NUREG/CR-6886
PNNL-15313

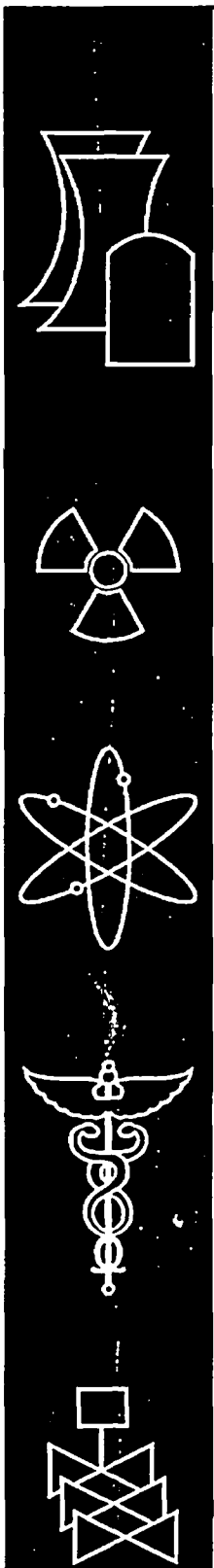

Spent Fuel Transportation Package Response to the Baltimore Tunnel Fire Scenario

Draft Report for Comment

Pacific Northwest National Laboratory

U.S. Nuclear Regulatory Commission
Office of Nuclear Material Safety and Safeguards
Washington, DC 20555-0001

AVAILABILITY OF REFERENCE MATERIALS IN NRC PUBLICATIONS

NRC Reference Material

As of November 1999, you may electronically access NUREG-series publications and other NRC records at NRC's Public Electronic Reading Room at http://www.nrc.gov/reading-rm.html. Publicly released records include, to name a few, NUREG-series publications; *Federal Register* notices; applicant, licensee, and vendor documents and correspondence; NRC correspondence and internal memoranda; bulletins and information notices; inspection and investigative reports; licensee event reports; and Commission papers and their attachments.

NRC publications in the NUREG series, NRC regulations, and *Title 10, Energy*, in the Code of *Federal Regulations* may also be purchased from one of these two sources.

1. The Superintendent of Documents
   U.S. Government Printing Office
   Mail Stop SSOP
   Washington, DC 20402–0001
   Internet: bookstore.gpo.gov
   Telephone: 202-512-1800
   Fax: 202-512-2250
2. The National Technical Information Service
   Springfield, VA 22161–0002
   www.ntis.gov
   1–800–553–6847 or, locally, 703–605–6000

A single copy of each NRC draft report for comment is available free, to the extent of supply, upon written request as follows:

Address: Office of the Chief Information Officer,
Reproduction and Distribution
Services Section
U.S. Nuclear Regulatory Commission
Washington, DC 20555-0001
E-mail: DISTRIBUTION@nrc.gov
Facsimile: 301–415–2289

Some publications in the NUREG series that are posted at NRC's Web site address http://www.nrc.gov/reading-rm/doc-collections/nuregs are updated periodically and may differ from the last printed version. Although references to material found on a Web site bear the date the material was accessed, the material available on the date cited may subsequently be removed from the site.

Non-NRC Reference Material

Documents available from public and special technical libraries include all open literature items, such as books, journal articles, and transactions, *Federal Register* notices, Federal and State legislation, and congressional reports. Such documents as theses, dissertations, foreign reports and translations, and non-NRC conference proceedings may be purchased from their sponsoring organization.

Copies of industry codes and standards used in a substantive manner in the NRC regulatory process are maintained at—

The NRC Technical Library
Two White Flint North
11545 Rockville Pike
Rockville, MD 20852–2738

These standards are available in the library for reference use by the public. Codes and standards are usually copyrighted and may be purchased from the originating organization or, if they are American National Standards, from—

American National Standards Institute
11 West 42nd Street
New York, NY 10036–8002
www.ansi.org
212–642–4900

Legally binding regulatory requirements are stated only in laws; NRC regulations; licenses, including technical specifications; or orders, not in NUREG-series publications. The views expressed in contractor-prepared publications in this series are not necessarily those of the NRC.

The NUREG series comprises (1) technical and administrative reports and books prepared by the staff (NUREG–XXXX) or agency contractors (NUREG/CR–XXXX), (2) proceedings of conferences (NUREG/CP–XXXX), (3) reports resulting from international agreements (NUREG/IA–XXXX), (4) brochures (NUREG/BR–XXXX), and (5) compilations of legal decisions and orders of the Commission and Atomic and Safety Licensing Boards and of Directors' decisions under Section 2.206 of NRC's regulations (NUREG–0750).

DISCLAIMER: This report was prepared as an account of work sponsored by an agency of the U.S. Government. Neither the U.S. Government nor any agency thereof, nor any employee, makes any warranty, expressed or implied, or assumes any legal liability or responsibility for any third party's use, or the results of such use, of any information, apparatus, product, or process disclosed in this publication, or represents that its use by such third party would not infringe privately owned rights.

NUREG/CR-6886
PNNL-15313

Spent Fuel Transportation Package Response to the Baltimore Tunnel Fire Scenario

Draft Report for Comment

Manuscript Completed: October 2005
Date Published: November 2005

Prepared by
H.E. Adkins, Jr., J.M. Cuta, B.J. Koeppel

Pacific Northwest National Laboratory
Richland, WA 99352

C. Bajwa and A. Hansen, NRC Project Managers

Prepared for
Spent Fuel Project Office
Office of Nuclear Material Safety and Safeguards
U.S. Nuclear Regulatory Commission
Washington, DC 20555-0001
Job Code J5167

COMMENTS ON DRAFT REPORT

Any interested party may submit comments on this report for consideration by the NRC staff. Comments may be accompanied by additional relevant information or supporting data. Please specify the report number NUREG/CR-6886, draft, in your comments, and send them by December 30, 2005 to the following address:

Chief, Rules Review and Directives Branch
U.S. Nuclear Regulatory Commission
Mail Stop T6-D59
Washington, DC 20555-0001

Electronic comments may be submitted to the NRC by the Internet at AGH@nrc.gov.

For any questions about the material in this report, please contact:

Allen Hansen
OWFN 13 D-13
U.S. Nuclear Regulatory Commission
Washington, DC 20555-0001
Phone: 301-415-1390
E-mail: AGH@nrc.gov
Fax: 301-415-8555

Note: The NUREG/CR-6886 draft report for comment is identical (except for format changes) to the NUREG/CR-DRAFT report posted in September in the NRC ADAMS document system (ML052500391) and announced in the Federal Register (page 54780) on Friday September 16, 2005.

NUREG/CR-6886 has been reproduced from the best available copy.

ABSTRACT

On July 18, 2001, a freight train carrying hazardous (non-nuclear) materials derailed and caught fire while passing through the Howard Street railroad tunnel in downtown Baltimore, Maryland. The United States Nuclear Regulatory Commission (USNRC), one of the agencies responsible for ensuring the safe transportation of radioactive materials in the United States, undertook an investigation of the train derailment and fire to determine the possible regulatory implications of this particular event for the transportation of spent nuclear fuel by railroad.

The USNRC met with the National Transportation Safety Board (NTSB) to discuss the details of the accident and the ensuing fire. Following these discussions, the USNRC assembled a team of experts from the National Institute of Standards and Technology (NIST), the Center for Nuclear Waste Regulatory Analyses (CNWRA), and Pacific Northwest National Laboratory (PNNL) to determine the thermal conditions that existed in the Howard Street tunnel fire and analyze the effects on various spent fuel transportation package designs.

The Fire Dynamics Simulator (FDS) code developed by NIST was used to determine the thermal environment in the Howard Street tunnel during the fire. The FDS results were used as boundary conditions in the COBRA-SFS and ANSYS® computer codes to evaluate the thermal performance of different package designs. The staff concluded that larger transportation packages resembling the HOLTEC Model No. HI-STAR 100 and TransNuclear Model No. TN-68 would withstand a fire with thermal conditions similar to those that existed in the Baltimore tunnel fire event with only minor damage to peripheral components. This is due to their sizable thermal inertia and design specifications in compliance with currently imposed regulatory requirements.

For the TN-68 and the NAC LWT, the maximum temperatures predicted in the regions of the lid, vent and drain ports exceed the seals' rated service temperatures, making it possible for a small release to occur, due to CRUD that might spall off the surfaces of the fuel rods. However, any release is expected to be very small due to a number of factors. These include (1) the tight clearances maintained between the lid and cask body by the closure bolts, (2) the low pressure differential between the cask interior and exterior, (3) the tendency of such small clearances to plug, and (4) the tendency of CRUD particles to settle or plate out.

USNRC staff evaluated the radiological consequences of the package responses to the Baltimore tunnel fire. The results of this evaluation strongly indicate that neither spent nuclear fuel (SNF) particles nor fission products would be released from a spent fuel shipping cask involved in a severe tunnel fire such as the Baltimore Tunnel Fire. None of the three cask designs analyzed for the Baltimore Tunnel fire scenario (TN-68, HI-STAR 100, and NAC LWT) experienced internal temperatures that would result in rupture of the fuel cladding. Therefore, radioactive material (i.e., SNF particles or fission products) would be retained within the fuel rods.

There would be no release from the HI-STAR 100, because the inner welded canister remains leak tight. The potential releases calculated for the TN-68 rail cask and the NAC LWT truck cask indicate that any release of CRUD from either cask would be very small - less than an A_2 quantity (see footnote 6, Section 8.)

DISCLAIMER

This report was prepared as an account of work sponsored by an agency of the United States Government. Neither the United States Government nor any agency thereof, nor Battelle Memorial Institute, nor any of their employees, makes any warranty, express or implied, or assumes any legal liability or responsibility for the accuracy, completeness, or usefulness of any information, apparatus, product, or process disclosed, or represents that its use would not infringe privately owned rights.

CONTENTS

ABSTRACT iii

ABBREVIATIONS xiii

1 INTRODUCTION 1.1

1.1 The Baltimore Tunnel Fire Event 1.1

2 NIST TUNNEL FIRE MODEL 2.1

3 CNWRA MATERIALS EXPOSURE ANALYSIS 3.1

4 TRANSPORTATION OF SPENT NUCLEAR FUEL 4.1

4.1 Transportation Packages Analyzed 4.1
4.1.1 TransNuclear TN-68 SNF Transportation Package 4.1
4.1.2 HOLTEC HI-STAR 100 SNF Transportation Package 4.2
4.1.3 NAC LWT SNF Transportation Package 4.3

5 ANALYSIS APPROACH 5.1

5.1 Model of TN-68 Transportation Package 5.1

5.2 Model of HI-STAR 100 Transportation Package 5.3

5.3 Model of NAC LWT Transportation Package 5.10

6 ANALYSIS METHOD 6.1

6.1 Fire Transient Assumptions and Boundary Conditions 6.1
6.1.1 Boundary Temperatures from FDS 6.2
6.1.2 Convection and Radiative Heat Transfer Boundary Conditions 6.3
6.1.3 Extrapolated Boundary Conditions for Long-Term Cool Down 6.5
6.1.4 Heat Transfer through Liquid Neutron Shield 6.7

6.2 Initial System Component Temperatures 6.8

6.3 Tunnel Fire Evaluations of Rail Packages 6.13

7 ANALYSIS RESULTS 7.1

7.1 TN-68 Fire Transient Results 7.1
7.1.1 TN-68 During the Fire 7.1

7.1.2 TN-68 Short-Term Post-Fire Response 7.3
7.1.3 TN-68 Long-Term Post-Fire Response 7.6

7.2 Holtec HI-STAR 100 Fire Transient Results 7.8
7.2.1 HI-STAR 100 During the Fire 7.8
7.2.2 HI-STAR 100 Short-Term Post-Fire Response 7.9
7.2.3 HI-STAR 100 Long-Term Post-Fire Response 7.11

7.3 NAC LWT Fire Transient Results 7.14
7.3.1 LWT During the Fire 7.14
7.3.2 LWT Short-Term Post-Fire Response 7.16
7.3.3 LWT Long-Term Post-Fire Response 7.18

8 POTENTIAL CONSEQUENCES 8.1

8.1 Results for the HI-STAR 100 Cask 8.1

8.2 Results for the TN-68 Cask 8.1

8.3 Results for the NAC LWT Cask 8.3

8.4 Summary of Potential Releases 8.5

9 REFERENCES 9.1

FIGURES

1.1 Liquid Tripropylene Tank Car 1.2
4.1 Cross-section of TN-68 Package (drawing 972-71-3 Rev. 4, "TN-68 Packaging General Arrangement: Parts List and Details") 4.1
4.2 TransNuclear TN-68 Spent Fuel Transportation Package 4.2
4.3 HOLTEC HI-STAR 100 Spent Fuel Package 4.2
4.4 Spent Fuel Transportation Package on Railcar 4.3
4.5 NAC LWT Transport Package (without ISO container) 4.3
4.6 NAC LWT Transport Package (with ISO container) 4.3
5.1 COBRA-SFS Model of TN-68 Basket and Support Rails 5.2
5.2 ANSYS HI-STAR 100 Package Analysis Model Element Plot 5.4
5.3 Cross-section of Package, Cradle, and Rail Car Section 5.4
5.4 Cross-section of HI-STAR Package and MPC-24 Canister 5.5
5.5 Close-up of Package Cross-section 5.5
5.6 Close-up of Canister Basket Structure and Fuel Compartment Configuration (without helium elements) 5.6
5.7 Close-up of Canister Basket Structure and Fuel Compartment Configuration (with helium elements) 5.6
5.8 Complete Impact Limiter (Except Skin) 5.7
5.9 Impact Limiter Skin and Primary Support Structure 5.7
5.10 Boundary Sections for Tunnel and Package Model 5.8
5.11 Surfaces Defined for Interaction with "Top" Gas Region 5.8
5.12 Surfaces Defined for Interaction with "Side" Gas Region 5.9
5.13 Surfaces Defined for Interaction with "Bottom" Gas Region 5.9
5.14 ANSYS NAC LWT Package Analysis Model Element Plot 5.10
5.15 Cross-section of NAC LWT Package 5.10
5.16 NAC LWT Package Geometry 5.11
5.17 Zones for Convection Heat Transfer Within the ISO Container 5.12
5.18 Zones for External Radiation Between ISO Container and Tunnel Surfaces 5.13
6.1 BTF Peak Transient Ambient Air Temperatures (smoothed values, NIST 20-m data) 6.3
6.2 BTF Peak Transient Tunnel Surface Temperatures for Floor, Walls, and Ceiling (smoothed values, NIST 20-m data) 6.3
6.3 BTF Peak Transient Horizontal Velocities near Package Surface (smoothed values, NIST 20-m data) 6.3
6.4 Heat Transfer Coefficients at Package Surface from NIST 20 m Air Temperature and Velocity Predictions 6.4
6.5 BTF Peak Transient Air Temperatures for Top, Side, and Bottom Regions (NIST and Extrapolated Data Sets) 6.5
6.6 BTF Peak Transient Surface Temperatures for Floor, Walls, and Ceiling (NIST and Extrapolated Data Sets) 6.6
6.7 Nusselt Number for Heat Transfer in Liquid Neutron Shield 6.8
6.8 Effective Conductivity of Neutron Shield Tank Contents 6.8

6.9 Effective Conductivity of Expansion Tank Contents 6.8
6.10 HI-STAR 100 Package Hot-Normal Condition Temperature Distribution 6.9
6.11 LWT Package Hot-Normal Condition Temperature Distribution (2.5 kW Decay Heat) 6.11
6.12 LWT Package Normal Condition Temperature Distribution (2.5 kW Decay Heat) 6.12
7.1 Maximum Temperature Histories for TN-68 Package Components During Fire Transient 7.2
7.2 Temperature Profiles Top-To-Bottom Through TN-68 Package Axis During Fire Transient 7.2
7.3 Maximum Temperature Histories for TN-68 Package Components During First 30 hr of Transient 7.3
7.4 Maximum TN-68 Package Surface Temperatures Compared to NIST Boundary Condition Temperatures 7.4
7.5 Peak Fuel Cladding Temperature History in TN-68 During First 50 hr of Transient 7.5
7.6 Maximum Global TN-68 Closure/ Port Seal Temperature History During First 30 hr of Transient 7.6
7.7 Temperature Profiles Top-To-Bottom Through TN-68 Package Axis: First 30 hr of Transient 7.6
7.8 Maximum Temperature Histories for TN-68 Package Components During 300 hr of Transient 7.7
7.9 Maximum Temperature Histories for HI-STAR 100 Package Components During Fire Transient 7.8
7.10 Maximum Temperature Histories for HI-STAR 100 Package Components During First 30 hr of Transient 7.9
7.11 Maximum HI-STAR 100 Package Surface Temperatures Compared to NIST Boundary Condition Temperatures 7.10
7.12 Peak Fuel Cladding Temperature History in HI-STAR 100 During First 50 hr of Transient 7.10
7.13 Maximum Global HI-STAR 100 Closure/Port Seal Temperature History During First 30 hr of Transient 7.11
7.14 Maximum Temperature Histories for HI-STAR 100 Package Components During 300 hrs of the Transient 7.12
7.15 NAC LWT Package Component Maximum Temperature Histories During Fire Transient 7.15
7.16 Lumped Fuel Assembly Temperature Distribution 7 hr Into Transient 7.15
7.17 NAC LWT Package Component Maximum Temperature Histories for First 30 hr of Fire Transient 7.16
7.18 Maximum ISO Container Surface Temperature History Compared with NIST Boundary Condition Temperatures 7.16
7.19 Peak and Average Fuel Cladding Temperature Histories for NAC LWT Package During First 30 hr of Fire Transient 7.17
7.20 Maximum Seal Temperature Histories for Drain/Vent Ports and Package Lid During First 30 hr of Fire Transient 7.17
7.21 NAC LWT Package Component Maximum Temperature Histories During 300 hr Transient 7.18

TABLES

6.1 TN-68 Hot-Normal Component Temperatures 6.9
6.2 HOLTEC HI-STAR 100 Hot-Normal Component Temperatures 6.10
6.3 NAC LWT Component Temperatures at Various Decay Heat Loads 6.11
6.4 NAC LWT Component Temperatures at 2.5 kW Decay Heat Load and 130°F Ambient 6.12
6.5 NAC LWT Pre-Fire Component Temperatures at 2.5 kW Decay Heat Load and 100°F Ambient 6.13
7.1 TN-68 Peak Component Temperatures During Fire Transient 7.7
7.2 HOLTEC HI-STAR 100 Peak Component Temperatures During Fire Transient 7.14
7.3 NAC LWT Peak Component Temperatures During Fire Transient 7.18
8.1 Assumptions Used for Release Estimate for TN-68 Cask 8.3
8.2 Potential Release Estimates for TN-68 Cask 8.3
8.3 Assumptions Used for Release Estimate for NAC LWT Cask 8.4
8.4 Potential Release Estimates for NAC LWT Cask 8.5

APPENDICES

APPENDIX A – Material Properties for COBRA-SFS Model of TN-68 Package A.1

APPENDIX B – Material Properties for ANSYS Model of HI-STAR 100 Package B.1

APPENDIX C – Material Properties for ANSYS Model of Legal Weight Truck Package C.1

APPENDIX D – Blackbody Viewfactors for COBRA-SFS Model of TN-68 Package D.1

APPENDIX E – HOLTEC HI-STAR 100 Component Temperature Distributions E.1

ABBREVIATIONS

APDL	ANSYS® Parametric Design Language
BTF	Baltimore Tunnel Fire
BWR	Boiling Water Reactor
CFD	Computational Fluid Dynamics
CNWRA	Center for Nuclear Waste Regulatory Analyses
CRUD	Chalk River Unknown Deposit (generic term for various residues deposited on fuel rod surfaces, originally coined by Atomic Energy of Canada, Ltd. (AECL) to describe deposits observed on fuel removed from the test reactor at Chalk River.)
FDS	Fire Dynamics Simulator (computational fluid dynamics computer code)
FEA	Finite Element Analysis
ISO	International Organization for Standardization (The International Organization for Standardization has decreed the use of the initials ISO for reference to the organization, regardless of the word order of the organization's name in any given language. This defines a uniform acronym in all languages.)
MPC	Multi-Purpose Canister
NIST	National Institute of Standards and Technology
NTSB	National Transportation Safety Board
OFA	Optimized Fuel Assembly
PNNL	Pacific Northwest National Laboratory
PWR	Pressurized Water Reactor
SFPO	USNRC Spent Fuel Project Office
SNF	Spent nuclear fuel
USNRC	United States Nuclear Regulatory Commission

1 INTRODUCTION

Current USNRC regulations specify that spent nuclear fuel shipping packages must be designed to survive exposure to a fully engulfing fire accident lasting no less than 30 minutes with an average flame temperature of no less than 1475°F (802°C)[1]. The package must maintain containment, shielding and criticality functions throughout the fire event and post-fire cool down in order to meet USNRC requirements.

On July 18, 2001, a CSX freight train carrying hazardous (non-nuclear) materials derailed and caught fire while passing through the Howard Street railroad tunnel in downtown Baltimore, Maryland. (A summary description of the event is given in Section 1.1.) The staff of the USNRC Spent Fuel Project Office (SFPO) undertook an investigation of the derailment and fire in order to determine what impact this event might have had on spent nuclear fuel transported by rail.

The severity of the Baltimore tunnel fire has raised questions about the performance of spent fuel transportation packages in such an accident. As one element of on-going evaluations related to this accident scenario, calculations were performed for three spent nuclear fuel transportation packages. The TransNuclear Model No. TN-68 ("TN-68") transport package was analyzed using the COBRA-SFS code [2]. The HOLTEC Model No. HI-STAR 100 ("HI-STAR 100") and the NAC International Model No. LWT ("NAC LWT") transport package were analyzed using the ANSYS® code [3]. The analyses were performed in parallel to expedite the work and to provide independent evaluation of different modeling approaches for the two relatively similar large package designs.

Air temperatures and temperatures of the tunnel wall, floor and ceiling derived from fire analyses performed by the National Institute of Standards and Technology (NIST) were used to define the boundary conditions for the transient calculations. The purpose of the evaluation was to obtain an estimate of the temperature response of the various components of each of these packages during and after the fire.

This report presents a detailed description of the analyses, including boundary conditions, modeling approach, and computational results. Section 2 describes the NIST tunnel fire model used to develop boundary conditions for the thermal analyses of the spent fuel transportation packages. Section 3 briefly describes the material exposure analysis used to verify the predicted temperatures obtained in the fire simulations performed by NIST. Section 4 presents a detailed description of the spent fuel transportation casks, and the computational models developed for the analyses are described in Section 5. Section 6 presents a detailed description of the analysis method. Section 7 presents the results of the simulation, giving a detailed evaluation of predicted response for each cask package during and after the fire. Section 8 provides an analysis to determine the magnitude of any potential release of radioactive material as a consequence of the effects of the fire on the casks.

1.1 The Baltimore Tunnel Fire Event

The Howard Street tunnel in Baltimore is a single track railroad tunnel of concrete and refractory brick. Originally constructed in 1859, later additions extended it to its current length of 1.65 mi (2.7 km). The tunnel has an average upward grade of 0.8% from the west portal to the east portal, and has no active ventilation system. The tunnel measures approximately 22 ft (6.7 m) high

by 27 ft (8.2 m) wide in the vicinity of the accident; however, the dimensions vary along the length.

The freight train involved in the accident had a total of 60 cars pulled by 3 locomotives, and was carrying paper products and pulp board in boxcars as well as hydrochloric acid, liquid tripropylene[1], and other hazardous liquids in tank cars [4,5]. As the train was passing through the tunnel, 11 of the 60 rail cars derailed. A tank car (see Figure 1.1) containing approximately 28,600 gallons (108,263 liters) of liquid tripropylene had a 1.5-inch (3.81-cm) diameter hole punctured in it by the car's brake mechanism during the derailment.

Ignition of the liquid tripropylene led to the ensuing fire. The exact duration of the fire is not known. Based on NTSB interviews of emergency responders, it was determined that the most severe portion of the fire lasted approximately 3 hours. Other, less severe fires burned for periods of time greater than 3 hours. Approximately 12 hours after the fire started, firefighters were able to visually confirm that the tripropylene tank car was no longer burning.

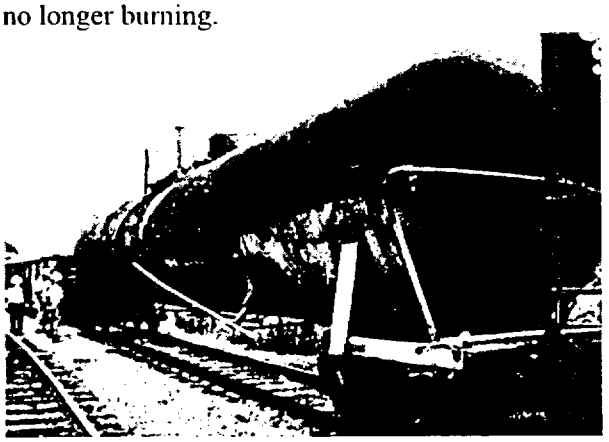

Figure 1.1. Liquid Tripropylene Tank Car

[1] Tripropylene carries an NFPA hazards rating of 3 for flammability, which is the same as that of gasoline.

2 NIST TUNNEL FIRE MODEL

Experts at the National Institute of Standards and Technology (NIST) developed a model [4] of the Baltimore tunnel fire using the Fire Dynamics Simulator (FDS) code [6, 7][2] to predict the range of temperatures present in the tunnel during the fire event. FDS is a computational fluid dynamics (CFD) code that models combustion and flow of hot gas in fire environments. FDS solves the mass, momentum, and energy equations for a given computational grid, and is also able to construct a visual representation of smoke flow for a given fire.

To validate FDS for tunnel fire applications, NIST developed fire models in FDS based on the geometry and test conditions from a series of fire experiments conducted by the Federal Highway Administration and Parsons Brinkerhoff, Inc. as part of the Memorial Tunnel Fire Ventilation Test Program [8]. NIST modeled both a 6.83×10^7 Btu/hr (20 MW) and a 1.71×10^8 Btu/hr (50 MW) unventilated fire test from the Memorial Tunnel Test Program, and achieved results using FDS that were within 100°F (56°C) of the recorded data[6,7].

The full-length 3-dimensional representation of the tunnel fire scenario developed by NIST included railcars positioned as they were found following the derailment and fire. The source of the fire was specified in the simulation as a pool of burning liquid tripropylene positioned below the location of the hole punctured in the tripropylene tank car. The computational grid for the tunnel fire model was relatively fine in the immediate vicinity of the fire, in order to properly capture fire and gas behavior. The mesh size was expanded at distances further from the fire source, where less resolution was needed.

Maximum temperatures calculated in the FDS model were on the order of 1800°F (982°C) in the flaming regions of the fire. The model results showed that the hot gas layer above the railcars within three rail car lengths of the fire was an average of 900°F (482°C). Temperatures on the tunnel wall surface were calculated to be in excess of 1500°F (816°C) where the fire directly impinged on the ceiling of the tunnel. The average tunnel ceiling temperature, within a distance of three rail cars from the fire, was 750°F (399°C).

Additional details associated with the analyses performed by NIST can be found in the report on the FDS analysis of the Howard Street tunnel fire [4].

[2] Formal publication of the FDS code documentation began in 2001 with Version 2. Continuing validation and development of the code led to Version 3 in 2002. Version 3 was used in the FDS analyses discussed in this report.

3 CNWRA MATERIALS EXPOSURE ANALYSIS

Staff from the Center for Nuclear Waste Regulatory Analysis (CNWRA), along with staff from NRC and NIST, examined railcars and tank cars removed from the Howard Street tunnel approximately one year after the fire. The examination of physical evidence provided the staff with further insight into the fire environment that existed in the tunnel during the accident. Staff from CNWRA also collected material samples from the boxcars and tank cars inspected.

By performing metallurgical analyses on the material samples collected, including sections of the boxcars exposed to the most severe portion of the fire and an air brake valve from the tripropylene tanker car, CNWRA was able to estimate the fire exposure time and temperature for the samples tested. The material time and temperature exposures determined by the CNWRA analyses were consistent with the conditions predicted by the NIST FDS model of the Howard Street tunnel fire [4].

Additional details associated with the analyses performed by CNWRA can be found in the report on the analysis of the rail car components [5].

4 TRANSPORTATION OF SPENT NUCLEAR FUEL

NRC regulations require that spent fuel transportation packages be evaluated for a series of hypothetical accident conditions that include a 30-ft (9 m) drop test, a 40-inch (1 m) pin puncture drop test, and a fully engulfing fire with an average flame temperature of 1475°F (802°C) for a period of 30 minutes. These tests are followed by the immersion of an undamaged package under 50 ft (15 m) of water [1]. The certification process must include either an open pool fire test or an analysis of the package for a fire exposure meeting the aforementioned criteria. Packages must maintain shielding and criticality control functions throughout the hypothetical accident conditions.

4.1 Transportation Packages Analyzed

This investigation evaluates how a fire similar to the Howard Street tunnel fire might affect three NRC-approved spent fuel transportation package designs. These include the HOLTEC HI-STAR 100 and TransNuclear TN-68 rail transportation packages, and NAC LWT transportation package. The LWT was selected because it represents a typical truck (over-the-road) package that can also be transported by rail. The design of each of these packages is briefly described below.

4.1.1 TransNuclear TN-68 SNF Transportation Package

The TN-68 spent fuel shipping package transports BWR spent fuel assemblies. The basic design is similar to that of the HOLTEC HI-STAR 100, except that the TN-68 package does not include an inner sealed canister. The containment boundary is provided by the package shell and lid seals.

The TN-68 package holds up to 68 BWR assemblies, with a maximum total decay heat load of 72,334 Btu/hr (21.2 kW). The fuel assemblies are contained within a basket structure consisting of 68 stainless steel tubes that have aluminum and borated aluminum (or boron carbide/aluminum composite) neutron poison plates sandwiched between the steel tubes. The general layout of the TN-68 package is illustrated in Figures 4.1 and 4.2. Detailed information on the design can be found in the appropriate sections of the TN-68 Safety Analysis Report (SAR) [9].

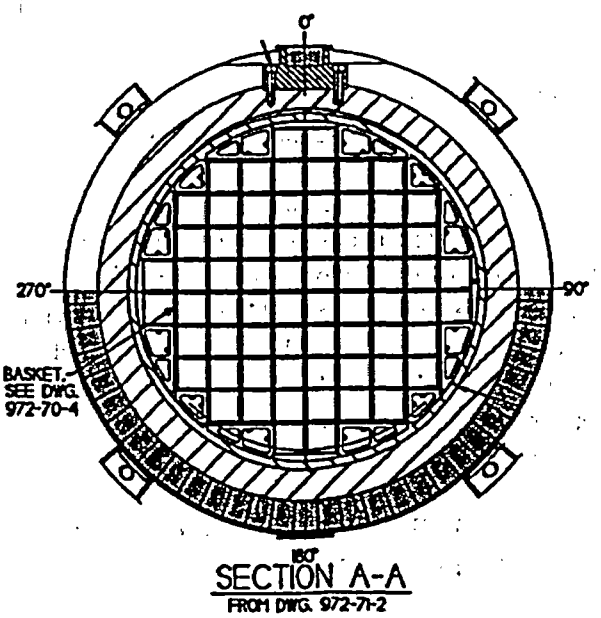

Figure 4.1. Cross-section of TN-68 Package (drawing 972-71-3 Rev. 4, "TN-68 Packaging General Arrangement: Parts List and Details")

The basket structure is supported by aluminum alloy support rails bolted to the inner carbon steel package shell, which also serves as the inner gamma shield. This inner steel shell is shrink-fitted within an outer carbon steel shell that serves as the outer gamma shield. The gamma shielding is surrounded by the neutron shielding, which

consists of a ring of aluminum boxes filled with borated polyester resin. The outer shell of the package is carbon steel.

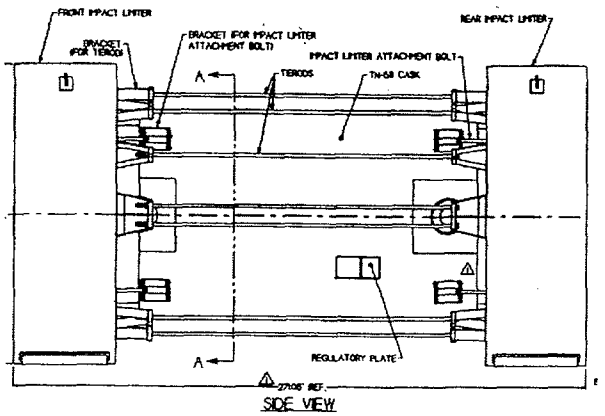

Figure 4.2. TransNuclear TN-68 Spent Fuel Transportation Package

The package bottom is carbon steel with an inner steel shield plate. The package lid is also carbon steel with a steel inner top shield plate. During transport, the ends of the package are capped with impact limiters made of redwood and balsa and covered in stainless steel plate. The TN-68 weighs approximately 260,400 lb (118,115 kg) when loaded for transport.

4.1.2 HOLTEC HI-STAR 100 SNF Transportation Package

This design provides an additional containment boundary in the form of a welded multi-purpose canister (MPC) enclosing the spent fuel. (The outermost containment boundary is provided by the package shell and lid seals.) HOLTEC has a variety of MPC configurations designed to accommodate three different spent fuel loading configurations: up to 24 PWR assemblies, up to 32 PWR assemblies, or up to 68 BWR assemblies. The MPC-24 configuration was selected for this evaluation. This design has an integral fuel basket that accommodates 24 PWR spent fuel assemblies with a maximum total decay heat load of 68,240 Btu/hr (20.0 kW). The MPC is placed in the transportation package (or overpack) for shipment after it has been loaded with spent nuclear fuel and welded shut. A diagram of the HI-STAR 100 package system (MPC and overpack) is provided in Figure 4.3. The package inner shell is stainless steel, and six layers of carbon steel plates comprise the gamma shield. The next layer is a polymeric neutron shield, strengthened by a network of carbon steel stiffening fins. The outer shell of the package is carbon steel, with a painted outer surface.

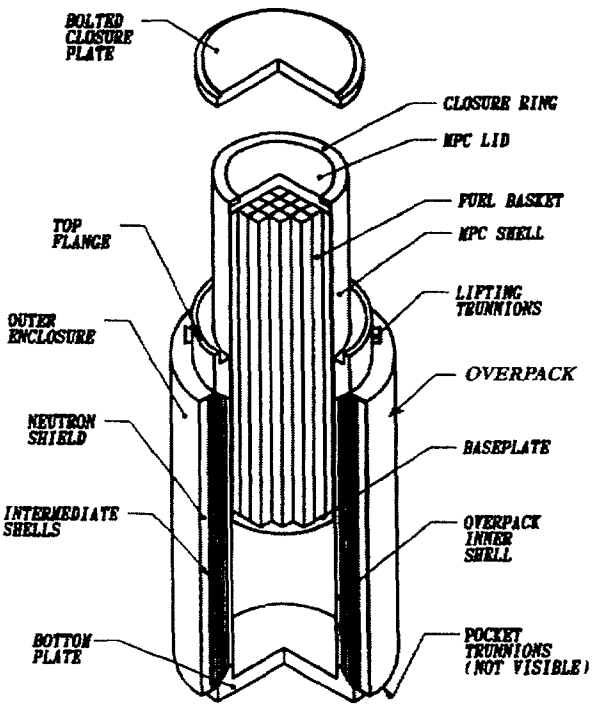

Figure 4.3. HOLTEC HI-STAR 100 Spent Fuel Package

Aluminum honeycomb impact limiters with stainless steel skin are installed on the ends of the package prior to shipping. Impact limiters protect the closure lid, MPC, fuel basket, and contents from damage in the event of a package drop accident. The impact limiters also provide thermal

insulation to the lid and port cover components in the event of a fire exposure. Figure 4.4 shows an illustration of this package secured to a railcar, with impact limiters installed. This package weighs approximately 277,300 lb (125,781 kg) when loaded for transport. Additional configuration details are provided in the HI-STAR 100 Package System SAR [10].

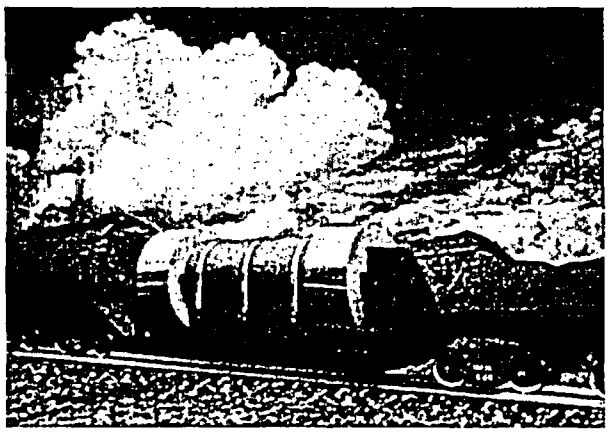

Figure 4.4. Spent Fuel Transportation Package on Railcar[3]

4.1.3 NAC LWT SNF Transportation Package

The NAC LWT is a small transportation package certified for transport on a standard tractor trailer truck, but can also be transported by rail. The NAC LWT is typically shipped within an International Organization for Standardization (ISO) shipping container. Figure 4.5 shows a picture of a NAC LWT package on a flat-bed trailer with a personnel barrier installed, but without an ISO container. Figure 4.6 shows an exterior view of the package within an ISO container on a flat-bed trailer.

This package is designed to transport a variety of commercial and test reactor fuel types with widely varying maximum decay heat load specifications for the different fuels. For the purposes of this analysis, the package was assumed to contain a single PWR spent nuclear fuel assembly, with a maximum decay heat load of 8,530 Btu/hr (2.5 kW). This is the highest heat load the package is rated for with any spent fuel it is designed to carry, and thus provides a conservative thermal load for the fire accident scenario. The loaded package weighs approximately 52,000 lb (23,586 kg). The containment boundary provided by the stainless steel package consists of a bottom plate, outer shell, upper ring forging, and closure lid.

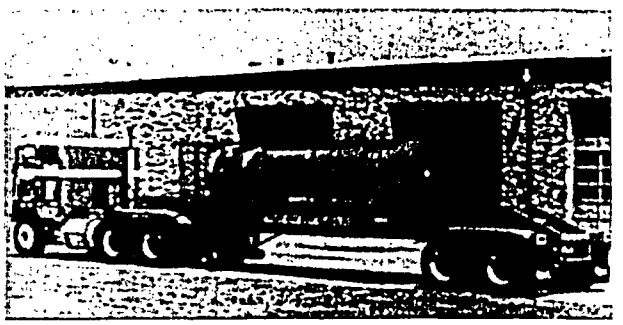

Figure 4.5. NAC LWT Transport Package (without ISO container)

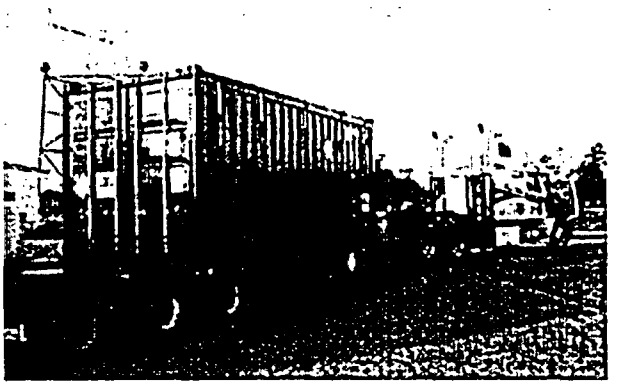

Figure 4.6. NAC LWT Transport Package (with ISO container)

The package has an additional outer stainless steel shell to protect the containment shell, and also to

[3] Image courtesy of HOLTEC International.

enclose the lead gamma shield. Neutron shielding is provided by a stainless steel neutron shield tank containing a water/ethylene glycol mixture. An additional annular expansion tank for the mixture is provided, external to the shield tank. This component is strengthened internally by a network of stainless steel stiffeners. Aluminum honeycomb impact limiters covered with an aluminum skin are attached to each end of the package. Additional configuration details are provided in the SAR for this transport package [11].

5 ANALYSIS APPROACH

The analytical approach used to evaluate the response of the selected transportation packages was to construct highly detailed 3-D models capable of accounting for all of the significant heat transfer paths, and exposing them to boundary conditions from the postulated Howard Street tunnel thermal environment. All three transportation package models were constructed in parallel to expedite the evaluation. Two different computer analysis codes were used for the large multi-assembly packages, to provide independent verification of the analytical results. The TN-68 package was modeled using the COBRA-SFS finite-difference thermal-hydraulic analysis code [2], while the HI-STAR 100 and NAC LWT packages were modeled using the ANSYS [3] general FEA code. Three-dimensional models of each of the packages were developed for these analyses.

These three-dimensional models were subjected to boundary conditions obtained from the results of the FDS simulation using the NIST model of the Howard Street tunnel. (See Section 6 for a detailed discussion of the analysis method.) The boundary conditions were developed from temperature and flow predictions for the postulated fire and post-fire scenario, and applied to the TN-68, HI-STAR 100, and LWT models.

Peak tunnel surface temperatures, peak gas temperatures, and associated gas velocities predicted in the FDS analysis were selected at 66 ft (20 m) down-stream from the fire source. This location corresponds to the shortest possible distance between the fire center and a SNF package being transported by rail. The distance was determined based on Department of Transportation regulations that require railcars carrying radioactive materials to be separated from other cars carrying hazardous materials or flammable liquids by at least one innocuous railcar (referred to as a buffer car) [12].

The package was assumed to be horizontal, with one end of the package facing the fire source. This orientation results in maximum possible exposure to the fire-driven flow of hot gas along the length of the package, and is the most adverse position for free convection cooling of the package during the post-fire cool down.

The FDS analysis predicted a 7-hour fire, and the calculation was extended out to a 23-hour post-fire cool-down, for a total simulation time of 30 hours. To determine the packages' complete transient temperature responses, and to explore the effects of prolonged exposure to post-fire conditions in the tunnel, the COBRA-SFS and ANSYS analyses extended the post-fire duration to 300 hours. Tunnel wall and air temperatures predicted in the FDS analysis at 30 hours were extrapolated from 30 hours to 300 hours using a power function, to realistically model cool-down of the tunnel environment.

5.1 Model of TN-68 Transportation Package

The TN-68 package was analyzed with COBRA-SFS, a code developed by PNNL for thermal-hydraulic analyses of multi-assembly spent fuel storage and transportation systems. The code uses a lumped-parameter finite-difference approach for predicting flow and temperature distributions in spent fuel storage systems and fuel assemblies under forced and natural circulation flow conditions. It is applicable to both steady-state and transient conditions in single-phase gas-cooled spent fuel packages with radiation, convection, and conduction heat transfer. The code has been validated in blind calculations using test data from

spent fuel packages loaded with actual spent fuel assemblies as well as electrically heated single-assembly tests [13,14,15].

The TN-68 package was modeled in COBRA-SFS as a one-half section of symmetry. Figure 5.1 shows a diagram of the center cross-section of the basket and support rails as represented in the COBRA-SFS model. The fuel assemblies within the basket are each modeled as detailed rod and subchannel arrays, and the tubes containing the fuel assemblies are represented using solid conduction nodes.

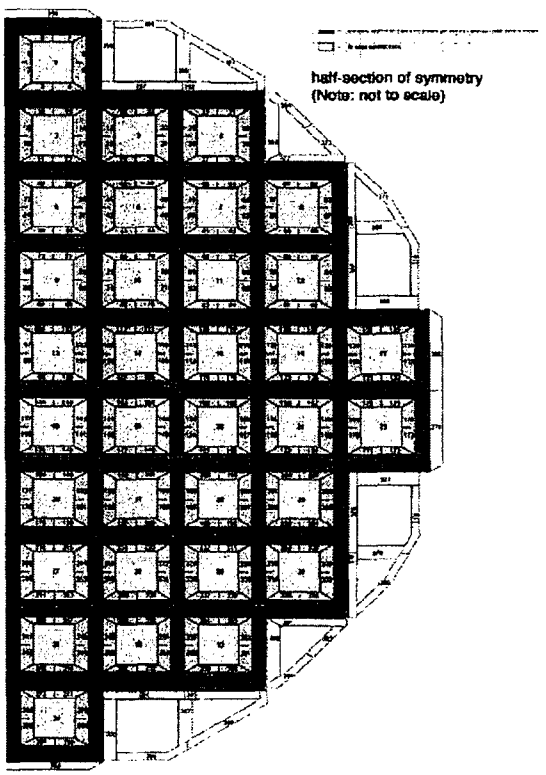

Figure 5.1. COBRA-SFS Model of TN-68 Basket and Support Rails

The aluminum and borated aluminum neutron poison plates sandwiched between the tubes are represented as an interconnected network of solid conduction nodes. The gamma shielding, neutron shielding, and outer steel shell are represented with concentric rings of interconnected solid conduction nodes with appropriate material properties. (For clarity, these nodes are not included in the diagram shown in Figure 5.1.) The half-section of the TN-68 package is represented with about 69,000 fluid nodes, 53,000 fuel nodes, and over 16,000 solid conduction nodes.

The solid conduction nodes extend over 32 axial divisions comprising the axial length of the package. In cross-section, the stainless steel tubes containing the fuel assemblies are represented using two solid conduction nodes on each face of the enclosure, for a total of eight nodes per tube. The aluminum and borated aluminum neutron poison plates sandwiched between the tubes are represented as an interconnected network of solid conduction nodes that are in intimate physical contact with the stainless steel tubes and with each other. A total of 272 nodes are used to represent the 34 steel tubes in the half-section of symmetry. The borated aluminum neutron poison plates making up the rest of the basket are modeled with a total of 83 solid conduction nodes. The aluminum alloy basket rails are represented with a total of 36 solid conduction nodes, and provide appropriate thermal connections between the basket and the steel inner gamma shield.

The gamma shielding, neutron shielding, and outer steel shell are represented in the COBRA-SFS model as concentric rings of interconnected solid conduction nodes. The spent fuel arrays within the basket are assumed to be 7 x 7 BWR assemblies (the design basis fuel loading for the TN-68, as specified in the SAR [9]). Each assembly is modeled in detail, with 49 rods and 64 subchannels.

In cross-section, the gamma shielding is represented with two rings of 16 nodes each, representing the inner and outer steel shells of this component. The neutron shield in cross-section is

represented with three rings of nodes (for a total of 48 nodes), with properties and connections defined to represent the material properties and thermal interactions of the ring of aluminum boxes filled with borated polyester. In cross-section, the outer steel shell of the package is represented with a ring of 16 nodes, with appropriate thermal connections to the neutron shielding on one side and ambient air on the other.

The COBRA-SFS model was verified by running the steady-state case for design basis normal hot transport conditions. The predicted peak clad temperature for these conditions was compared with the peak temperature reported in the SAR. The code predicts a peak clad temperature of 485°F (252°C); the SAR gives a value of 490°F (254°C) for these conditions (see Chapter 3, Table 3-1 in the TN-68 SAR [9]).

The steady-state solution obtained for normal hot transport conditions was used to define the pre-fire condition for the package in the transient calculations simulating the Baltimore tunnel fire. This provides a conservative estimate of the initial temperatures throughout the package, since the boundary conditions for normal hot transport are specified as 100°F (38°C) ambient temperature in still air with insolation.

The external air temperatures predicted for the fire in the NIST simulation are sufficiently high to boil off the borated polyester neutron shield and completely char the wooden impact limiters. In both cases, the normal material would be replaced with material that would tend to insulate the package from the fire (i.e., air in place of the borated polyester, charred wood in place of the wooden impact limiter material.)

To maximize the heat load to the package from the fire, it was assumed for the purposes of the calculation that these materials would persist intact throughout the fire (rather than gradually degrading or burning off.) Then at the end of the fire (6.75 hours into the transient), these materials would be instantly transformed to a degraded condition. For the nodes modeling the neutron shield, this was simulated in the calculation by changing the material properties to hot air at the end of the fire. The material properties specified for the nodes modeling the wooden impact limiters were changed from redwood to charcoal at the end of the fire.

The material properties from the package vendor's Safety Analysis Report (SAR) were verified and then used in the analyses [9]. The material properties used in this evaluation are given in Appendix A.

5.2 Model of HI-STAR 100 Transportation Package

The ANSYS model of the HI-STAR 100 package consists of a detailed three-dimensional representation of a half-section of symmetry for the package, its cradle support[4], and the rail car decking directly below the cradle. (The remainder of the rail car was omitted from the model because it would partially shield the package from thermal radiation from the hot tunnel surfaces and block convection heat transfer to the package due to the flow of hot gas generated by the fire.) This half-section model of the package was placed within a complete cross-section of the surrounding tunnel.

The model developed for the HI-STAR 100 package utilized 120,412 SOLID70 and 1,542 SHELL57 thermal elements for conduction. It used two groups of 13,573 SURF152 surface effect elements for handling convection states in

[4]Dimensions and materials for the rail car decking and the cradle were based on current (as of June 2005) specifications from the package vendor. Cradle design determines the height of the cask within the tunnel, the

the pre-fire steady state and the fire accident transient. For radiation interaction, 288 highly structured AUX-12 generated MATRIX50 superelements were constructed using SHELL57 elements. Solar insolation (from 10CFR71 [1]) for the pre-fire condition was assigned via heat generation to the first group of 13,573 SURF152 surface effect elements. A portion of the model is shown in Figure 5.2. (In this figure most of the tunnel has been omitted for clarity.)

The material properties from the package vendor's Safety Analysis Report were verified and used in the analysis [10]. The model explicitly represents the geometry of the package, including the internal geometry of the fuel basket, all gaps associated with the basket construction, as well as the integral neutron absorber plates. Figures 5.3 through 5.6 show cross-sections of the HI-STAR model highlighting key features that were included.

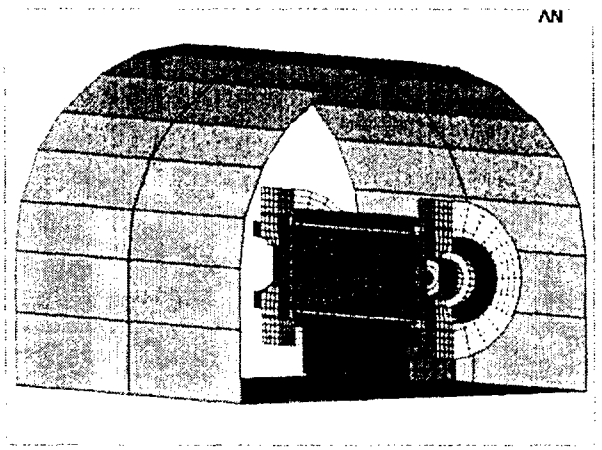

Figure 5.2. ANSYS HI-STAR 100 Package Analysis Model Element Plot

Figure 5.3 shows the cross-section of the package, canister, cradle, and transport car section. In this figure, all helium conduction volumes have been removed for visualization purposes. The cradle section and rail car section were modeled as hollow enclosures. All internal radiation and convection influences associated with these two enclosures were accounted for using AUX-12 generated MATRIX50 superelements (constructed with SHELL57 elements) and SURF152's with the extra node option, respectively.

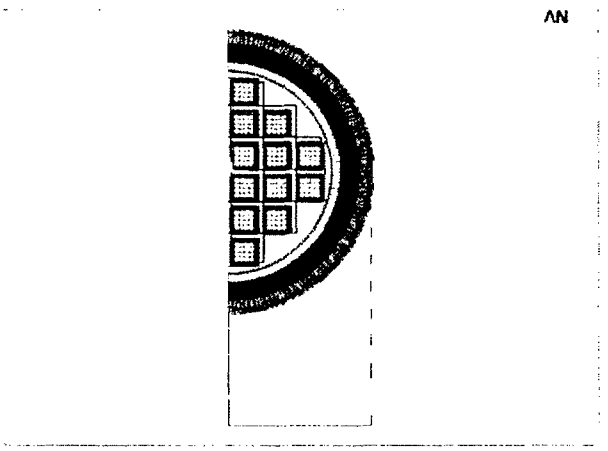

Figure 5.3. Cross-section of Package, Cradle, and Rail Car Section

Conduction within the cradle and trailer material sections was also accounted for using additional SHELL57 elements with thickness option applied. Natural convection correlations and specially constructed automated subroutines written in ANSYS Parametric Design Language (APDL) were used to continuously evaluate and update the convective coefficients of heat conductance. Fourteen separate passive computation nodes were assigned as "extra nodes" for the SURF152 surface effect elements used in specifying the convection interaction within the cradle and rail car section (seven for each – not shown in Figure 5.3). Section 6 presents a discussion of the natural convection correlations used in this analysis.

Figure 5.4 shows the cross-section of the package and canister, with the overall basket structure. As in Figure 5.3, all helium conduction volumes have been removed for visualization purposes. This

geometry of direct conduction paths from the cask, and can affect thermal shielding of the cask during the fire.

figure displays the general fuel compartment layout within the MPC-24 basket structure, and includes the inner shell (light green), gamma shield (dark blue), and the neutron shield (purple) components of the HI-STAR 100.

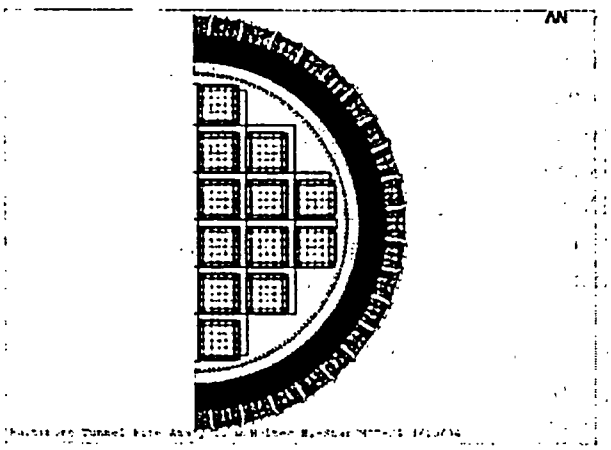

Figure 5.4. Cross-section of HI-STAR Package and MPC-24 Canister

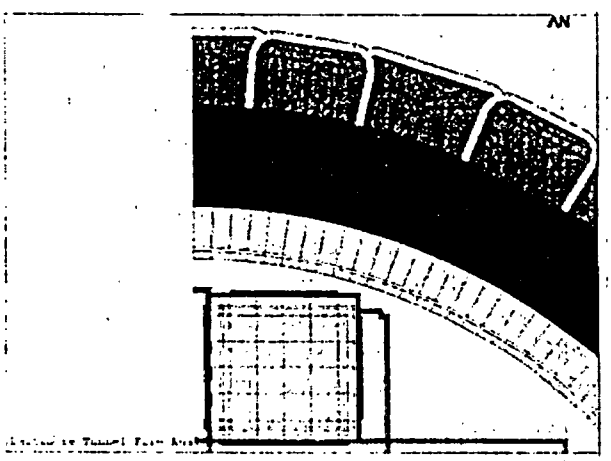

Figure 5.5. Close-up of Package Cross-section

The model cross-section in Figure 5.5 shows that the fillet welds joining the sections of the package outer skin and the expansion foam in the neutron shield area have been modeled explicitly. Special element material definitions were created for the elements providing the connection between the fins enclosing the neutron shield and the gamma shield. The material definition was specified such that the thermal conductivity could be readily degraded to represent the effect of single-sided fillet welds (i.e., not full penetration) that are used in this connection. Since the thermal conductivity through single-sided fillet welds is difficult to determine objectively, the conductivity of this material in the pre-fire steady state and post-fire transient was conservatively reduced to half of that of the solid base material. The effect of this assumption is to conservatively minimize the rejection of internal heat. During the fire, however, the thermal conductivity of these elements was assumed to be the same as the solid base material, mimicking that of a full penetration weld. This approach was used to conservatively maximize the heat input into the package during the fire.

Special material definitions were also created for the elements making up the multi-layer steel gamma shield (dark blue in Figures 5.5 and 5.6.) To account for the probability of gaps between the five steel sheets due to standard manufacturing practices, a gap of 0.01 inch was assumed to exist between each layer. Effective material thermal conductivities were then calculated for the gaps, accounting for conduction through gas in the gap and radiation across the gap. These material property definitions were used in the pre-fire steady state and the post-fire transient to conservatively minimize the rejection of internal heat. However, the conduction properties of these elements were reassigned to that of solid material (i.e., equivalent to assuming no gaps between these layers during the fire), to conservatively maximize the heat input into the package.

Figure 5.6 presents a detailed view of the basket cross-section showing a typical basket fuel compartment (purple) containing a homogenized fuel assembly (light blue) surrounded by Boral sheets and their associated sheathing. Also shown in this figure are the MPC canister shell (blue-green) and

the package containment/inner shell (lime). The same features are shown in Figure 5.7 with the elements for the helium regions included.

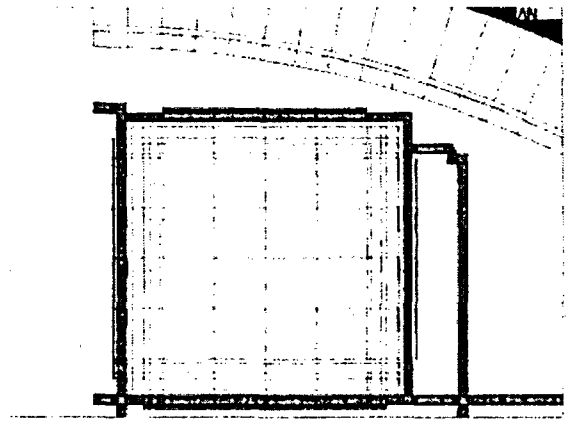

Figure 5.6. Close-up of Canister Basket Structure and Fuel Compartment Configuration (without helium elements)

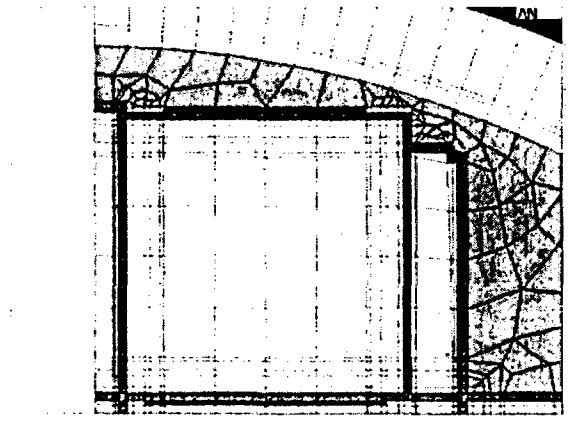

Figure 5.7. Close-up of Canister Basket Structure and Fuel Compartment Configuration (with helium elements)

Westinghouse 17x17 OFA fuel was selected for this evaluation. The effective fuel conductivity in the radial direction was determined using the approach documented in the HOLTEC SAR [10]. This approach uses a homogenization scheme similar to that presented by Bahney and Lotz [16], modified to include a helium gap between the homogenized fuel region and the fuel compartment, and the effect of cover gas pressurization.

Axial conductivity for the homogenized fuel region was modeled with the cladding as the only conduction medium, using a cross-sectional area weighting scheme. The remaining portion of the homogenized region was considered to be helium. Density and heat capacity were based on volumetric averages of the cover gas, cladding, upper and lower end fittings, and uranium oxide fuel. A normalized peaking factor of 1.1 (from the design basis axial power distribution in the SAR [10]) was used to establish the volumetric heat generation of 2,843 Btu/hr (0.833 kW) over each assembly along the active fuel length.

Orthotropic effective conductivity properties were developed for the Boral to include the radiation and conduction heat transfer components through an assumed helium gap of 0.0035 inch between the Boral sheet and its stainless sheathing, and between the Boral and stainless basket structure.

Modeling of the radiation interaction within the basket, canister, and package was accomplished by unselecting all helium regions and coating each respective interacting set of surfaces forming enclosures with SHELL57 elements with specified emissive material properties. The SHELL57 elements were then used to produce highly structured AUX-12 generated MATRIX50 super-elements, each defined by a enclosure. A total of 269 MATRIX50 superelements were defined to capture the radiation interaction within the package and canister.

Helium conduction and convection within the gas regions inside the canister were accounted for by computing effective conduction properties, assuming limited internal convection and

pressurization. The effective conductivity for these regions was established to be roughly 2.25 times the thermal conductivity of helium. Standard helium properties were used for the helium gas between the canister and the package.

Figure 5.8 shows an element plot of the top impact limiter honeycomb core and steel substructure of the HI-STAR 100 package, including the Holtite-A neutron shield material sections. (The impact limiter skin is omitted for visual clarity.) The bottom impact limiter is similar to the top impact limiter, except for the bolting configuration and the extended steel ring covering the top forging, lid, and buttress plate. Figure 5.9 shows the top impact limiter skin and support structure, without the honeycomb core and the neutron shield materials included.

The impact limiters are assembled with five different types of honeycomb sections. Gaps between the honeycomb sections, the steel substructure, and skin were conservatively ignored to maximize heat input during the fire. Thermal properties for the honeycomb sections were based on volumetric averages of each section using properties published by the honeycomb manufacturer [17].

Radiation interaction between the package ends and impact limiters was modeled by coating each respective interacting set of surfaces with SHELL57 elements with specified emissive material properties. The SHELL57 elements were then used to produce highly structured AUX-12 generated MATRIX50 superelements. A total of 16 MATRIX50 superelements were defined to capture the radiation interaction between the package and impact limiter surfaces.

Conduction and natural convection heat transfer between the package and impact limiter surfaces was handled using SURF152 surface effect elements. Correlations and specially constructed automated subroutines written in APDL were used to continuously evaluate and update the assigned convection coefficients of heat conductance.

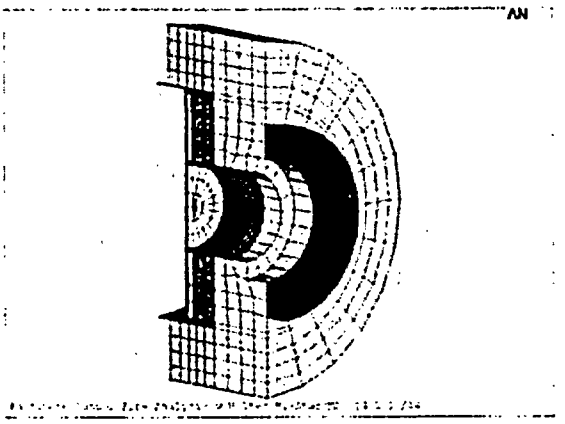

Figure 5.8. Complete Impact Limiter (Except Skin)

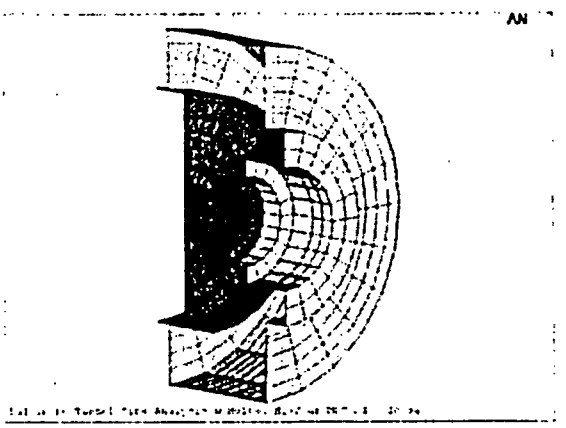

Figure 5.9. Impact Limiter Skin and Primary Support Structure

Sixteen separate passive computation nodes were assigned as "extra nodes" for the SURF152 surface effect elements used in specifying the convection interaction within the cradle and rail car section (eight for each package end.) (The natural convection correlations used are presented in Section 6.) Convection coefficients of heat conductance were conservatively boosted by a multiplicative factor of 100 between limiter and package during the fire to mimic enhanced heat conduction at this interface due to rapid thermal

expansion. These values were returned to normal after the end of the fire.

The tunnel structure for this evaluation was represented by an enclosure approximately 22 ft (6.7 m) high by 27 ft (8.2 m) wide and 42 ft (12.8 m) long. The enclosure was capped at both ends and assigned the same boundary condition on the end caps as on the walls and ceiling. As specified by dimensions of the rail car decking and cradle, the transport system was located such that the center axis was 8.2 ft (2.5 m) above the tunnel floor, leaving 12.2 inches (31 cm) underneath the lowest part of the rail car decking.

The tunnel enclosure was divided into three sections; top, side, and bottom. The floor of the enclosure was considered the bottom. The top was conservatively considered to be all surfaces (including the end caps) in the range from 15.8 to 22 ft (4.8 to 6.7 m). All surfaces from the floor to 15.8 ft (4.8 m) were considered to be the side region. These divisions are shown in Figure 5.10.

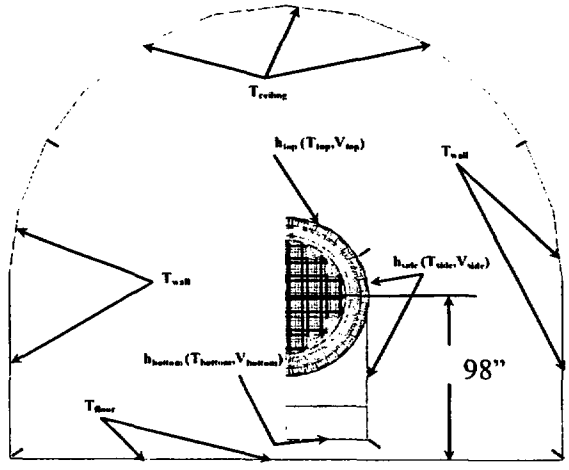

Figure 5.10. Boundary Sections for Tunnel and Package Model

The selected boundary temperatures for each section were the maximum in that region (top, side, and bottom, corresponding to ceiling, wall, and floor in the FDS simulation from NIST; see Section 6.)

To determine the convection heat transfer to the package during the fire scenario, the exposed surfaces of the package were also divided into three section. The top section was defined as all surfaces above 9.4 ft (2.9 m). The bottom section was defined as the bottom of the rail car segment of the model. The side surfaces of the package were conservatively defined to be all remaining outer surfaces of the package. The surface elements of these sections are pictured in Figures 5.11 through 5.13.

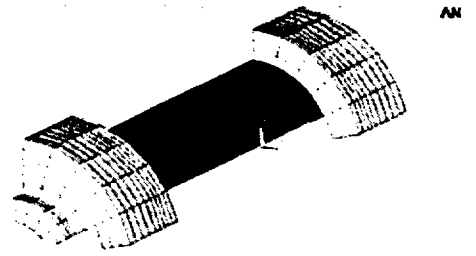

Figure 5.11. Surfaces Defined for Interaction with "Top" Gas Region

The bottom surface of the rail car section was the only surface influenced by convection heat transfer in the bottom gas region. In actuality, none of the "top" surfaces would be directly exposed to the highest temperature gas region at the top of the tunnel, because the package is not positioned that high in the tunnel. This assumption therefore represents an additional conservatism in the analysis.

Forced and natural convection correlations and specially constructed automated subroutines written in APDL were used to continuously evaluate and update the assigned convective

coefficients of heat conductance for the surface of the package during pre-fire, fire, and post-fire phases based on gas velocity.

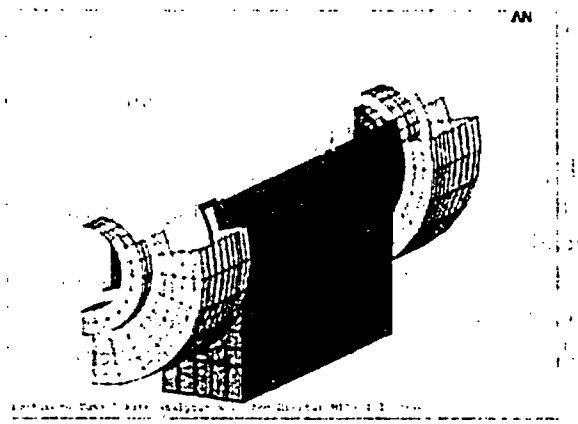

Figure 5.12. Surfaces Defined for Interaction with "Side" Gas Region

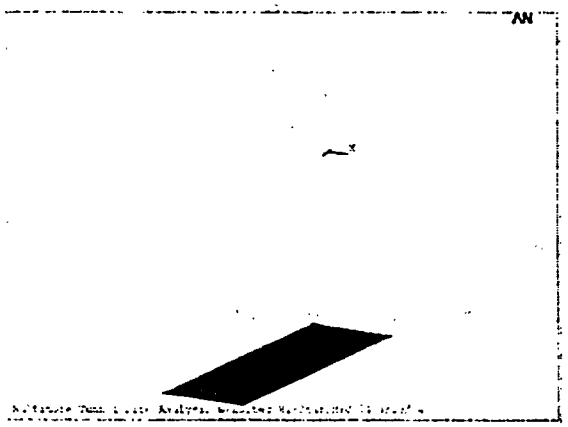

Figure 5.13. Surfaces Defined for Interaction with "Bottom" Gas Region

Radiation interaction between the transport system and its partial conveyance and the tunnel was established by coating all respective interacting surfaces with SHELL57 elements with specified emissive material properties. The SHELL57 elements were then used to produce a highly structured AUX-12 generated MATRIX50 superelement.

The Baltimore tunnel fire evaluation of the HI-STAR 100 was conducted in three phases. These were the pre-fire, fire, and post-fire phases. For the pre-fire phase, the hot-normal conditions of transport were evaluated assuming solar insolation and a 100°F (38°C) ambient temperature, in accordance with 10CFR71.71 [1]. This conservatively established initial component temperatures. During this phase, the fillet welds joining the fins to the gamma shield were specified with their realistically reduced conduction and conservative gas gaps were assumed between the layers of the gamma shield.

For the fire phase of the evaluation ($0 \leq t \leq 7$ hr), solar insolation was shut off, the tunnel surfaces were introduced, and the transport package and tunnel surfaces were assigned an emissivity of 0.9 to represent surfaces affected by sooting. Air gaps originally assumed to be present between the gamma shield plates were removed, and good conduction contact was assumed to exist where the heat fins attach to the gamma shield. Convection coefficients of heat conductance were conservatively multiplied by a factor of 100 between the impact limiters and package body to mimic enhanced heat conduction due to rapid thermal expansion. In addition to these conservative measures, to maximize heat input during the fire, all aluminum honeycomb and neutron shield resin materials were assumed to remain intact during the full duration of the fire.

For the post-fire phase of the evaluation ($t > 7$ hr), aluminum honeycomb sections exceeding an average temperature of 1220°F (660°C) and all neutron shield material sections were degraded to thermal properties identical to that of air. Conservatively, the energy that would be absorbed due to phase change in this material was not subtracted from the heat input to the package. In addition, all gamma shield gaps and reduced fin fillet weld conduction properties were reintroduced. Finally, convection coefficients of heat

conductance between the impact limiters and package body were returned to normal for the remainder of the simulation.

The material properties from the package vendor's SAR [10]were verified and then used in the analyses. The material properties used in this evaluation are listed in Appendix B.

5.3 Model of NAC LWT Transportation Package

The model for the NAC LWT package constructed in ANSYS is similar in structure to the HI-STAR 100 model described in Section 5.2. A detailed three-dimensional model of a half-section of symmetry was developed for the package and ISO container, within the same tunnel geometry. A diagram of the package and shipping container model and partial tunnel is shown in Figure 5.14.

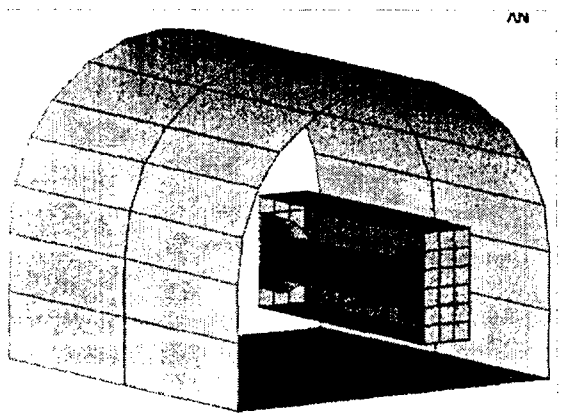

Figure 5.14. ANSYS NAC LWT Package Analysis Model Element Plot

The model used 40,333 SOLID70 8-node brick elements and 3,409 SHELL57 4-node quadrilateral thermal elements to represent the structural components. A total of 6,931 SURF152 elements were used to incorporate radiation and convection heat transfer to the ISO container and tunnel environment for the various surfaces, and 12 MATRIX50 elements were used to model radiation heat exchange between package surfaces. The surface effect elements were also used to generate solar insolation loads for calculation of the initial temperature distribution for the package.

The model geometry was developed from the vendor's engineering drawings from the package SAR [11]. The model cross-section is shown in Figure 5.15. The package contains a cylindrical solid aluminum basket that holds a single fuel assembly. The helium gaps between the fuel and the basket, and between the basket and package shell, were explicitly modeled with solid elements.

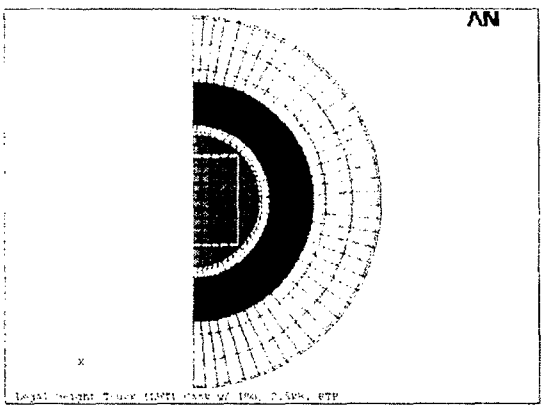

Figure 5.15. Cross-section of NAC LWT Package

The package body is constructed of several stainless steel shells to provide structural support and gamma shielding. The innermost shell is surrounded by a layer of lead that acts as a gamma shield. The outermost stainless steel shell is surrounded by an annular tank containing a solution of ethylene glycol and water which acts as a neutron shield. The tank is contained by an outer stainless steel skin and an annular overflow tank that extends approximately one-third of the axial length of the package body. All of these components were modeled using brick elements.

The tank is constructed with eight stainless steel support ribs (in the half section) connecting the skin to the outer shell. These structures were modeled with shell elements. The package bottom is constructed with a stainless steel base, a layer of lead shielding, and a steel cover. The upper end of the package is sealed with a stainless steel lid (see Figure 5.16). Impact limiters attached to the ends of the package consist of an internal aluminum honeycomb structure covered by an aluminum skin. The expansion tank to handle overflow of the liquid neutron shield consists of an outer stainless steel skin.

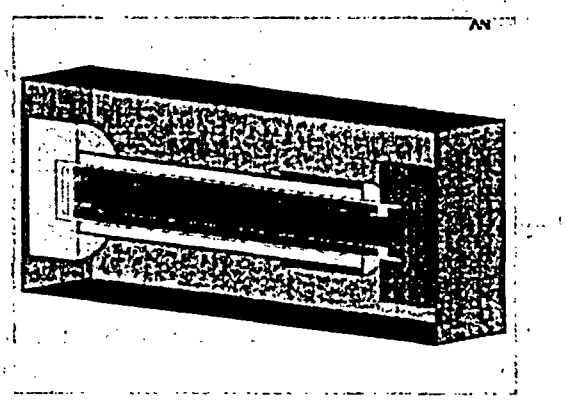

Figure 5.16. NAC LWT Package Geometry

The entire package is contained in an ISO container constructed of stainless steel plate. This is based on the assumption that an ISO container would be required if the NAC LWT were shipped by rail. (The consequences of this hypothetical accident scenario on a package shipped without an ISO container are discussed with the results of this analysis in Section 7.3.) The package and container model is oriented horizontally in the tunnel with the center of the ISO container is 97.7 inches (248 cm) above the tunnel floor.

Heat exchange via conduction, convection, and radiation was carefully modeled between all of the components to provide a sound estimate of package temperatures during the transient fire event. Conduction is handled inherently by the elements modeling each component, but convective and radiation mechanisms must be carefully implemented.

Westinghouse 17x17 OFA fuel was used in this evaluation. The fuel assembly was modeled with an effective conductivity determined using a homogenization scheme similar to that presented by Bahney and Lotz [16], modified to include a helium gap between the homogenized fuel region and the fuel basket. This yields a more realistic representation of the temperature profile through the assembly, and takes into account the effect of the non-uniform wall temperature distribution around the assembly.

Axial conduction in the homogeneous fuel region was conservatively neglected in the fuel itself, and was modeled only in the cladding, using the conductivity of Zircaloy modified by a weighting scheme based on the cross-sectional area. The effective density and heat capacity for the fuel region was based on volumetric averages of the properties of the helium cover gas, fuel rod cladding, and uranium oxide fuel pellets. The design basis axial power profile from the SAR [11], which has a normalized peaking factor of 1.2, was used to establish the volumetric heat generation of 8,532 Btu/hr (2.5 kW) over the assembly along the active fuel length.

The 0.225-inch (0.57-cm) gap filled with helium cover gas between the fuel and the basket was modeled with solid elements and used standard helium thermal properties for conduction and specific heat. Convection was ignored in this small gap. Radiation exchange between the adjacent surfaces was modeled using MATRIX50 superelements. These were created by using SHELL57 to designate the discrete enclosure, and the AUX-12 hidden ray-tracing method was used to compute view factors for each element in the superelement. The 0.25-inch (0.64-cm) gap between the basket and the inner shell was

modeled in the same manner, also assuming negligible convection.

The entire package model was enclosed within elements modeling the ISO container. For the large air volumes in the ISO container, conduction across the gaseous medium is negligible but significant convection currents will be created by the buoyant forces due to the heated surfaces. Surfaces with unobstructed views of other surfaces will also experience significant radiation exchange that is highly dependent on the surface geometry. Therefore, heat exchange between the package exterior and the container interior was modeled with internal free convection and radiation between adjacent surfaces.

The radiation was implemented using the MATRIX50 superelement procedure described in Section 5.2 for the Holtec HI-STAR 100 model. The convection calculations were based on empirical relations for free convection over flat plates and cylinders (see Section 6). Convection was implemented using SURF152 elements. These elements are placed on the exterior surface of a body and communicate with the designated sink temperature assigned to a single node (called the "space node") to compute the heat flux.

Because convection heat transfer rates are expected to vary in different regions throughout the ISO container, the single volume was divided into 17 zones. These consisted of a zone on each end of the package, three zones representing the top, side, and bottom radial surfaces for each impact limiter, and similar zones for the package for three locations along its axial length (see Figure 5.17.)

A sink temperature was defined for each zone, computed as the average surface temperature of the participating package and container elements for that zone. The convective heat transfer coefficient was assigned to the package and container elements based on the temperature difference between the surface and sink temperature, and the surface geometry, as described in Section 6. The heat exchange between these surfaces and the space node was then computed by ANSYS during the solution.

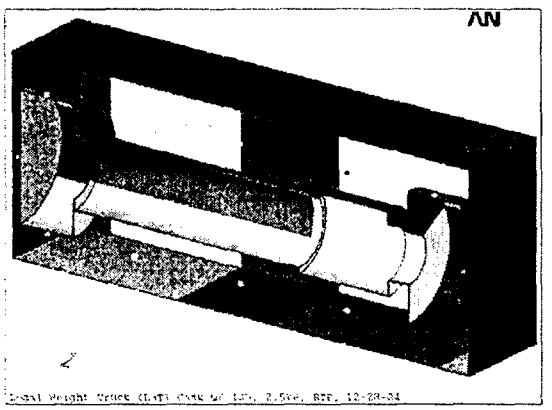

Figure 5.17. Zones for Convection Heat Transfer Within the ISO Container

Convection and radiation are also the two mechanisms required to model thermal exchange from the exterior of the ISO container. In the fire analysis, the initial temperature distribution is obtained from a steady-state solution with conditions specified by 10CFR71.71 [1], followed by a transient solution representative of the fire. For the steady-state solution, convection is handled by SURF152 elements with a constant convection coefficient of 0.891 Btu/hr-ft^2-°F (5.06 W/m^2-°K) and an ambient temperature of 100°F (38°C). Solar insolation is incorporated by using SURF152 elements with heat generation on the outer surface at the rate specified in 10CFR71 [1].

During the fire, the sink node temperature for the SURF152 elements is set and the external convection coefficient is computed using a forced convection relation derived using the gas temperatures and velocities from the results of the NIST fire simulation using FDS. These results were obtained for the top, side, and bottom of the

tunnel, and applied to three zones defined on the top, sides, and bottom of the ISO container, as illustrated in Figure 5.18. By the end of the transient simulation using FDS (i.e., 30 hours), the predicted gas velocities have dropped to the point that free convection is the only significant mode of convection heat transfer. From this point in the transient, the convection coefficient is computed in the same manner as described for the steady-state initial conditions.

Thermal radiation between the container and the tunnel during and after the fire is incorporated by the MATRIX50 elements, as described previously, where the top, side, and bottom temperatures of the tunnel from the NIST fire simulation are imposed as boundary conditions. A conservative emissivity value of 0.9 was used for the tunnel surfaces and ISO container exterior, to account for the effect of sooting.

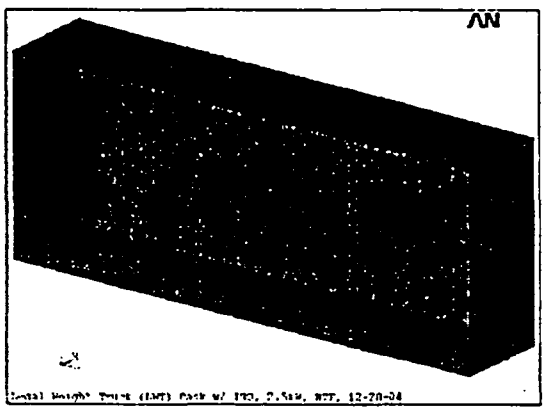

Figure 5.18. Zones for External Radiation Between ISO Container and Tunnel Surfaces

The material thermal properties used in the model are listed in Appendix C, and were obtained primarily from the vendor's SAR [11]. Some modifications were made to the material properties to account for structural configuration and expected effects of the fire. For the aluminum honeycomb material, the significant void volume reduces the heat transfer capability compared to solid material. The thermal conductivity assigned to the impact limiters was scaled by the ratio of the honeycomb density to the solid aluminum density.

Modeling of the liquid neutron shield was complicated by the expectation that the 56% ethylene glycol liquid will exceed its boiling point during a fire transient, leading to tank rupture and vaporization of the contents, which significantly affects the heat transfer of the package. Prior to rupture, the liquid in the tank is expected to sustain convective currents due to temperature gradients through the liquid between the tank surfaces. After rupture, empirical relations were used to obtain separate effective conductivities for the shield tank and expansion tank.

The empirical relations were based on correlations by Raithby and Hollands [18], as described in Section 6. The effective conductivity was then determined as a function of the average tank temperature and the radial temperature difference between the tank inner and outer surfaces. The material properties were updated between each time step during the transient solution using APDL. They were computed for 56% ethylene glycol solution up to the point where the average temperature reached its boiling point of 350°F (177°C).

When the average temperature in the tank exceeded the boiling point, it was assumed that rupture occurred and the liquid was immediately vaporized. Subsequently, the effective conductivity was computed using dry air as the medium. This calculation was continued during the cool down period also. This formulation conservatively neglects energy absorbed by the phase change (i.e., the heat of vaporization for the liquid), although this is mainly as a matter of convenience, since this would constitute a very small deduction from the total energy imparted to the package.

The general solution procedure for this model was similar to that for the HI-STAR 100 described previously. The steady-state temperature solution for normal hot conditions was computed using solar insolation and 100°F (38°C) ambient temperature per 10CFR71.71 [1], and used as the initial temperature state. The insolation was removed and the tunnel was introduced for the transient fire analysis. The transient solution was then obtained for the 30 hours of the NIST simulation, representing the 7-hour fire and 23-hour cool down. The solution was also extended for a total simulation time of 300 hours, in the same fashion as described in Sections 5.1 and 5.2 for the other two package models.

6 ANALYSIS METHOD

The National Institute of Standards and Technology (NIST) performed analyses using the FDS code, based on the type of fire that could have been sustained during the accident in the Howard Street tunnel and the time required to consume the available fuel. The results were used to define boundary conditions for COBRA-SFS and ANSYS evaluations of the thermal response of the selected spent fuel transportation packages. Section 6.1 lists the conservative assumptions underlying the analytical approach used and describes the boundary conditions in detail. This includes temperature boundary conditions and the approach used to define convection and radiation heat transfer rates. Section 6.2 describes the initial steady-state conditions for each cask package. Section 6.3 describes the procedure used for the transient calculations.

6.1 Fire Transient Assumptions and Boundary Conditions

A number of conservative assumptions were made in developing models and performing evaluations of the thermal response of the three spent fuel transport packages (TN-68, HI-STAR 100, and NAC LWT) to the Baltimore tunnel fire transient. The assumptions of greatest impact are listed below.

1) Boundary conditions were taken from predictions of peak gas temperatures in the lower, middle, and upper zones of the tunnel and peak surface temperatures on the tunnel floor, walls, and ceiling. The peak values in each region were used to define boundary temperatures over the entire region, rather than using the local temperature distributions predicted in the FDS calculation. This approach ensures a conservative estimate of the boundary temperatures, since the package does not see the peak temperatures on all surfaces, and in some cases may not see the peak temperature on any surface. (For example, the top of the package is not high enough to be directly exposed to the peak gas temperature at the top of the tunnel, but this value was used as the ambient temperature for convective heat transfer to the upper surface of the package.)

2) The package cradle and the rail car section beneath the cradle were included in the ANSYS model of the HI-STAR 100, but the rail car ends and honeycomb end blocks adjacent to the impact limiters were omitted. These structures were neglected because they would partially shield the package from thermal radiation from the hot tunnel surfaces and block convection heat transfer to the package due to the flow of hot gas generated by the fire. The rail car was omitted from the COBRA-SFS model of the TN-68 cask and the ANSYS model of the NAC LWT cask within the ISO container. This approach eliminated any potential shielding of these packages from thermal radiation and convective heat transfer from the tunnel environment.

3) During the fire and the short-term post-fire cool down period (7 hr $< t <$ 30 hr), it was assumed that convection heat transfer at the package surface was due to forced convection only (due to air flow induced in the tunnel by the temperature gradients of the fire), using the gas velocities predicted in the NIST analysis. This approach neglects the possible contribution of free convection around the package (due to non-uniform circumferential temperatures around the package outer shell), which would tend to remove heat from the package. The boundary condition was switched to solely free

convection after 30 hours, in the extrapolated portion of the transient. This conservatively neglects any forced convection cooling of the package during the extended cool down period, when the gas velocities in the tunnel are predicted to have dropped to negligible values.

4) The effects of optical densification due to combustion products and material degradation, which would tend to attenuate the radiation influence between the tunnel and package surfaces, were not taken into account in the boundary conditions defining the fire. Radiation views were treated as clear and unobscured at all times. Radiation attenuation was also neglected between the ISO container inner surfaces and the NAC LWT package.

5) Materials that could be expected to burn, boil off or melt during the transient were assumed to remain intact during the fire, to maximize the heat input into the package. At the end of the fire, the thermal conductivity values for these materials were reduced to that of air. As a result, the affected components then present an added thermal barrier to heat removal from the package following the fire. In addition, the energy absorbed by these materials, due to latent heat of diffusion or vaporization, was not subtracted from the energy input to the package from the fire.

6) The cask package was assumed to be the shortest possible distance away from the center of the fire, in order to obtain the highest possible boundary temperatures due to the fire. Based on Department of Transportation regulations [12] that require railcars carrying radioactive materials to be separated by at least one railcar (a buffer car) from other cars carrying hazardous materials or flammable liquids, this distance must be at least 66 ft (20 m).

Given these assumptions, the ANSYS and COBRA-SFS analyses constitute conservative evaluations of the response of the spent fuel transportation packages. The FDS simulations for the NIST model of the Howard Street tunnel fire produced detailed predictions of gas flow rates, gas temperatures, and tunnel wall, ceiling, and floor temperatures during the 7-hour fire and 23-hour post-fire cool down.

6.1.1 Boundary Temperatures from FDS

The FDS simulations included a significant portion of the tunnel length, from the fire location to the tunnel entrance. The results obtained for the radial plane of the model at the location 66 ft (20 m) from the center of the fire were used to determine the boundary conditions for the analyses with COBRA-SFS and ANSYS. As a conservative simplification of the finely detailed noding in the FDS simulation, the tunnel radial geometry was divided into three regions; top, side, and bottom (refer to the diagram in Figure 5.10.) Within each of these regions, the predicted peak wall temperatures and peak gas temperatures as a function of time (with the associated gas velocities) were taken as representative of the transient behavior of the entire region, rather than following the local gradients obtained in the detailed NIST simulation with FDS.

These temperature-vs.-time and velocity-vs.-time values were smoothed to conservatively remove the rapid stochastic variations typical of dynamic fire behavior, preserving only the major peaks and troughs related to the general physical behavior of the simulated fire. Figure 6.1 shows these smoothed peak air temperatures for the top, sides and bottom regions in the tunnel at 66 ft (20 m) from the fire center. The smoothed peak surface temperatures for the walls, floor and ceiling of the tunnel at this location for the same fire scenario are shown in Figure 6.2. Figure 6.3 shows the smoothed velocities predicted in the NIST

analyses at the locations of the peak gas temperatures in Figure 6.1.

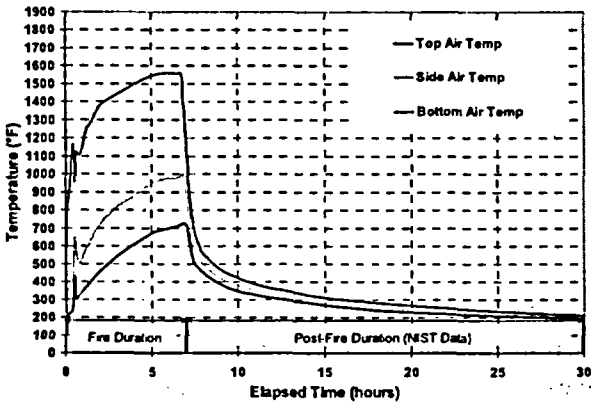

Figure 6.1. BTF Peak Transient Ambient Air Temperatures (smoothed values, NIST 20-m data)

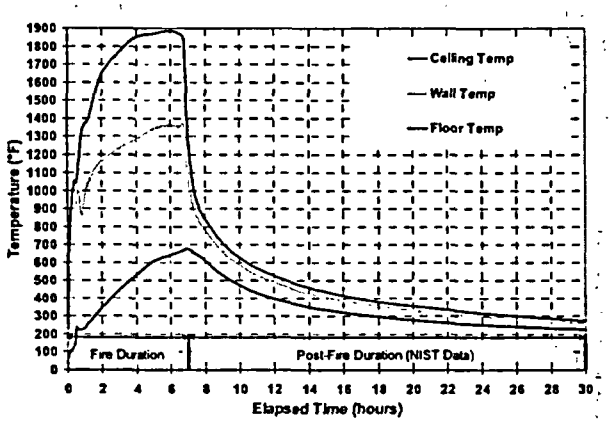

Figure 6.2. BTF Peak Transient Tunnel Surface Temperatures for Floor, Walls, and Ceiling (smoothed values, NIST 20-m data)

The NIST fire simulation results shown in Figures 6.1 through 6.3 were used to develop the boundary conditions applied to the TN-68, HI-STAR 100, and LWT models. The peak surface temperatures in Figure 6.2 were applied to all corresponding tunnel surfaces in the top, side, and bottom regions of the ANSYS models for the HI-STAR 100 and LWT packages. These temperature values defined the boundary conditions for radiation heat transfer between the tunnel walls and the exposed surfaces of the cask package.

The COBRA-SFS model for the TN-68 package incorporated the effect of the tunnel walls, ceiling and floor by calculating a radiation heat flux at the package surface using the local package surface temperature and the regional tunnel surface temperatures defined in Figure 6.2. Blackbody view factors between the package surface and the tunnel ceiling, walls and floor were determined using a conventional ray-tracing scheme. (The radiation exchange values for this geometry are listed in Appendix D.)

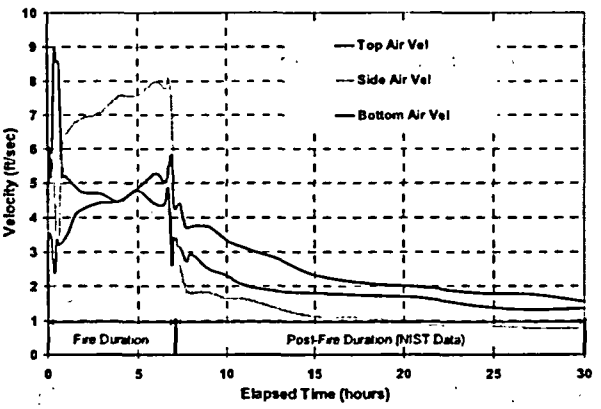

Figure 6.3. BTF Peak Transient Horizontal Velocities near Package Surface (smoothed values, NIST 20-m data)

6.1.2 Convection and Radiative Heat Transfer Boundary Conditions

The NIST analyses showed that the thermal gradients created in the tunnel due to the fire would result in significant air flow past a body located near the fire. This fire-forced convection would significantly affect heat transfer around the package and could have a strong influence on the package outer shell surface temperatures. The smoothed air temperatures in Figure 6.1 and velocities in Figure 6.3 were used to define local

time-dependent Nusselt number values at the top, sides and bottom of the package. These values were used to define the local surface heat transfer coefficient for the three computational models.

To maintain consistency between the three models, the same Nusselt number correlation was used to define convection heat transfer at the package surface. The selected correlation gives the Nusselt number for gas flow over a flat or slightly curved surface at zero angle of attack [19], and has the form

for laminar flow ($Re_L < 500{,}000$)

$$Nu_L = 0.665\, Re_L^{1/2}\, Pr^{1/3}$$

for turbulent flow ($Re_L > 500{,}000$)

$$Nu_L = 0.032\, Re_L^{0.8}\, Pr^{1/3}$$

The characteristic length, L, used to define the Nusselt number and Reynolds number for this application is the package body horizontal length. In the COBRA-SFS modeling of the TN-68, the characteristic length was specified as 160 inches, based on the length of exposed package body. In the ANSYS model of the HI-STAR 100, the characteristic length of 173 inches was used, based on the length of exposed package body. For the NAC LWT, a value of 240 inches was used, based on the ISO container wetted surface length.

The peak air temperatures (see Figure 6.2) from the NIST analysis define the ambient sink temperature around the package during the fire and post-fire intervals. The Nusselt number defines the rate of heat transfer from the package surface, which allows both codes (COBRA-SFS and ANSYS) to calculate the convection heat flux at the package surface. Using the above relationship, local surface temperatures, T_s, are calculated, and the convection component of the heat flux at the surface is solved for using the formula

$$q''_{conv} = Nu_L \frac{k}{L}(T_s - T_{air})$$

where k = thermal conductivity of ambient air
L = characteristic length
T_s = package surface temperature
T_{air} = ambient external air temperature.

Separate boundary types were defined for the top, sides, and bottom surfaces of the package using the external air temperatures shown in Figure 6.1. The velocities in Figure 6.3 were used to define the Reynolds number so the boundary conditions on the package could change with time as the transient proceeded. Figure 6.4 shows the resulting local heat transfer coefficients calculated for the COBRA-SFS evaluation during the 30 hours of the NIST transient calculation, at the top, sides and bottom of the TN-68 package.

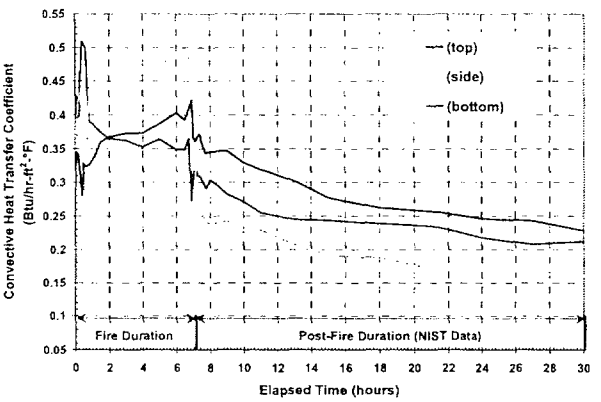

Figure 6.4. Heat Transfer Coefficients at Package Surface from NIST 20 m Air Temperature and Velocity Predictions

In addition to convection heat transfer between the transport package and the surrounding air during the transient, radiation heat transfer between the package surface and the tunnel ceiling, walls, and floor was also captured. Boundary conditions to

define radiation heat transfer between the package surface and the tunnel ceiling, walls, and floor were included in the COBRA-SFS model in the following fashion. The total heat flux at the surface of the package is the sum of the two components:

$$q'' = q''_{conv} + q''_{rad}$$

The tunnel surface temperature profiles shown in Figure 6.2 were used to define the radiation heat flux as an additional boundary condition at the package surface using the relationship

$$q''_{rad} = \varepsilon_i B_{ij} \sigma_{SB} \left(T^4_{package} - T^4_{surf} \right)$$

where ε_i = emissivity of surface i
B_{ij} = blackbody viewfactor from surface i to j
σ_{SB} = Stefan-Boltzmann constant
T_{surf} = tunnel ceiling, wall or floor surface temperature
$T_{package}$ = package surface temperature.

The blackbody view factors between the package surface and the tunnel ceiling, walls, and floor were determined using a Monte Carlo ray tracing scheme based on the package diameter and a uniform axial node length along the length of the package. These are presented in Appendix D.

Radiation interaction between the tunnel surfaces and the package surfaces in the HI-STAR 100 model (and the ISO container surfaces in the NAC LWT system) was established through the use of ANSYS superelement definitions, as described in Section 5 above. The NIST tunnel surface temperature predictions (see Figure 6.2) were then used to establish the tunnel surface boundary condition temperatures. The emissivity of all tunnel surfaces and the package surface was assumed to be 0.9 for all evaluations during the fire and post-fire transient.

6.1.3 Extrapolated Boundary Conditions for Long-Term Cool Down

NIST's FDS analysis was carried out for a 7-hour fire and 23-hour post-fire cool-down. To determine the long-term temperature responses and explore the effects of prolonged exposure to post-fire conditions in the tunnel, the post-fire duration was extended to 300 hours (273 hours after fire cessation). Temperatures predicted in the NIST analysis for 30 hours were extrapolated from 30 hours to 300 hours using a power function to realistically model cool-down of the tunnel environment. The extrapolated predictions are presented in Figures 6.5 and 6.6 for the air temperatures and wall temperatures, respectively.

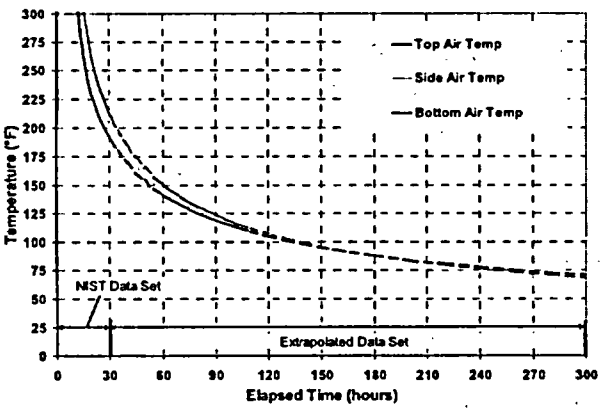

Figure 6.5. BTF Peak Transient Air Temperatures for Top, Side, and Bottom Regions (NIST and Extrapolated Data Sets)

About 20 hours into the transient, the velocities predicted in the NIST calculations have dropped to values of 1 to 2 ft/s (0.3 to 0.6 m/s) or less (refer to Figure 6.3). Heat transfer at the package surface for these flow conditions is a complex mixture of forced convection (due to air flow induced in the tunnel by the wall temperature gradients of the fire) and free convection (driven by the non-uniform circumferential temperatures of the package outer shell). At velocities below about 3

to 5 ft/s (1 to 1.5 m/s), heat transfer rates predicted assuming forced convection are generally lower than the heat transfer rates due to natural convection around the package body for these temperature conditions.

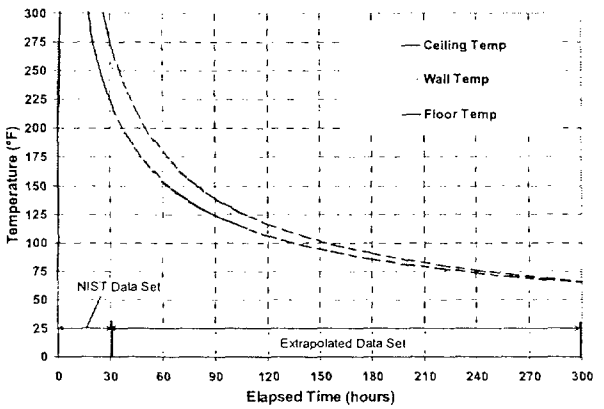

Figure 6.6. BTF Peak Transient Surface Temperatures for Floor, Walls, and Ceiling (NIST and Extrapolated Data Sets)

To avoid the modeling uncertainties associated with mixed-mode heat transfer, forced convection only was assumed until the end of the NIST simulation, at 30 hours into the transient. From 30 hours to 300 hours, the heat transfer was assumed to be natural convection only. This ensured a conservative treatment of convection heat transfer from the package surface during the entire calculation, since free convection to surface heat transfer from the package is ignored in the cool down from 7 to 30 hours, and forced convection is neglected in the period from 30 to 300 hours.

For consistency, the natural or buoyant convection coefficients were those utilized for determining the pre-fire component temperature distributions (i.e., Hot-normal Conditions of Transport, as defined in 10 CFR 71.71(c)(1)([1].) The heat transfer coefficients were defined for the appropriate surface geometries using the following relationships [20]:

--for flow along a vertical plane or cylinder :

--laminar flow ($10^4 < Gr_f \cdot Pr_f < 10^9$)

$$h = 1.42\left(\frac{\Delta T}{L}\right)^{1/4}$$

--turbulent flow ($Gr_f \cdot Pr_f > 10^9$)

$$h = 1.31(\Delta T)^{1/3}$$

where

h = heat transfer coefficient, $W/(m - °C)$

$\Delta T = T_w - T_\infty$, $°C$

T_w = surface or wall temperature, $°C$

T_∞ = ambient temperature, $°C$

L = vertical or horizontal dimension, m

Gr_f = Grashoff number of the gas at film temperature, $T_f = (T_w + T_\infty)/2$

Pr_f = Prandtl number of the gas at film temperature, $T_f = (T_w + T_\infty)/2$

--for flow over a horizontal cylinder:

--laminar flow ($10^4 < Gr_f \cdot Pr_f < 10^9$),

$$h = 1.32\left(\frac{\Delta T}{d}\right)^{1/4}$$

where

d = diameter, m

--turbulent flow ($Gr_f \cdot Pr_f > 10^9$),

$$h = 1.24(\Delta T)^{1/3}$$

--for flow over a horizontal heated plate facing upward (cool side facing downward):

-- laminar flow ($10^4 < Gr_f \cdot Pr_f < 10^9$),

$$h = 1.32\left(\frac{\Delta T}{L}\right)^{1/4}$$

-- turbulent flow ($Gr_f \cdot Pr_f > 10^9$),

$$h = 1.52(\Delta T)^{1/3}$$

--for laminar flow ($10^4 < Gr_f \cdot Pr_f < 10^9$) over a heated plate facing downward (cool side facing upward):

$$h = 0.59\left(\frac{\Delta T}{L}\right)^{1/4}$$

Definitions of material properties for use with these correlations were taken from Table A-3 of Kreith [21].

6.1.4 Heat Transfer through Liquid Neutron Shield

An empirical relationship for effective conductivity incorporating the effects of both conduction and convection was used to determine heat exchange through the liquid neutron shield. In the SAR analysis for the LWT package [11], the effective conductivity of the ethylene glycol mixture for conditions below 350°F was determined using the correlation of Bucholz [22], which defines the ratio of the effective conductivity to the actual thermal conductivity as equal to the Nusselt number, such that

$$\frac{k_{eff}}{k_c} = Nu = 0.135(Pr^2\, Gr/(1.36 + Pr))^{0.278}$$

where k_{eff} = effective thermal conductivity of material in node
k_c = thermal conductivity of motionless fluid in node
Nu = Nusselt number
Pr = Prandtl number
Gr = Grashoff number

The BTF transient is outside the range of the Bucholz correlation, and it yields unrealistically large values for k_{eff} for these conditions. An alternative correlation from Raithby and Hollands [18], based on heat transfer between two concentric cylinders, was used in this analysis instead. This correlation produces reasonable values of k_{eff}, and the transient conditions are generally within its applicable range.

The form of this correlation is similar to the Bucholz correlation in that it equates the Nusselt number to the ratio of the effective conductivity over the actual conductivity, but in the Raithby and Hollands formulation, the Nusselt number is expressed as

$$\frac{k_{eff}}{k_c} = Nu = 0.386 D_r (Pr/(0.861 + Pr))^{0.25} Ra^{0.25}$$

where Ra = Rayleigh number (Ra = Pr*Gr)
Pr = Prandtl number
Gr = Grashoff number (based on the temperature difference across the annular gap)

The variable D_r is a dimensionless parameter based on the geometry of the annulus, and is defined:

$$D_r = \left[\frac{\ln(D_o/D_i)}{d^{3/4}(1/D_i^{3/5} + 1/D_o^{3/5})^{5/4}}\right]$$

where D_o = annulus outer diameter
D_i = annulus inner diameter
d = width of annulus.

Figure 6.7 shows a plot of the Nusselt number predicted with these two correlations for the liquid (56% ethylene glycol and water mixture) in the neutron shield annulus.

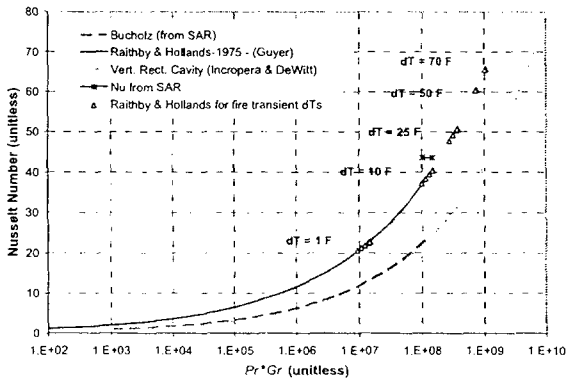

Figure 6.7. Nusselt Number for Heat Transfer in Liquid Neutron Shield

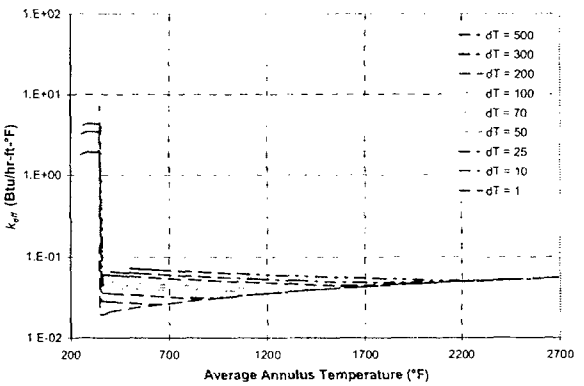

Figure 6.9. Effective Conductivity of Expansion Tank Contents

Figures 6.8 and 6.9 show the effective conductivity for the annulus as a function of the average temperature and temperature difference for the liquid neutron shield tank and expansion tank, respectively. (The sharp discontinuity in the

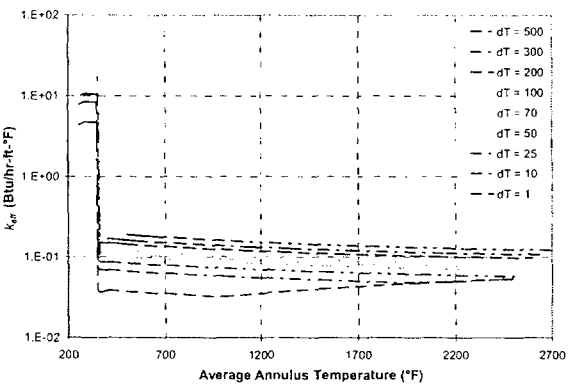

Figure 6.8. Effective Conductivity of Neutron Shield Tank Contents

curves on both plots represents the abrupt phase change assumed when the average temperature of the liquid reaches the boiling point of the ethylene glycol and water mixture.) For low values of the temperature difference, the results approach those for the conduction-only case.

6.2 Initial System Component Temperatures

The normal conditions of transport described in 10 CFR 71.71 [1] were used as initial conditions for each analysis. All three packages were subjected to an ambient temperature of 100°F (38°C), with solar insolation. For pre-fire conditions, the package surface was given an emissivity value representative of its surface finish (e.g., 0.3 for bare stainless steel, 0.85 for painted surfaces.) In the ANSYS models for the HI-STAR 100 and NAC LWT systems, thermal radiation heat transfer to ambient was modeled using surface effect elements (SURF152).

Convection from the surface of each package was modeled with a similar set of surface effect elements. The natural convection correlations for buoyancy driven flow discussed above were used to simulate convection heat transfer at the package surface. For the COBRA-SFS model of the TN-68 package, the surface boundary conditions also included natural convection and thermal radiation.

Heat generation rates for decay heat loads of 68,240 Btu/hr (20kW) for the HOLTEC HI-STAR 100, 8,530 Btu/hr (2.5kW) for the NAC LWT, and 72,334 Btu/hr (21.2kW) for the TN-68, were

applied, with appropriate peaking factors, over the active fuel region.

A steady state normal condition temperature distribution for each package was obtained to establish pre-fire conditions. The hot-normal condition temperatures for each package were verified against the results reported in the relevant SAR. Normal condition temperatures from the ANSYS solution for the HI-STAR 100 are provided in Figure 6.10. (Appendix E contains additional plots showing the detailed temperature distributions for these conditions predicted for the HI-STAR 100.) The peak clad temperature predicted with ANSYS for the HI-STAR 100 is 673°F (356°C), compared to 701°F (372°C) reported in the SAR[10].

Since COBRA-SFS does not have a graphical post-processing module, it is not possible to produce similar color-flooded thermographs for the TN-68 evaluation. However, the analysis results are similarly in very good agreement with the corresponding SAR values. The COBRA-SFS calculations predicted a peak clad temperature of 485°F (252°C) in the TN-68 package, compared to 490°F (254°C) reported in the TN-68 SAR [9].

Component temperature comparisons of results determined in this study and those published in the applicant's SAR documentation are presented in Table 6.1 for the TN-68 analysis with COBRA-SFS and Table 6.2 for the HI-STAR 100 analysis with ANSYS. These tables show that the analytical results obtained for the TN-68 and HI-STAR 100 are in very good agreement with the results presented for the corresponding cases in the respective SARs. Minor differences between the SAR results and those obtained in the current study are due to differences in modeling detail and simplifying assumptions employed in the SAR models. For example, the SAR analysis of the HI-STAR 100 neglects the effect of the support cradle on component temperatures in the evaluation for the hot-normal conditions of transport.

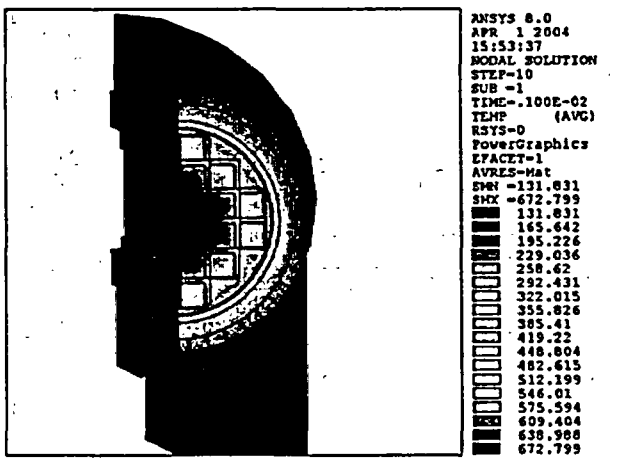

Figure 6.10. HI-STAR 100 Package Hot-Normal Condition Temperature Distribution

For the TN-68 model and the HI-STAR 100 model, the results presented in Tables 6.1 and 6.2 are representative of the initial conditions for the fire transient analysis. For the NAC LWT, convection from the surface of the ISO container was modeled with a similar set of surface effect elements. The natural convection correlations for buoyancy-driven flow discussed above were used to simulate the convective heat transfer within and at the ISO container surface.

Table 6.1. TN-68 Hot-Normal Component Temperatures

Component	Current Study (COBRA-SFS) °F (°C)	SAR Values °F (°C) (Table 3-1 [9])
Fuel Cladding	485 (252)	490 (254)
Basket plate	467 (242)	469 (243)
Basket Rail	332 (167)	319 (159)
Inner Shell	292 (144)	262 (128)
Gamma Shell	285 (141)	260 (127)
Package Bottom	261 (127)	254 (123)
Seals	260 (127)	234 (112)
Radial Neutron	256 (124)	244 (118)
Outer Shell	243 (117)	204 (96)

Table 6.2. HOLTEC HI-STAR 100 Hot-Normal Component Temperatures

Component	Current Study (ANSYS) °F (°C)	SAR Values °F (°C) (Table 3.4.10 [10])
Fuel Cladding	673 (356)	701 (372)
MPC Basket Centerline	667 (353)	667 (353)
MPC Basket Periphery	432 (222)	430 (221)
MPC Outer Shell	345 (174)	315 (157)
MPC/Overpack Helium Gap Outer Surface	305 (152)	291 (144)
Radial Neutron Shield Inner Surface	270 (132)	271 (133)
Overpack Enclosure Shell Surface	250 (121)	222 (106)
Axial Neutron Shield	223 (106)	292 (144)
Impact Limiter Exposed Surface	160 (71)	121 (49)
Overpack Closure Plate	250 (121)	163 (73)
Overpack Bottom Plate	375 (191)	295 (146)

A heat generation rate equivalent to a decay heat load of 8,530 Btu/hr (2.5 kW) was applied, with appropriate peaking factor, over the active fuel region. The NAC LWT is currently licensed for a maximum decay heat load of only 2.1 kW. The value of 2.5 kW was selected for this analysis because an Amendment to the SAR that would increase the decay heat load limit to 2.5 kW is currently under review [11]. This approach ensures a conservative decay heat load for the package in the fire transient analysis.

The steady-state initial condition temperature distribution predicted for the NAC LWT package was verified against the results reported in the SAR [11]. Direct comparison is not possible, because the SAR [11] does not include any analytical cases similar to the detailed 3-D model used in this study. Due to the relatively low associated decay heat load capacity, the applicant chose to perform a series of highly conservative evaluations to qualify the system for its Certificate of Compliance (CoC).

The most complex models presented in the SAR [11] involve simple 2-D ANSYS cross-sections in which the cutting plane includes the expansion tank as well as the neutron shield tank. This approach does not allow axial heat flow out of the plane of the 2-D cross-section, and also assumes that the decay heat load axial peak occurs on that plan, placing the spent nuclear fuel peak decay heat location under two concentric neutron shields. This provides conservatism for a steady-state analysis, since the expansion tank makes a longer conduction path over which to dissipate the decay heat. For the fire transient, however, the assumptions in this 2-D model would have the effect of limiting the heat input to the cask from the fire, and would not constitute a conservative approach.

ANSYS cross-sectional models were also used to represent a 1.41 kW 25-rod BWR basket assembly and a 2.1 kW high burn-up PWR assembly, with detailed representation of the fuel pins, pin tubes, and can weldments with the pins resting on the pin tubes via point contact. These models included the ISO container, with boundary conditions that included solar insolation and 100°F (38°C) ambient temperature.

The design basis model presented in Amendment 34 of the SAR [11] for a 2.5 kW PWR assembly also used a 2D representation of the cask. This is a HEATING5 model, and consists of a 2-D axisymmetric representation using effective diameters for the basket and fuel assembly. This model does not include an ISO container or impact limiters, convection at the assembly end cavities is neglected, and the ambient temperature boundary is specified as 130°F (54°C).
None of these cases from the SAR [11] use assumptions or boundary conditions identical to the initial conditions assumed for the fire transient in this analysis, but there are sufficient similarities to allow reasonable comparisons to be made for

verification of the 3-D ANSYS model predictions. The results for these three cases are reported in Table 6.3.

Table 6.3. NAC LWT Component Temperatures at Various Decay Heat Loads

Component	2.5 kW °F (°C) (Table 3.4-2 [11])	1.41 kW °F (°C) (Table 3.4-7 [11])	2.1 kW °F (°C) (Table 3.4-10 [11])
Fuel Cladding	472 (244)	358 (181)	671 (355)
Aluminum PWR Insert	276 (136)	*	394 (201)
Inner Shell	274 (134)	249 (121)	385 (196)
Gamma Shield	273 (134)	248 (120)	375 (191)
Outer Package Surface	229 (109)	185 (85)	308 (153)
Neutron Shield	238 (114)	235 (113)	306 (152)
Lid Seal	227 (108)	*	*
Drain/Vent Ports	231 (111)	*	*
Impact Limiters	*	*	*
ISO Container	*	*	*

* value not reported by applicant

Figure 6.11 shows the predicted temperature distribution from the ANSYS solution for the 3-D model developed for the current study, obtained using 130°F (54°C) ambient temperature with a 2.5 kW decay heat load. This calculation was performed in addition to the initial conditions case at 100°F (38°C) ambient temperature, as a verification case for comparison to the results obtained for the 2.5 kW case reported in the SAR [11]. The 2-D axisymmetric model in the SAR [11], which used an ambient temperature of 130°F (54°C), is the most similar to the initial conditions in the fire transient for the purposes of this comparison, despite the exclusion of the ISO container.

Table 6.4 presents detailed component temperature results obtained with the 3-D ANSYS model, compared to the values published in the SAR [11] for this decay heat load.

At first glance, the differences between the results obtained with the two models appear to be rather sizable. The peak clad temperature predicted with the ANSYS 3-D model is 434°F (223°C), compared to 472°F (244°C) reported in the SAR [11]. The other temperatures shown in the table are also considerably lower for the ANSYS model, compared to the corresponding SAR values. However, this is an expected result, given the modeling differences between the two cases. A more significant observation for the purposes of this comparison is to note that the differences in peak component temperatures between the two models are consistent.

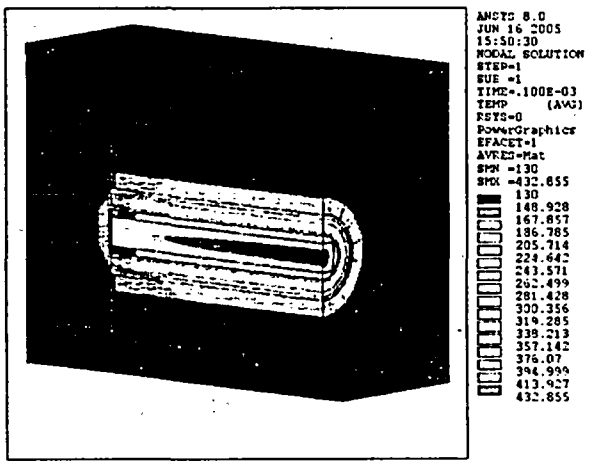

Figure 6.11. LWT Package Hot-Normal Condition Temperature Distribution (2.5 kW Decay Heat)

The radial temperature drop from the peak fuel cladding temperature to the outer cask surface temperature is 234°F (130°C) for the 3-D ANSYS model, compared to 243°F (135°C) for the HEATING5 axisymmetric model. This close agreement strongly suggests that the axisymmetric model featured in the SAR predicts essentially the components temperature distribution as the more detailed ANSYS model, and that most of the differences in the point-to-point temperatures predicted with each model are due to the

differences in assumed external boundary conditions (100°F vs. 130°F (38°C vs. 54°C)) and differences in modeling details.

Table 6.4. NAC LWT Component Temperatures at 2.5 kW Decay Heat Load and 130°F Ambient

Component	Current Study (ANSYS) °F (°C)	SAR Values (Table 3.4-2 [11]) °F (°C)	ΔT °F (°C)
Fuel Cladding	434 (223)	472 (244)	38 (21)
Aluminum PWR Insert	265 (129)	276 (136)	11 (6)
Inner Shell	228 (109)	274 (134)	46 (26)
Gamma Shield	227 (108)	273 (134)	46 (26)
Outer Package Surface	200 (93)	229 (109)	29 (16)
Neutron Shield	204 (96)	238 (114)	34 (19)
Lid Seal	164 (73)	227 (108)	63 (35)
Drain/Vent Ports	164 (73)	231 (111)	67 (37)
Impact Limiters	167 (75)	Not Modeled	--
ISO Container	167 (75)	Not Modeled	--

Figure 6.12 shows the temperature distribution predicted with the ANSYS 3-D model for the initial steady-state conditions before the fire transient. The boundary conditions for this calculation are from the Normal Transport Condition case, as described in 10 CFT 71.21 [1]. The hottest fuel temperature is predicted to occur near the center of the assembly, at a location that corresponds closely to the cross-section with the highest decay heat (i.e., the location of the maximum axial peaking factor.) This location is some distance away from the part of the cask covered by the expansion tank. This shows that the assumption placing the peak location under the expansion tank, which was used in the 2-D cross-section model in the SAR [11], is markedly conservative, and therefore can be expected to yield a higher estimate of the peak temperature.

As shown in Figure 6.12, the temperature gradients in the cask are such that heat spreads and dissipates axially as well as radially. As a result, the 3D geometry yields a more realistic representation of the heat flow in the cask. The conservative measures used in the simpler 2-D ANSYS cross-sectional models and the HEATING5 axisymmetric cross-sectional model (as reported in the SAR [11]) will tend to result in higher predicted temperatures for steady-state conditions. Other associated modeling assumptions and simplifications, including boundary conditions developed by the applicant, also tend to drive up component temperatures, compared to what might be obtained with a detailed 3-D representation.

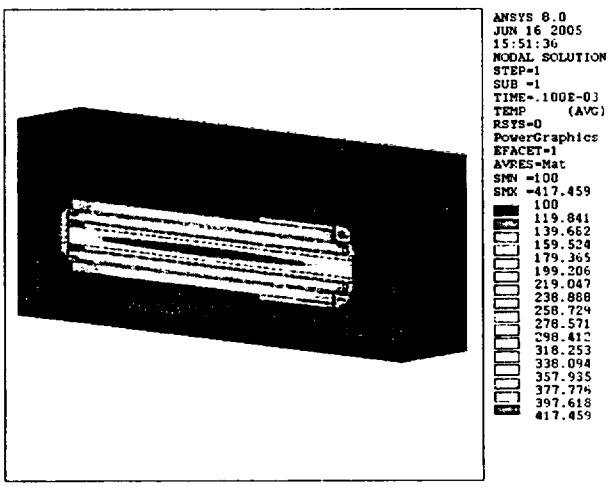

Figure 6.12. LWT Package Normal Condition Temperature Distribution (2.5 kW Decay Heat)

The main concern in analyses for normal transport conditions is to determine a conservative rate of heat removal *from* the package. The approach employed in the SAR should yield conservative estimates of peak internal temperatures for the analysis. However, for the fire transient, the main

concern is the amount of heat that the external fire can put *into* the package. In the fire transient calculations, a best estimate of component temperature distributions and heat transfer paths is more appropriate.

The conservative approach is to choose assumptions that tend to enhance the heat transfer paths, making it easier for heat to move into the package from outside. For example, the treatment of internal gaps between components is conservative in the SAR, in that gaps are assumed to be as large as possible. In the ANSYS model for the fire analysis, the shrinkage gap between the lead shielding and cask shell is included during the initial steady-state calculation, but is ignored during the fire transient. This approach tends to minimize heat loss from the package at the initial conditions, but then maximizes the heat input into the package internal components during the fire.

The pre-fire peak component temperature results determined in this study for the Normal Transport Condition case at 100°F (38°C), as described in 10 CFR 71.71 [1] are shown in Table 6.5.

Table 6.5. NAC LWT Pre-Fire Component Temperatures at 2.5 kW Decay Heat Load and 100°F Ambient

Component	Component Temperature °F (°C)
Fuel Cladding	418 (214)
Aluminum PWR Insert	242 (117)
Inner Shell	205 (96)
Gamma Shield	204 (96)
Outer Package Surface	176 (80)
Neutron Shield	180 (82)
Lid Seal	138 (59)
Drain/Vent Ports	138 (59)
Impact Limiters	141 (61)
ISO Container	140 (60)

6.3 Tunnel Fire Evaluations of Rail Packages

The Baltimore tunnel fire simulations for the three transport packages were conducted in three phases. These were the pre-fire steady-state (hot-normal) conditions of transport, the fire (consisting of the first 7 hours of the transient), and the post-fire phase. For the pre-fire steady state, the hot-normal conditions of transport were evaluated with solar insolation and a 100°F (38°C) ambient temperature, according to 10 CFR 71.71(c)(1) [1]. External heat transfer was assumed to be free convection in still air with radiation to the environment. This conservatively established component temperatures to serve as initial conditions for the transient.

For the fire phase of the evaluation ($0 \leq t \leq 7$ hours), the energy input due to solar insolation was set to zero, the tunnel surfaces were introduced, and the transport package and tunnel surfaces were assign an emissivity of 0.9 to represent surfaces affected by sooting. A forced convection regime was assumed to exist on the exterior of the package, based on the gas velocity results from the analysis performed by NIST. These results were used to determine the surface heat transfer coefficient, and with the gas temperatures from the NIST analysis defining the ambient boundary temperature, the convective heat flux at the package surface could be determined in the solution for the local surface temperature. Tunnel wall temperatures were also taken as boundary conditions from the NIST calculations, and radiation from the tunnel walls was also accounted for in the evaluations. In addition to these measures, all aluminum honeycomb, neutron shield resin materials, or wood were assumed to remain intact during the full duration of the fire to maximize heat input during the fire.

For the post-fire phase of the evaluation (t > 7 hours), properties of the neutron shield resin materials, wood, and selected portions of aluminum honeycomb sections were replaced with thermal properties identical to those of air. This change in material properties simulates the degradation of the materials due to the fire and has the effect of reducing the rate of heat release during the post-fire phase. Conservatively, the energy absorbed in the degradation of these materials was not subtracted from the heat input of the fire to the package. Other model-specific conservatisms were also incorporated, as described above in Section 5.

Analysis of the post-fire phase was carried out for a duration of 293 hours. This included the 23 hours of the post-fire portion of the transient predicted by the FDS analysis, plus an additional 270 hours in which boundary conditions at 30 hours were extrapolated to 300 hours, using a power function (as discussed in Section 5 above.) Purely forced convection heat transfer correlations (based on the NIST gas velocities and temperatures) were imposed for the post-fire phase of the simulation from 7 hours to 30 hours. The forced convection boundary condition at the package surface was then transitioned to free convection correlations, to establish the buoyant convective coefficients of heat conductance for the remainder of the evaluation period.

Results obtained in the evaluations of the three packages are discussed in Section 7.

7 ANALYSIS RESULTS

Due to the temperature limits on the spent fuel cladding, closure seals, impact limiter core materials, and neutron shield core materials, these components are the most important elements to consider in evaluating the response of the transport systems to the fire scenario. The peak cladding temperature limit is important because the cladding is the primary fission product containment boundary for the spent fuel. The temperature limit for the closure seals is important because these seals constitute the outer-most containment boundary for the package. The temperature limits for the neutron shield material and impact limiters are important because these materials are the most vulnerable to damage or destruction during the fire. The results of the analyses for the three rail packages were evaluated primarily in relation to the peak predicted temperatures for these components in the fire transient.

These analyses indicate that the spent fuel cladding reaches a peak temperature of 887°F (475°C) in the HI-STAR 100 package, 845°F (452°C) in the TN-68 package, and 1099°F (593°C) in the NAC LWT system. Peak cladding temperatures for the TN-68 and HI-STAR 100 packages are below the currently accepted short term temperature limit[5] of 1058°F (570°C) for Zircaloy clad spent nuclear fuel under accident conditions [23]. The peak cladding temperature determined for the LWT exposed to this hypothetical accident event exceeds the currently accepted short term temperature limit by approximately 41°F (23°C).

The transient results for each of the three systems are discussed in detail below. Section 7.1 discusses the response of the TN-68 package during the fire. Section 7.2 presents results for the HI-STAR 100 package. Section 7.3 discusses the response of the NAC LWT package.

7.1 TN-68 Fire Transient Results

The COBRA-SFS model of the TN-68 package consists of a total of 530,228 computational nodes that are solved for each time step. This yields an overwhelming volume of output that must be sorted, sifted, and processed to produce a coherent picture of the response of the package to this fire scenario. The following three subsections present the peak temperatures versus time for selected components, as determined with COBRA-SFS for the TN-68 package subjected to the fire transient conditions described in detail in Section 6. The results are presented separately for the three main phases of the transient. Section 7.1.1 discusses the predicted response of the TN-68 package during the fire. Section 7.1.2 presents results for the post-fire transient over the duration of the NIST simulation (to 30 hours.) Section 7.1.3 discusses the response to the postulated long-term post-fire conditions, out to 300 hours.

7.1.1 TN-68 During the Fire

Figure 7.1 shows the initial temperature response of the TN-68 package predicted with COBRA-SFS during the fire portion of the transient. The fire burns for the first 6.75 to 7 hours of the transient (see Figures 6.1 and 6.2 for boundary temperatures representing the fire with the package 66 ft (20 m) from the fire center.) During this time, the outer

[5] The short-term temperature limit of 1058°F (570°C) is based on creep experiments performed on two fuel cladding test samples which remained undamaged (i.e., no significant observable damage) when held at 1058°F (570°C) for up to 30 and 71 days [24]. This temperature limit is a relatively conservative limit, since the temperature at which Zircaloy fuel rods actually fail by burst rupture is approximately 1382°F (750°C)[25].

surface temperature of the package shell increases quite rapidly. The maximum temperature of the package surface increases at a rate of up to 10.5°F/min. (5.8°C/min.), reaching a peak temperature of 1789°F (976°C) at about 6.3 hours into the fire. The maximum temperature of the neutron shield material also shows a relatively rapid increase, reaching a peak of 1355°F (735°C) at approximately 6.9 hours into the fire.

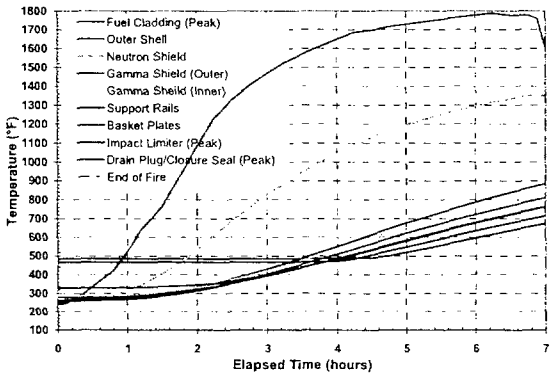

Figure 7.1. Maximum Temperature Histories for TN-68 Package Components During Fire Transient

The internal components of the package show a very slow thermal response during the fire. The support rails and gamma shields take more than an hour to show any noticeable increase in temperature. Approximately 3.5 hours elapse before the peak fuel cladding temperature rises as much as 1°F above the initial steady-state peak temperature of 486°F (252°C). The peak temperatures of the basket tubes and poison plates rise only about 4°F (2.2°C) in the first four hours of the fire. During this time period, the peak temperature on the outer shell of the package is predicted to go up to 1647°F (897°C), the predicted peak temperature of the neutron shield rises to 1042°F (561°C), and the peak temperature on the gamma shields increases to 549°F (287°C).

By the end of the fire, marking the point at which all volatile flammables are consumed, the peak clad temperature has risen to only 673°F (356°C), and the peak temperature of the basket tubes and poison plates is at about 714°F (379°C). The outer shell of the package is predicted to have a peak temperature of 1599°F (871°C) at the end of the fire, with the neutron shield at 1347°F (731°C) and the outer gamma shield at 886°F (474°C).

Figure 7.2 shows midline temperature profiles from top to bottom vertically through the package cross-section, including the package shell, support rails, and basket structure during the fire at approximately hourly intervals. The large difference in the predicted rate of increase in temperature for the internal and external components of the package is illustrated by these profiles. The temperatures of the nodes modeling the basket tubes and poison plates change very little during the fire. The support rails and gamma shield nodes heat up relatively slowly, while the outer shell and neutron shield region increase rapidly in temperature in response to the fire.

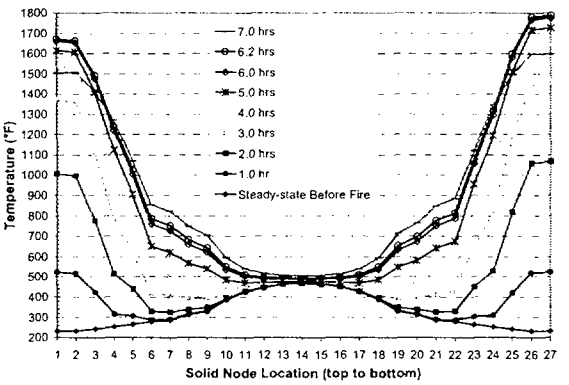

Figure 7.2. Temperature Profiles Top-To-Bottom Through TN-68 Package Axis During Fire Transient

The neutron shield and gamma shields insulate the basket and fuel assemblies from the fire, but the slow response is also due in large part to the huge thermal inertia of the package components. The 68 assemblies within the package comprise on the order of 20 to 25 metric tons of material (mainly

uranium dioxide and Zircaloy), with roughly 8 metric tons of material in the basket (mainly steel and borated aluminum.) The inner and outer gamma shields consist of approximately 40 metric tons of carbon steel, while the outer shell of the package is approximately 5 metric tons of steel. Even under the severe heat load imposed by the sustained high temperatures of a fire lasting 7 hours, it takes time to raise the temperature of such a large mass of material, even with its internal heat generation due to the spent fuel assemblies.

A significant detail discovered during the evaluation of the TN-68 is that during the first quarter of the fire transient, the total heat flux associated with radiation heat transfer from the tunnel to the package is nearly an order of magnitude greater than the total heat flux associated with convection heat transfer from the tunnel environment to the package. As a consequence, the most severe conditions for this transient are those that result in the package receiving the greatest exposure to radiation heat transfer. This means that a horizontal orientation will result in the greatest possible heat input for a given fire scenario. Any package orientation other than the horizontal orientation during the fire (e.g., the package bounced into a vertical orientation as a result of an accident) would yield less severe heat input to the package.

7.1.2 TN-68 Short-Term Post-Fire Response

Figure 7.3 shows the temperature response of the package during the first 30 hours of the COBRA-SFS simulation of the transient. (This time period represents the total duration of the NIST analysis that is the source of the boundary conditions for this calculation, in which the package is positioned 66 ft (20 m) from the fire center.) During the fire, the material in the neutron shield reaches temperatures that would heavily degrade the borated polyester. This does not mean, however, that the package would fail to meet the requirement of maintaining appropriate shielding in this scenario. This spent fuel transportation package is expected to lose its neutron shield material in the fire accident specified in current regulations, and therefore the design does not rely on the neutron shield material remaining intact in order to maintain shielding. This package is designed to attenuate neutron radiation to acceptable levels (see 10 CFR 71.51 [1]) following an accident without the assistance of the neutron shield material. However, the loss of the shield material means that the neutron shield's heat transfer capability would be expected to deteriorate rapidly during the fire.

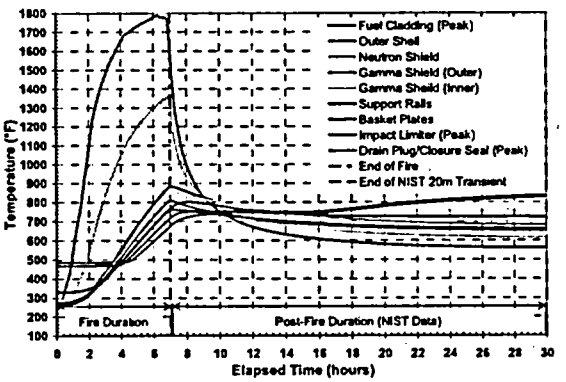

Figure 7.3. Maximum Temperature Histories for TN-68 Package Components During First 30 hr of Transient

In the COBRA-SFS evaluation, it was assumed that the borated polyester remains in place and is unaffected during the fire, but instantly degrades at the end of the fire and is replaced by hot air. This maximizes the heat input into the package during the fire, then imposes an additional barrier to heat transfer from the package after the fire. From the standpoint of the thermal response of the system, this is a conservative representation of the effect of the fire on the neutron shield. The thermal conductivity of the borated polyester is about 140 times that of air, so extending the residence time of the polyester to the end of the fire results in a

calculation that overestimates the rate of heat flow into the package during the fire. This will tend to result in higher calculated temperatures on the package internals than would be obtained if it were assumed that the polyester was replaced with air earlier in the transient. In reality, the change would be more gradual and would occur earlier in the transient as the neutron shield burned away. The heat absorbed in the process of melting the polyester material is not subtracted from the heat of the fire, as an associated conservatism.

The temperatures in Figure 7.3 show that once the fire is over, the peak temperatures on the package shell and neutron shield are predicted to begin to drop precipitately. This is primarily a response to the rapid decrease of the boundary temperatures, as can be seen in Figure 7.4. This plot shows the outer shell surface temperature predicted with COBRA-SFS compared to the tunnel ceiling temperature and the temperature of the air above the package, which are derived from the NIST calculations and used as boundary conditions.

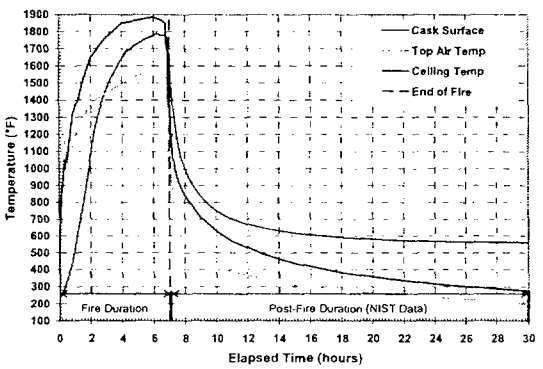

Figure 7.4. Maximum TN-68 Package Surface Temperatures Compared to NIST Boundary Condition Temperatures

Figure 7.3 also shows that the peak temperatures on the gamma shields and support rails of the package decrease after the fire ends. However, the temperature decrease for these components is much slower than for the neutron shield region and outer shell because the internal components must also absorb the thermal load from the fuel. For the same reason, the peak temperature of the basket shows a continuous increase even after the end of the fire, as does the peak clad temperature.

The plot of the predicted peak clad temperature in Figure 7.3 shows that the thermal output of the fire itself does not have much of an effect on the fuel. The observed rise in peak clad temperature is mainly a response to the effect of the external boundary conditions on the rate of heat transfer from the package. The heat of the fire does not result in much of an increase in the package internal temperatures, but the increase in the external air temperature severely compromises the rate of heat rejection from the package and continues to do so long after the fire is out. This is illustrated very clearly by the plot of the global peak clad temperature alone, shown in Figure 7.5 for 50 hours of the transient (i.e., the 30 hours of the NIST transient, plus an additional 20 hours of the extended cool down beyond the NIST calculation.)

As shown by the plot in Figure 7.5, at about 4.5 hours into the fire the peak clad temperature begins an almost adiabatic heat up (approximately 77°F/hr (43°C/hr)) because the fire is preventing normal heat removal from the package (which occurs by thermal radiation to the external environment and natural convection at the surface.) This adiabatic heat-up continues for about an hour after the end of the fire, until the package shell temperature drops low enough to permit some heat removal from the package by radiation to the tunnel surfaces.

The fuel cladding temperature increase observed shortly before the end of the fire (at ~4.5 hours) occurs in fuel in the outer periphery of the basket, because the fire is heating the outer cylinder of the package. This causes the peak fuel cladding temperature to shift first to the bottom assembly in

the horizontal basket cross-section, then to the top assembly. The rate of increase in the predicted peak cladding temperature slows briefly to 1-2°F/hr (0.5-1°C/hr) before increasing again as the peak temperature location shifts back to the center assembly in the core of the basket. (The peak fuel clad temperature location is automatically tracked in these results during the transient.)

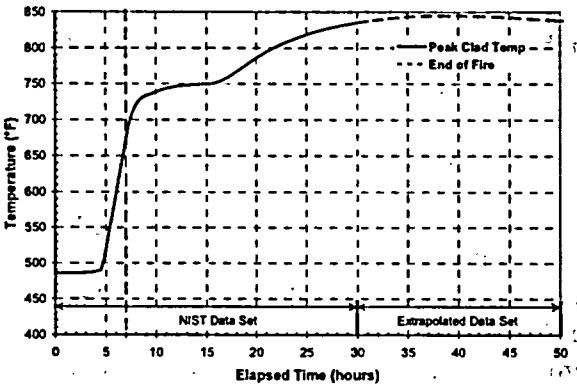

Figure 7.5. Peak Fuel Cladding Temperature History in TN-68 During First 50 hr of Transient

The peak clad temperature continues to increase after the fire, because thermal radiation from the tunnel ceiling, walls and floor is continuing to add heat to the package and the external ambient air temperature slows the rate of heat removal by convection. However, the rate of increase drops to only about 2°F/hr (~1°C/hr). At about 15 hours into the transient, the rate of increase of the peak clad temperature begins to climb again, to a rate of about 10°F/hr (6°C/hr), then again drops to only 3°F/hr (~2°C/hr) after about 20 hours. This behavior is due to the decrease in the rate of heat removal via thermal radiation as the tunnel surfaces cool down, and the more gradual decrease in the rate at which heat is being removed from the package by forced convection from the hot air flowing past the package.

By the end of the NIST transient at 30 hours, the rate of increase of the peak clad temperature has dropped to less than 3°F/hr (<2°C/hr). The global peak cladding temperature of 845°F (452°C) is finally reached at ~40 hours into the transient. (The dashed portion of the curve in Figure 7.5 denotes results that stem from the boundary conditions extrapolated beyond the results obtained in the 30-hour NIST calculation.)

The maximum temperature history of the seals in the package closure and vacuum port is shown in Figure 7.6. The curve in this figure represents the global peak of all seal material used in the TN-68. As shown in this figure, the Helicoflex® seal material is predicted to reach a maximum temperature of 811°F (433°C) right at the end of the fire, then gradually begins to cool as the transient proceeds into the post-fire duration. This peak temperature exceeds the maximum operating temperature of 536°F (280°C) for this material.

Bolts and other subcomponents were not explicitly represented at the package ends in the COBRA-SFS model of the TN-68. However, the depicted temperature history (see Figure 7.6) conservatively represents the peak temperature history of the closure bolts due to the manner in which heat must migrate around the top impact limiter into the package upper forging, through the closure seal location, and then into the closure. This is due to the limited conduction offered by the steel-encapsulated wooden impact-damping material.

The thermal response of the package after the end of the fire is further illustrated in Figure 7.7, with plots showing radial temperature profiles through the package at selected time intervals through the transient. These profiles show that the outer shell and former neutron shield cool rapidly once the fire is over, while the temperatures of the internal nodes representing the basket tubes and poison plates continue to rise in response to the heat load from the spent nuclear fuel.

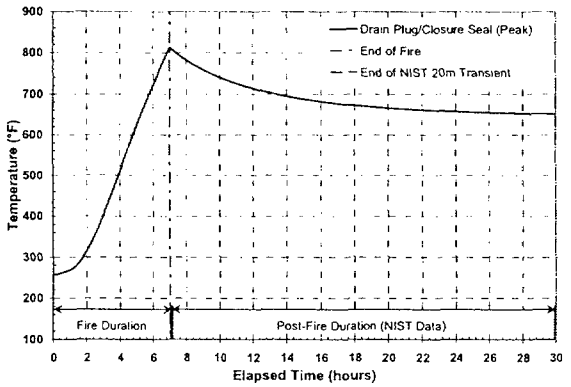

Figure 7.6. Maximum Global TN-68 Closure/ Port Seal Temperature History During First 30 hr of Transient

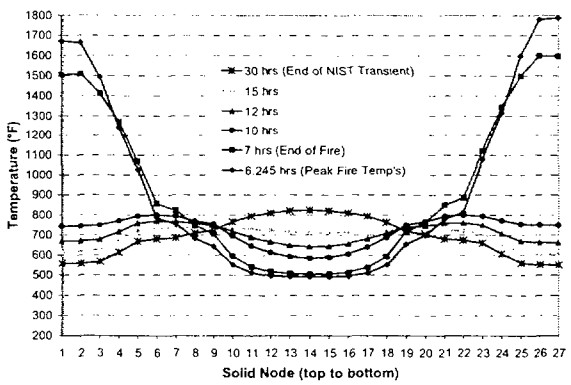

Figure 7.7. Temperature Profiles Top-To-Bottom Through TN-68 Package Axis: First 30 hr of Transient

7.1.3 TN-68 Long-Term Post-Fire Response

The NIST calculation used to define the boundary conditions for the COBRA-SFS analysis simulated the fire transient and its aftermath out to 30 hours. However, the trends exhibited by the temperatures of the various components of the package at the end of the transient indicate that the system is not yet at a new steady state by then. Temperatures predicted by NIST for the first 30 hours were extrapolated from 30 hours out to 300 hours using a power function to realistically model cool-down of the tunnel environment. (The extrapolated values are presented in Figures 6.5 and 6.6 for the air and wall temperatures, respectively.)

To explore the effects of prolonged exposure to post-fire conditions in the tunnel, the calculations were carried out for the full 300 hours (273 hours after fire cessation). This is equivalent to assuming that the package will be left in the tunnel for an extended period (days or weeks rather than merely hours) without any emergency responder intervention. This assumption is not very realistic but is highly conservative in that it defines a relatively severe long-term ambient environment.

During the first 30 hours of the transient, the heat transfer at the package surface was assumed to be forced convection at the velocities predicted in the tunnel by the NIST calculation. The basis for this approach is discussed in Section 6.0. This is a relatively conservative assumption, particularly for conditions after about 20 hours into the transient, when the velocities predicted in the NIST calculation have dropped to values of 1 to 2 ft/s (0.3 to 0.6 m/s) or less. For the latter portion of the transient ($t \geq 20$ hours), heat transfer at the package surface is a complex mixture of forced convection (due to air flow induced in the tunnel by the temperature gradients of the fire) and free convection (driven by the non-uniform circumferential temperatures of the package outer shell.) This was conservatively approximated by imposing a purely forced convection heat transfer coefficient (based on the NIST air velocities and temperatures) for the first 30 hours of the simulation, then imposing a free convection coefficient for the remainder of the calculation.

Figure 7.8 shows the temperature response of the various components of the package for the long term transient calculation to 300 hours. (As previously indicated, the dashed portion of the curve is used to distinguish the results that stem from the boundary conditions that were

extrapolated from the NIST simulation.) As shown in Figure 7.8, the highest peak clad temperature, 845°F (452°C), is reached at approximately 40 hours. The peak temperature for the basket structure is also reached at about the same time. The predicted maximum in the peak clad temperature is below the regulatory limit of 1058°F (570°C) by a difference of 213°F (110°C). All other temperatures in the package have been decreasing steadily since the end of the fire.

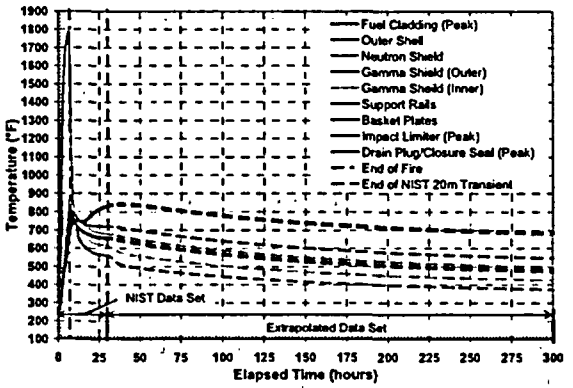

Figure 7.8. Maximum Temperature Histories for TN-68 Package Components During 300 hr of Transient

By 100 hours, the peak clad temperature has dropped to 784°F (418°C), with temperatures decreasing at rates of about -1°F/hr (-0.6°C/hr). After 200 hours, the peak clad temperature has dropped to 719°F (382°C), and at 300 hours is predicted to be down to 690°F (366°C) for the specified boundary conditions. At this point in the transient calculation, the rate of change of local temperatures in the system is about -0.2°F/hr (-0.1°C/hr). The rate of cooling is very slow due to the huge thermal mass of the package and its fuel load. Projections of the cooling rate indicate that it would take an additional 175-200 hours to reach a new post-fire steady state.

The trends in Figure 7.8 show that the overall thermal response of the package to the fire transient is essentially an accommodation to the new higher-temperature boundary conditions extrapolated from the conditions predicted at the end of 30 hours in the NIST fire analysis. The temperature of the fuel and basket is largely unaffected by the heat input to the package from the fire; the increase in peak clad temperature and peak basket temperature is due almost entirely to having no heat removal from the package during the fire and for about an hour immediately afterwards. After the ambient temperatures drop enough to allow heat removal from the package, the rate of increase of the peak clad temperature begins to level off and then finally turn around about 40 hours into the transient.

Viewed on the scale of 300 hours, the fire portion of the transient appears as a relatively short-lived spike in the boundary conditions that significantly affects only the outer shell, neutron shield, and impact limiters, and to a lesser extent the outer and inner gamma shielding. These components show a rapid temperature increase during the fire, but after the end of the fire immediately begin to rapidly cool down.

Peak component temperatures for the TN-68 package over the transient fire simulation are summarized in Table 7.1.

Table 7.1. TN-68 Peak Component Temperatures During Fire Transient

Component	Maximum Temperature (COBRA-SFS) °F (°C)	Time (hours)
Fuel Cladding	845 (452)	40
Basket Plate	836 (447)	40
Basket Rail	801 (427)	8.3
Inner Shell	857 (458)	7.0
Gamma Shell	886 (474)	7.0
Package Bottom	762 (406)	7.0
Seals	811 (433)	7.0
Neutron Shield	1355 (735)	6.9
Outer Shell	1789 (976)	6.3

7.2 Holtec HI-STAR 100 Fire Transient Results

The ANSYS model of the HI-STAR 100 package consists of a total of 149,100 standard computational elements and 288 superelements that are solved for each time step. Similar to the COBRA-SFS model of the TN-68, this model yields an overwhelming volume of output that must be processed to produce a coherent picture of the package response. The following three subsections present the peak temperatures versus time for selected components, as determined with ANSYS for the HI-STAR 100 subject to the hypothetical fire transient conditions described in Section 6.

7.2.1 HI-STAR 100 During the Fire

Figure 7.9 shows the initial temperature response of the HI-STAR 100 package predicted with ANSYS during the fire portion of the transient. The maximum temperature of the HI-STAR 100 package surface increases rapidly to a peak temperature of 1831°F (999°C) around 6 hours into the fire. The maximum temperature of the inner shell material, which defines the primary containment boundary, also shows a relatively rapid increase, reaching a peak of 1444°F (784°C) approximately 6.75 hours into the fire. This corresponds to the peak boundary condition temperatures defined by the fire. The fire temperatures predicted in the NIST analysis peak at 6.75 hours, and then drop off rapidly thereafter as the fire burns itself out. The peak temperature of the inner shell material is predicted to lead the gamma shield material peak temperature because the elements selected to define the primary containment boundary include the bottom and top forgings and lid. A large section of the top forging is directly exposed to the fire (un-shrouded by the gamma shield, neutron shield/fin section and upper impact limiter.)

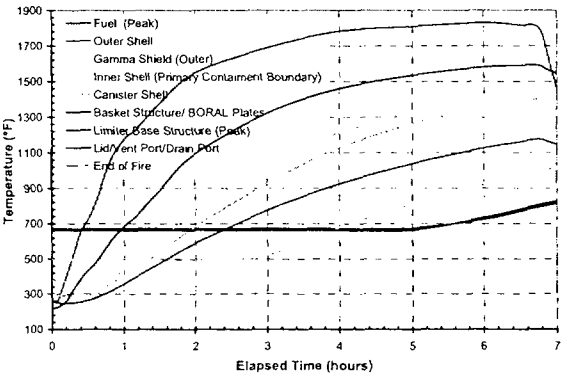

Figure 7.9. Maximum Temperature Histories for HI-STAR 100 Package Components During Fire Transient

Similar to the TN-68 results with the COBRA-SFS model, the internal components of this package also show a very slow thermal response during the fire. The gamma shield takes nearly an hour to show any noticeable increase in temperature. Two hours elapse before the internal canister shell temperature rises as much as 1°F above the initial steady-state peak temperature of 494°F (257°C). The peak temperatures of the basket structure, poison plates, and fuel rise only by about 2°F (1°C) in the first five hours of the fire.

This is approximately an hour later than the TN-68 response and can be attributed to the additional thermal barrier represented by the canister in this particular design. During this time period, the peak temperature on the outer skin surrounding the neutron shield of this package is predicted to go up to 1831°F (999°C), and the peak temperature on the gamma shields increases to 1400°F (760°C).

By the end of the fire, marking the point at which all volatile flammables are consumed, the peak clad temperature has risen to only 813°F (434°C). The outer shell of the package is predicted to have a peak temperature of 1449°F (787°C) at the end of the fire, with the outer gamma shield at 1322°F (717°C). This is a bit cooler than the TN-68 at this point in time. The difference is due mainly to the

larger thermal resistance to radial heat flow in the thinner skin of the HI-STAR 100, compared to the TN-68. However, both packages tend to perform similarly overall.

As with the TN-68 results, the large difference in the predicted rate of increase in temperature for the internal and external components of the HI-STAR 100 is because the neutron shield and gamma shield insulate the basket and fuel assemblies from the fire. The slow response is due mainly to the huge thermal inertia of the package components themselves. Even under the severe heat load imposed by the sustained high temperatures of a fire lasting nearly 7 hours, it takes time to raise the temperature of such a large mass of material despite its internal heat generation component.

7.2.2 HI-STAR 100 Short-Term Post-Fire Response

Figure 7.10 shows the temperature response of the package during the first 30 hours of the ANSYS transient simulation. During the fire, the material in the neutron shield is predicted to achieve temperatures that will heavily degrade it. As noted in Section 7.1.1 for the predicted loss of the TN-68 cask's neutron shield, the HI-STAR 100 is also designed to attenuate neutron radiation to acceptable levels (see 10 CFR 71.51 [1]) following an accident without the assistance of the neutron shield material. However, the neutron shield's heat transfer capability is expected to deteriorate rapidly during the fire. In the ANSYS evaluation, it was assumed that the neutron shield material (HOLTITE-A) remains in place and unaffected during the fire, but instantly degrades at the end of the fire, to be replaced by hot air. This maximizes the heat input into the package.

This is a conservative representation of the effect of the fire on the neutron shield from the standpoint of the thermal response of the system. The thermal conductivity of HOLTITE-A is approximately 16 times that of air, so extending the residence time to the end of the fire results in the calculation somewhat overestimating the rate of heat flow into the package during the fire. This will result in higher calculated temperatures on the package internals than would occur if degradation were accounted for at a more realistic rate during the fire. As an additional associated conservatism, the latent heat absorbed in the degradation of the material, which would tend to decrease the external heat flux due to the fire, is also neglected.

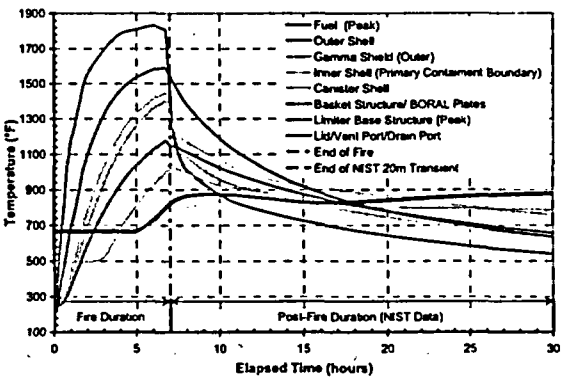

Figure 7.10. Maximum Temperature Histories for HI-STAR 100 Package Components During First 30 hr of Transient

Figure 7.10 shows the peak temperatures predicted in the ANSYS analysis for the various components of the package during the full 30 hours of the transient as defined by the NIST calculations. These results show that once the fire is over, the predicted peak temperatures on outboard components begin to drop rapidly (i.e., outer shell, gamma shield, etc.). This is primarily a response to the rapid decrease of the boundary temperatures, as can be seen in Figure 7.11, which shows the outer shell surface temperature predicted with ANSYS compared to the tunnel ceiling temperature and the temperature of the air above the package derived from the NIST calculations and used as boundary conditions.

Figure 7.10 shows that the peak temperatures on the gamma shields and inner shell of the package decrease after the end of the fire. However, the temperature decrease for these components is much slower than for the outer shell because the internal components must absorb the thermal load from the fuel. Similarly, the peak temperature of the basket shows a continuous increase even after the end of the fire, as does the peak clad temperature.

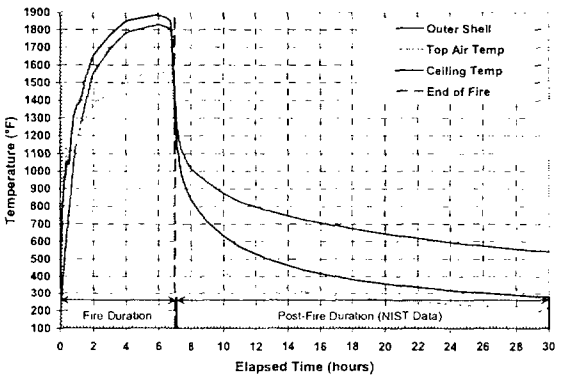

Figure 7.11. Maximum HI-STAR 100 Package Surface Temperature Compared to NIST Boundary Condition Temperatures

The plot of the predicted peak clad temperature in Figure 7.10 shows that the thermal output of the fire itself has little effect on the fuel or its accommodating basket. As discussed above for the TN-68, the observed rise in peak clad temperature is mainly a response to the effects of the external boundary conditions on the rate of heat transfer from the package. The heat of the fire does not result in much of an increase in the package internal temperatures, but the increase in the external air temperature severely compromises the rate of heat rejection from the package, and continues to do so long after the fire is out. This is illustrated very clearly by the plot of the peak clad temperature alone shown in Figure 7.12 for the first 50 hours of the NIST transient. The fire is very nearly over before the peak clad temperatures show a discernable increase.

Figure 7.12 shows that a little after 5 hours into the fire, the global peak clad temperature begins an almost adiabatic heat up (approximately 69°F/hr (38°C/hr)) because the fire prevents normal heat removal from the package by natural convection at the surface. This adiabatic heat-up continues for about an hour after the end of the fire, until the package shell temperature drops low enough to permit some heat removal from the package by radiation to the tunnel surfaces.

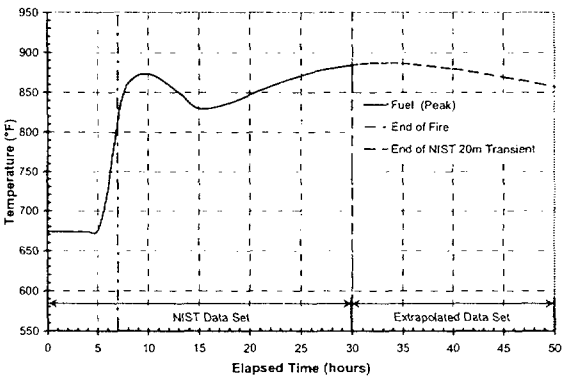

Figure 7.12. Peak Fuel Cladding Temperature History in HI-STAR 100 During First 50 hr of Transient

The initial fuel cladding temperature rise shown to initiate shortly before the end of the fire (~5.5 hours) occurs on fuel in the outer periphery of the basket in a portion of the package facing the top of the tunnel. The fuel in this region is initially rising in temperature faster than that residing in the center of the basket. This continues until ~8 hours into the transient. However, by this time the fire has ended (at ~7 hours) and the internal heat begins spread as component temperatures redistribute radially throughout the package, causing the peak fuel cladding temperature to shift from one assembly to another.

The peak cladding temperature begins to drop for a brief period, before rising again as fuel in the core of the basket begins to heat up and exceed the temperature of the fuel on the outer periphery. (Just as with the TN-68 results, the peak fuel clad temperature is captured in the global summary as it moves from assembly to assembly within the fuel basket during the transient.) The peak clad temperature continues to increase, because the hot air flow and hot tunnel surfaces resulting from the fire are continuing to compromise heat rejection from the package surface.

The package is designed to reject heat to ambient at 100°F (38°C), but the air within the tunnel environment is still above 200°F (93°C) at 30 hours, decreasing from a peak of 1557°F (847°C) at the end of the fire. However, by the end of 30 hours, the rate of increase in the peak clad temperature has dropped to only about 2°F/hour (1°C/hour), in response to the decreasing boundary temperatures. The global peak cladding temperature reaches a maximum of 887°F (475°C) at approximately 32 hours into the transient.

The maximum temperature history of the seals in the package lid closure, ports, and port covers is shown in Figure 7.13. The curve in this figure represents the global peak of all seal material utilized in the HI-STAR 100. These temperatures are gathered by querying nodes at the seals' locations, even though the seals were not explicitly represented in the model. As shown in this figure, the metallic mechanical seal material reaches a maximum temperature of 1177°F (636°C) right at the end of the fire, then gradually begins to cool as the transient proceeds into the post-fire cool down. Despite an abrupt rise in temperature during the fire, the peak seal temperature remains below the lowest reported maximum continuous-use seal temperature limit of 1200°F (649°C) (see Table 4.1.1 of the HI-STAR 100 SAR [10].)

Bolts were not explicitly represented at the package lid and buttress interface in the ANSYS model of the HI-STAR 100. However, the depicted seal temperature history conservatively represents the peak temperature history of the closure bolts due to the manner in which heat has to migrate around the top impact limiter, into the package upper forging (between the top limiter and neutron shield/fin section), through the closure seal location, and then into the closure. This is due to the limited conduction offered by the stainless steel-encapsulated cellular honeycomb material.

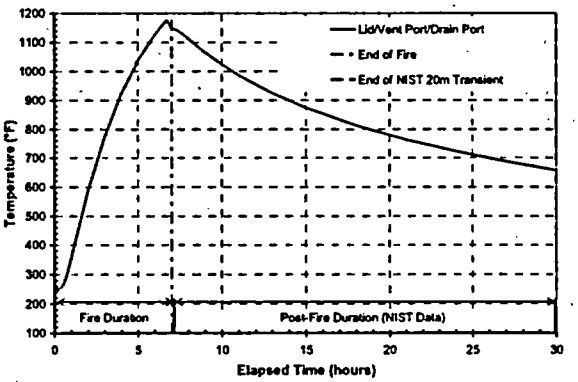

Figure 7.13. Maximum Global HI-STAR 100 Closure/Port Seal Temperature History During First 30 hr of Transient

7.2.3 HI-STAR 100 Long-Term Post-Fire Response

The trends exhibited by the temperatures of the various components of the HI-STAR 100 package at the end of the 30 hour transient indicate that the system is not yet at a new steady state. Boundary temperatures predicted by NIST were extrapolated from 30 hours out to 300 hours using a power function to realistically model cool down of the tunnel environment. (The extrapolated values are presented in Figures 6.5 and 6.6 for the air temperatures and wall temperatures, respectively.)

To explore the effects of prolonged exposure to post-fire conditions in the tunnel, the calculations were carried out for the full 300 hours (273 hours after fire cessation). As discussed previously, this is equivalent to assuming that the package will be left in the tunnel for up to 12.5 days without any emergency response. This assumption is not very realistic, but is highly conservative in that it defines a relatively severe long-term ambient environment around the package.

The same relatively conservative assumptions applied to the TN-68 evaluation for external convection during the fire and post-fire duration were applied to the HI-STAR 100 evaluation. A purely forced convection heat transfer regime and associated heat transfer coefficient was assumed for the first 30 hours of the simulation, then a purely free convection regime and associated coefficient was assumed for the remainder of the calculation ($t \geq 30$ hours). (Refer to Section 6 for detailed discussion of the heat transfer boundary conditions on the package surfaces.)

Figure 7.14 shows the temperature response of the various components of the package for the long term transient calculation to 300 hours. As previously discussed, the dashed portion of the curve is used to distinguish the results that stem from the boundary conditions that were extrapolated from the original NIST calculation. As noted in Section 7.2.2 (see Figure 7.12), the highest peak clad temperature is reached at approximately 32 hours, with a value of 887°F (475°C). This is 171°F (95°C) below the regulatory limit. The peak temperature for the basket/poison plate structure is reached at about the same time.

All other temperatures in the package have been decreasing steadily since the end of the fire. By 100 hours, the peak clad temperature has dropped to 757°F (403°C). Similar to the results for the TN-68, this system is not yet at a new post-fire steady-state by this time (see Section 7.1.3, Figure 7.8). The HI-STAR 100 is nearing its new post-fire steady-state at about 200 hours, with rates of temperature change on the order of approximately -0.3°F/hr (-0.2°C/hr). After 250 hours, the peak clad temperature has dropped to 681°F (361°C), and at 300 hours, it is predicted to be 674°F (357°C) for the specified boundary conditions. At this point in the transient calculation, the rate of change of local temperatures in the system is less than -0.1°F/hr (-0.06°C/hr), and the conditions can be treated as being essentially at a new post-fire steady state.

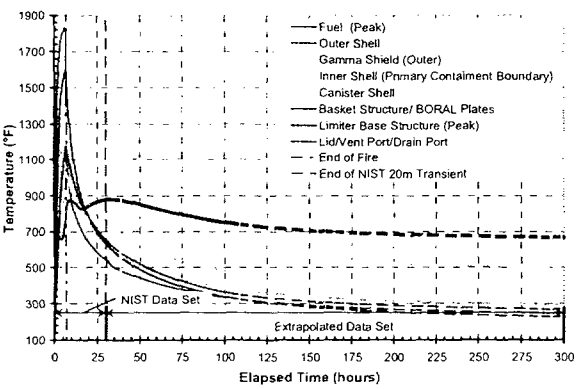

Figure 7.14. Maximum Temperature Histories for HI-STAR 100 Package Components During 300 hrs of the Transient

The trends in Figure 7.14 show that the overall thermal response of the package to the fire transient is essentially an accommodation to the new higher temperature boundary conditions represented by the conditions predicted at the end of 30 hours in the NIST fire analysis. Viewed on the scale of 300 hours (i.e., from pre-fire to post-fire steady state), the fire portion of the transient appears as a relatively short-lived spike in the boundary conditions that significantly affects only the outer shell, impact limiters, and the neutron shield, and to a lesser extent, the gamma shield, inner shell, and canister. The outer shell and

neutron shield show a rapid temperature increase during the fire, but after the end of the fire immediately begin to rapidly cool down.

The temperature of the fuel and basket is largely unaffected by the heat input to the package from the fire. The increase in peak clad temperature and peak basket temperature is due almost exclusively to having no heat removal from the package during the fire and for about an hour immediately afterward. After the ambient temperatures drop enough to allow heat removal from the package, the rate of increase of the peak clad temperature begins to level off, and then finally turns around at about 32 hours into the transient.

The TN-68 system displays a rapid peak cladding temperature increase during the interval from about 6 to 8 hours of the transient, followed by a much slower rate of increase until about 16 hours, at which point it begins to rise again toward its final peak value, reached at approximately 40 hours. The peak cladding temperature predicted for the HI-STAR 100 follows a similar pattern, but with a somewhat more dynamic response. After reaching a peak at approximately 8 hours, the peak cladding temperature actually decreases for a time, until about 16 hours, at which point it begins to rise toward its final peak value, reached at about 32 hours.

The difference in response of the peak clad temperature in the two packages is due to three main factors. There are significant differences in construction and thickness of the finned neutron shield regions in the two package designs. There is about a 15% difference in the thermal inertia associated with the spent fuel assemblies in each package (the HI-STAR 100 contains 24 PWR fuel assemblies, compared to 68 BWR fuel assemblies within the TN-68 package), and the two packages have very different basket designs. In addition, the high thermal conductivity of the HI-STAR 100 aluminum honeycomb impact limiters aids in ramping up component temperatures faster in the ends of the package, compared to the effect of the redwood impact limiters on the TN-68 package.

The TN-68 does not utilize an internal canister to hold spent fuel. It relies instead on seals to prevent radioactive releases from the fuel compartment. The maximum predicted seal temperature, which is seen by the package lid seal, is 811°F (433°C), and occurs at the end of the fire. This is below the peak seal temperature predicted for the HI-STAR 100 and is primarily due to the relatively low conductivity of the redwood material used in the TN-68 impact limiter design, compared to the aluminum honeycomb in the HI-STAR 100 impact limiter design.

When comparing the heating trends associated with the HI-STAR 100 and the TN-68 (compare results shown in Figure 7.14 and in Figure 7.8) , it appears that the HI-STAR 100 generally heats up faster during the fire than the TN-68. However, this is mainly an artifact of the differences between the initial steady-state conditions in the two packages, different exterior packaging, and differences in their respective fuel loading. The HI-STAR 100 components enter the fire transient anywhere from 100°F to 200°F (56°C to 111°C) hotter than the corresponding components of the TN-68. These temperature differences are due to the redundant encapsulation provided by the MPC canister in the HI-STAR system, the number of fuel assemblies that the decay heat is distributed over (24 for the HI-STAR 100 versus 68 for the TN-68), and the level of shrouding of the package surface by the support device. HI-STAR 100 is heavily shrouded by its support cradle; the TN-68 outer surface is essentially bare to ambient conditions.

In addition to these essentially incidental differences, there are some small differences in design that affect the rate of heat-up of the outer

shells of the two packages. The TN-68 has a 50% thicker solid outer skin which distributes the heat from the fire transient circumferentially to cooler regions of the package more effectively than the thinner outer skin of the HI-STAR 100 package. The outer skin of the HI-STAR 100 package consists of relatively narrow welded metal strips, rather than a single steel sheet. The 0.19-inch (0.48 cm) fillet welds joining the metal strips (which were explicitly accounted for in the ANSYS model) present an additional barrier to circumferential heat flow in the HI-STAR 100 package outer shell. However, because both packages present a very large thermal mass to the fire and have very similar overall designs, they respond in essentially the same manner to the fire transient. The differences shown in these two sets of results consist mainly of minor time-shifts in the response to the imposed boundary conditions, and in general the behavior of the two sets of curves make them almost indistinguishable.

Peak component temperatures for the HI-STAR 100 over the transient fire simulation are reported in Table 7.2.

Table 7.2. HOLTEC HI-STAR 100 Peak Component Temperatures During Fire Transient

Component	Maximum Temperature (ANSYS) °F (°C)	Time (hours)
Fuel Cladding	887 (475)	32
MPC Basket	878 (470)	9
Boral	876 (469)	9
Canister Shell	1020 (549)	7.3
Inner Shell and Forgings	1444 (784)	6.8
Gamma Shield	1400 (760)	6.8
Package Skin	1831 (999)	6
Lid/Vent/Drain Port Seals	1177 (636)	6.8
Impact Limiter Skin	1826 (997)	6
Impact Limiter Structure	1591 (866)	6.8

7.3 NAC LWT Fire Transient Results

The ANSYS model of the NAC LWT package consists of a total of 50,673 standard computational elements and 12 superelements that are solved for each time step. Similar to the TN-68 and HI-STAR 100 models, this model yields a large amount of output that has been processed to characterize the package response. The following three subsections present the peak temperatures versus time for selected components, as determined with ANSYS for the NAC LWT package subject to the hypothetical fire transient conditions described in Section 6.

7.3.1 LWT During the Fire

Figure 7.15 shows the initial temperature response for the NAC LWT package and ISO container as predicted with ANSYS during the fire portion of the transient. Similar to the HI-STAR 100, the maximum temperature of the exterior surface of the ISO container surrounding the NAC LWT package increases rapidly to a peak temperature of 1592°F (867°C) around 6 hours into the fire. This is roughly 200°F (111°C) below that of the HI-STAR 100 external surface peak temperature, and is due to the substantial view that the hottest portion (top) of the ISO container has of cooler surfaces (i.e., the package body, and the sides and bottom of the ISO container.)

The maximum temperature of the exterior surface of the package is slightly lower, at 1526°F (830°C). The maximum temperature of the cask inner shell material, which defines the primary containment boundary along with the bolted lid, shows a more gradual increase, reaching a peak of 1272°F (689°C) at about 7 hours into the fire.

Unlike the TN-68 and the HI-STAR 100, the internal components of the LWT package, particularly the fuel assembly, exhibit a noticeable

thermal response during the fire. The peak fuel cladding temperature begins to rise at about two hours elapsed time, and the package structural components show a fairly rapid rise in temperature in the first hour of the fire. This occurs primarily because this package has considerably less thermal inertia than the two larger multi-assembly packages. The additional heat transfer paths available into the LWT package are also contributing factors, resulting from the fuel assembly being exposed within a cavity at each end of the cask. As the inner shell surrounding the assembly ends heats up, radiation exchange within the cavities generates cladding temperatures at the ends of the fuel rods that are significantly higher than the temperatures at the center, as illustrated in Figure 7.16.

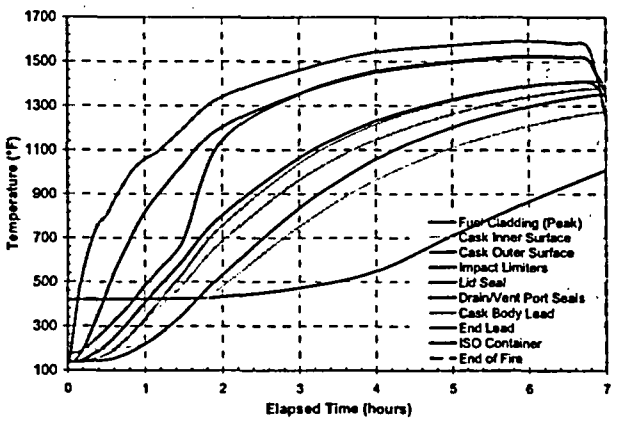

Figure 7.15. NAC LWT Package Component Maximum Temperature Histories During Fire Transient

By the end of the fire (at approximately 7 hours), the predicted peak fuel cladding temperature in the end region of the fuel has reached 1010°F (543°C) and is still rising. This value is approaching (and eventually will exceed—see Section 7.3.2) the currently accepted short term temperature limit of 1058°F (570°C) for Zircaloy clad spent nuclear fuel under accident conditions [23].

Other components of the package, in contrast to the peak cladding temperature, reach their peak temperature values at or very close to the end of the fire. This behavior closely follows the sudden decrease in the external thermal load on the package as the fire burns itself out. This can readily be seen in the peak temperatures reached on the gamma shield and the neutron shielding.

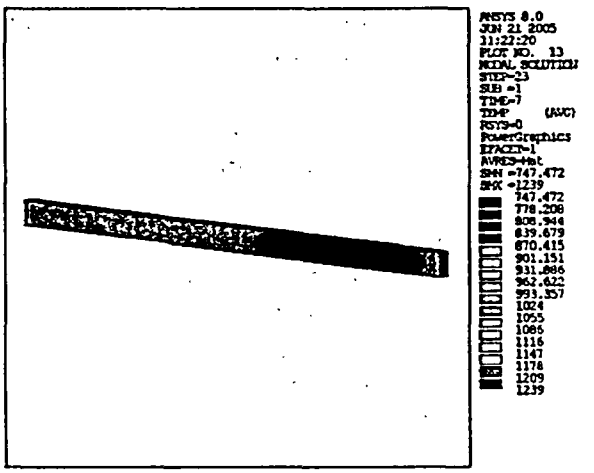

Figure 7.16. Lumped Fuel Assembly Temperature Distribution 7 hr into Transient

The gamma shielding is provided by a lead layer between the inner and outer shells as well as a lead section in the welded base (i.e., the end opposite the package lid). The lead temperature reaches a maximum of 1378°F (748°C) at 6.75 hours elapsed time. This is considerably greater than the established safe operating limit of 600°F (316°C) [11] for this material, and could result in reduced gamma shielding due to melting and slumping of the lead. However, in this calculation the lead is assumed to remains intact, to conservatively maximize heat input during the transient.

Neutron shielding is provided by the tanks of ethylene glycol solution on the package exterior. As described in Section 5.3, the temperatures of the nodes representing the main tank and overflow

tank were monitored for temperatures indicating rupture and evaporation throughout the transient solution. Similar to assumptions in the standard fire analysis included in the SAR [11], the liquid in the tank is expected to lose its shielding capability when the temperature exceeds its 350°F (177°C) boiling point. As noted for the TN-68 and HI-STAR 100 casks, the NAC LWT is also designed to attenuate neutron radiation to acceptable levels (see 10 CFR 71.51 [1]) following an accident without the assistance of the neutron shield material. However, the loss of the neutron shield affects the rate of heat transfer into and out of the cask during and after the fire transient.

As a measure of conservatism, tank rupture was considered to occur only after the minimum ethylene glycol temperature for each tank exceeded 350°F (177°C). This assumption effectively delays rupture to a slightly later point in the transient than might be expected, thus maximizing heat input into the package. The model predicted that the inner neutron shield tank and the outer expansion tank rupture at ~1.5 hours. Following rupture, the effective conductivity of the tank was significantly decreased, due to the ethylene glycol volume being expelled and replaced with air.

7.3.2 LWT Short-Term Post-Fire Response

Figure 7.17 shows the peak temperatures predicted for various components of the package during the first 30 hours of the ANSYS transient simulation based on the NIST simulation results. The cladding peak and average temperatures continue to rise after the fire, just as in the analyses for the TN-68 and HI-STAR 100 packages, and for much the same reason. The ambient conditions in the tunnel immediately following the fire severely retard the rate at which the fuel decay heat can be removed from the package.

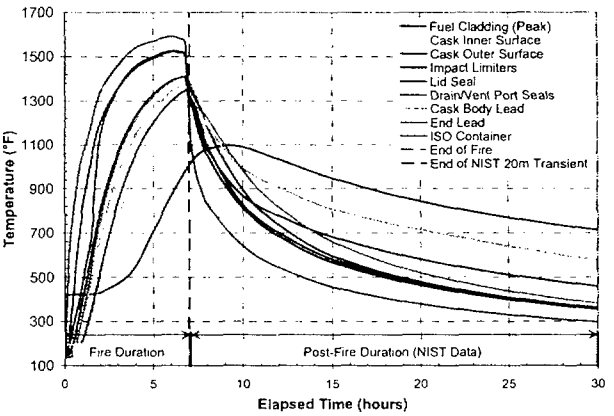

Figure 7.17. NAC LWT Package Component Maximum Temperature Histories for First 30 hr of Fire Transient

However, once the fire is over, the predicted peak temperatures on outboard components (i.e., the ISO container and cask outer surface) begin to drop rapidly in response to the rapid decrease in the boundary temperatures (see Figure 7.18). This figure shows the outer shell surface temperature predicted with ANSYS, compared to the tunnel ceiling temperature and the temperature of the air above the ISO container, derived from the NIST calculations and used as boundary conditions.

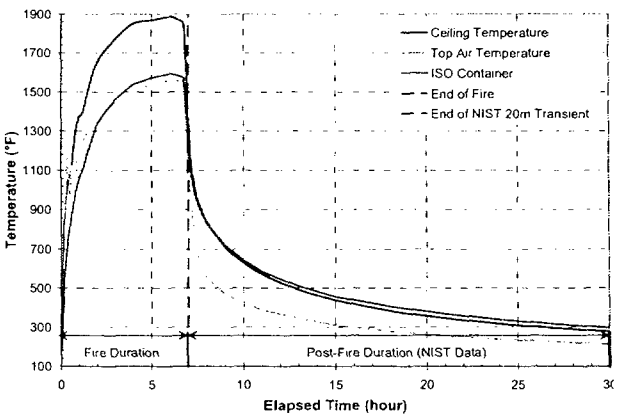

Figure 7.18. Maximum ISO Container Surface Temperature History Compared with NIST Boundary Condition Temperatures

Figure 7.17 shows that the peak temperatures for all package components begin to decrease shortly after the end of the fire. The peak cladding temperature reaches its maximum value of 1099°F (593°C) at 9 hours. This is 41°F (23°C) above the short term limit of 1058°F (570°C), but is still 283°F (157°C) below the temperature at which Zircaloy fuel rods actually fail by burst rupture, which is approximately 1382°F (750°C) [25]. (The maximum temperature for the basket reaches its peak of 1069°F (576°C) at about 8 hours into the transient, but this temperature curve is omitted from Figure 7.17 for clarity.)

As a result of the low thermal inertia of this package, peak temperatures in the various components occur within two hours of the fire being extinguished, rather than 25 or 33 hours later, as in the HI-STAR 100 and TN-68, respectively. Because of the heating of the ends of the fuel rods due to thermal radiation as a result of the fire, the *average* fuel temperature gradually increases to a maximum of 988°F (531°C). This peak is reached at 9 hours elapsed time, as shown in Figure 7.19.

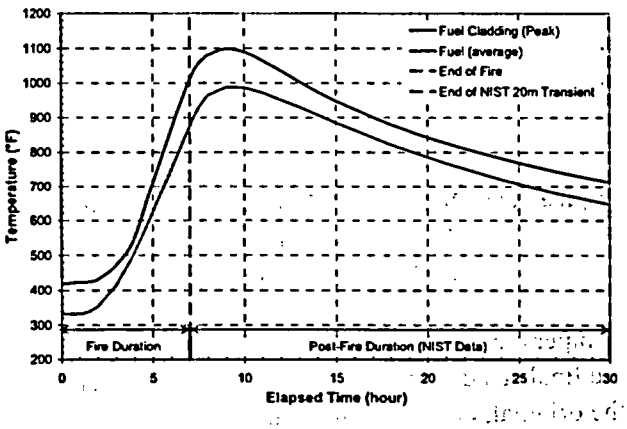

Figure 7.19. Peak and Average Fuel Cladding Temperature Histories for NAC LWT Package During First 30 hr of Fire Transient

The maximum temperature histories of the seals in the drain/vent ports and the lid are shown for the first 30 hours in Figure 7.20. (The calculated values were gathered by querying nodes at the seals' locations, since the seals were not explicitly represented in the model.) The drain and vent ports are sealed with Teflon O-rings. The bolted lid is sealed by both metallic and Teflon O-ring seals. The drain and vent ports reach a maximum temperature of 1410°F (766°C), and the lid seal reaches 1350°F (732°C) at the end of the fire.

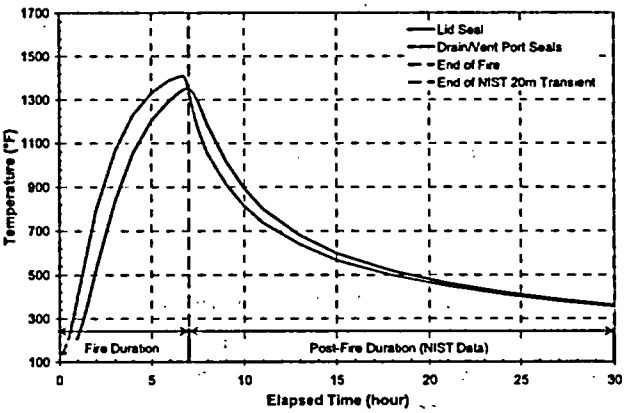

Figure 7.20. Maximum Seal Temperature Histories for Drain/Vent Ports and Package Lid During First 30 hr of Fire Transient

These materials then gradually cool as the transient proceeds into the post-fire cool down. The extreme rise in temperature is due to the low thermal inertia associated with the LWT package and the close proximity of the seals to exterior surfaces subject to thermal radiation from the thin ISO container.

The ISO container is itself subject to thermal radiation and convection heat input from the tunnel environment. If the NAC LWT cask were not enclosed in an ISO container, the cask components would reach even higher temperatures during the postulated accident scenario. However, with or without an ISO container, the predicted

seal temperatures are far greater than the maximum continuous-use seal temperature limits of 735°F (391°C) for Teflon seals and 800°F (427°C) for the metallic seals.

7.3.3 LWT Long-Term Post-Fire Response

As with the TN-68 and HI-STAR 100 analyses, the temperatures predicted in the NIST analysis were extrapolated from 30 hours to 300 hours using a power function in order to realistically model cool down of the tunnel environment. (The extrapolated values are presented in Figures 6.5 and 6.6.)

Peak component temperatures for the LWT over the transient fire simulation are reported in Table 7.3. To explore the effects of prolonged exposure to post-fire conditions in the tunnel, the calculations for the NAC LWT were carried out for the full 300 hours (273 hours after the end of the fire). As discussed previously, this conservative approach is equivalent to assuming that the package will be left in the tunnel indefinitely, without any emergency responder intervention. The same conservative assumptions used in the analysis of the TN-68 and HI-STAR 100 were used to define the convection heat transfer boundary on the NAC LWT package. A purely forced convection heat transfer regime was assumed for the first 30 hours of the simulation, then a purely free convection regime was assumed for the remainder of the calculation ($t \geq 30$ hours).

Figure 7.21 shows the temperature response of the various components of the package for the long term transient calculation to 300 hours. The maximum temperatures were reached within a short time after the end of the fire, and the LWT at 100 hours is very close to its new steady-state condition. This behavior is consistent with its lower thermal inertia, in comparison to the larger multi-assembly packages.

Table 7.3. NAC LWT Peak Component Temperatures During Fire Transient

Component	Maximum Temperature (ANSYS) °F (°C)	Time (hours)
Fuel Cladding	1099 (593)	9
Aluminum PWR Insert	1069 (576)	8
Inner Shell	1272 (689)	7
Lead Gamma Shield	1378 (748)	6.75
Outer Shell	1526 (830)	6
Liquid Neutron Shield	1525 (829)	6
Lid Seal	1350 (732)	6.9
Drain/Vent Ports	1410 (766)	6.75
Impact Limiters	1521 (827)	6
ISO Container	1592 (867)	6

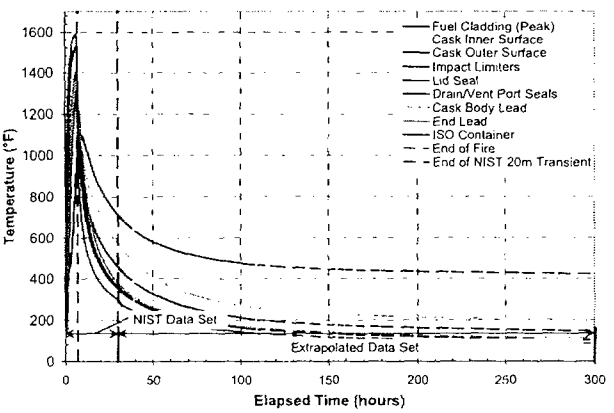

Figure 7.21. NAC LWT Package Component Maximum Temperature Histories During 300 hr Transient

Temperature distributions within the package for the final steady state will be slightly different than the original, due to the dissipation of the liquid neutron shield, changes in the surface emissivities because of the fire, and tunnel ambient conditions that differ from the hot-normal conditions assumed for the pre-fire steady state (i.e., lower ambient temperature and the absence of solar insolation.)

8 POTENTIAL CONSEQUENCES

USNRC Staff evaluated the potential for a release of radioactive material from each of the three transportation casks (HI-STAR 100, TN-68 and NAC LWT) analyzed for the Baltimore tunnel fire scenario. The analysis indicates that there would be no release expected from the HI-STAR 100 cask. However, the possibility of a small release cannot be entirely ruled out for either the TN-68 or NAC LWT casks, because cask temperatures during the fire or cool-down period exceed the long-term service temperature limits for the cask lid seals.

Staff performed an analysis to determine the magnitude of any potential release. Based on that analysis (which is described below), it was determined that any potential release from either the TN-68 or NAC LWT cask would be small—less than an A_2 quantity.[6] The potential release would not involve a release of spent fuel or fission products, but could possibly result from CRUD spalling off the fuel rods.

8.1 Results for the HI-STAR 100 Cask

The thermal analysis shows that the HI-STAR 100 cask design would maintain three important barriers throughout the fire and subsequent cool down period, which would prevent the release of radioactive materials. The welded inner canister remains intact and leak tight, preventing any release from the fuel rods themselves or as a result of CRUD spalling off the fuel rods. The temperature of the fuel cladding would peak at about 990°F (532°C), well below the short-term temperature limit of 1058°F (570°C) for Zircaloy cladding and significantly below its projected burst temperature of 1382°F (750°C). This would prevent the release of fission products from the fuel rods. The maximum temperature of 1177°F (636°C) predicted for the cask's metallic O-rings is below their rated continuous-use service temperature of 1200°F (649°C). Thus, the O-rings would not be expected to significantly degrade.

8.2 Results for the TN-68 Cask

The thermal analysis for the TN-68 cask shows that during the Baltimore tunnel fire scenario, this cask design would maintain the integrity of the fuel cladding, which is the single most important barrier to prevent the release of radioactive materials. At approximately 40 hours elapsed time, the temperature of the fuel cladding would peak at about 845°F (452°C), well below the short-term temperature limit of 1058°F (570°C) for Zircaloy cladding and significantly below its projected burst temperature of 1382°F (750°C). This would prevent the release of fission products from the fuel rods. However, the metallic helicoflex seals used on the TN-68 lid and vent and drain ports reach a maximum temperature of 811°F (433°C) by the end of the fire (at 7 hours elapsed time.) This exceeds the seals' rated service temperature of 536°F (280°C) by 275°F (153°C).

Exceeding the service temperature of the seals on the TN-68 cask lid or vent and drain ports means that there is a potential for a release to occur. Potential releases would be limited, however, by the narrow convoluted flow paths of the drain and vent ports and by the tight

[6] An A_2 quantity represents the threshold below which an accident resistant package is not required. The acceptance requirement for Type B packages is that they release less than an A_2 quantity/week after being subjected to the hypothetical accident conditions in 10 CFR Part 71 [1].

clearances of the close metal-to-metal contact between the lid and cask body. The close contact is maintained by the pre-load created by the initial torque on the lid bolts. Because the fuel cladding remains intact, it is not expected that any radioactive material would be released from inside the fuel rods. This limits any release from the cask to CRUD particles that may flake off or spall from individual fuel rods.

The amount of releasable CRUD in the TN-68 cask was estimated using data developed by Sandia National Laboratory for analysis of CRUD contribution to shipping cask containment requirements [26], based on cask contents consisting of 68 BWR fuel assemblies, each assembly containing 49 fuel rods. An estimate of the maximum "spot" CRUD activity shows that for 90% of BWR spent fuel rods the maximum activity is 300μCi/cm^2 or less [26, Table I-17]. The ratio of the peak to average concentration on the rod surface (i.e., the maximum "spot" CRUD activity over the average value) varies by a factor of two for BWR fuel rods [26, Table I-17].

The CRUD activity estimates [26] are based on newly discharged spent nuclear fuel. The CRUD activity is expected to decay by a factor of one-half for five-year cooled fuel, based on the decay rate for Co^{60}. This proves to be a good approximation because 98% of the activity for five-year cooled BWR fuel comes from Co^{60}. Based on this data, the average CRUD activity for a BWR rod with a surface area of 1600 cm^2 is about 0.12 Ci for five-year cooled fuel. The average CRUD activity for a typical 7 x 7 BWR assembly is about 5.9 Ci.

The amount of CRUD that might flake or spall from the surface of a BWR rod due to thermal stresses induced by temperature change in the fuel rods is estimated to be a maximum of 15% [26, Table I-10]. The major driving force for material release results from the increased gas pressure inside the cask due to increases in internal temperature. The temperature change in the cask is bounded by the difference between the maximum gas temperature predicted during the fire transient and the gas temperature at the time the cask is loaded. For this analysis, the loading temperature is defined as 100°F (38°C), based on the temperature reported in the SAR [9]. The maximum gas temperature is assumed to be the maximum peak clad temperature predicted during the transient. This yields a conservative estimate of the temperature change.

A deposition factor of 0.90 was used to account for the settling and deposition of CRUD particles on cask surfaces and fuel assemblies. The deposition factor was developed as part of NRC's security assessments for spent nuclear fuel transport and storage casks, and is based on an analysis of the gravitational settling of small particles. The value of 0.90 is conservative because it does not consider the effects of particle conglomeration and plugging. It is also consistent with the values used in other studies [25]. The major assumptions used to estimate the potential CRUD release are given in Table 8.1.

To estimate the potential release from the TN-68 cask, a methodology similar to that developed by Sandia National Laboratory (for NUREG-6672 [25]) was used. This methodology was developed for evaluation of the generic risks associated with the transport of spent fuel by truck and rail from commercial power plants to potential interim storage and disposal sites.

The potential release from the TN-68 cask can be estimated by adapting the equation developed in NUREG/CR-6672 ([25]) to estimate the releases from a severe fire accident. The estimated release is given by the relationship

$$R = C_I S(1-D)\left(1-\frac{T_i}{T_p}\right)$$

where R = release (curies)
C_I = amount of CRUD on fuel assemblies (curies)
S = fraction of CRUD released due to heating
D = deposition factor
T_p = peak internal temperature (°R)
T_i = initial internal temperature (°R)

Table 8.1. Assumptions Used for Release Estimate for TN-68 Cask

Parameter	Assumed value
Number of Assemblies in TN-68 Cask	68 BWR
Rods per Assembly	49
Maximum "spot" CRUD Activity on Fuel Rod	300μCi/cm^2
Peak to axial average variation	2
CRUD decay factor (5 yr) (based on Co^{60})	0.5
Average surface area per rod	1600 cm^2
Average CRUD Activity on BWR Fuel Rod (5 yr cooled)	0.12 Ci
Average CRUD Activity on BWR Assembly (5 yr cooled)	5.9 Ci
Fraction of CRUD released due to heating	0.15
Deposition Factor	0.90

Table 8.2 shows the results obtained when this equation is applied using the parameter values from Table 8.1 and the temperatures predicted for the TN-68 cask in this accident scenario.

Table 8.2. Potential Release Estimate for TN-68 Cask

Initial temperature °F (°R)	Peak temperature °F (°R)	Potential release (curies)
100 (560)	845 (1305)	3.4

The potential release from the TN-68 cask based on five-year cooled fuel is estimated to be approximately 3.4 curies of Co^{60}. Since the A_2 value for Co^{60} is 11 curies, the potential release is about 0.3 of an A_2 quantity (see footnote 6).

8.3 Results for the NAC LWT Cask

The thermal analysis for the NAC LWT cask shows that this cask design would also maintain the integrity of the fuel cladding during the Baltimore tunnel fire scenario, and thus would maintain the single most important barrier to prevent the release of radioactive materials. The peak temperature of the fuel cladding is conservatively predicted to reach 1099°F (593°C), a temperature that is below the projected burst temperature of 1382°F (750°C) for Zircaloy cladding. This peak temperature occurs at approximately 9 hours after the start of the fire (i.e., after a 7-hour fire and 2-hour cool down period).

However, at about 6.9 hours elapsed time, the maximum temperature predicted for the Teflon and metallic helicoflex seals used on the NAC LWT lid reaches 1350°F (732°C). This value exceeds the continuous-use rated service temperature limits of 735°F (391°C) for the Teflon seals and 800°F (427°C) for the metallic helicoflex seals. Similarly, the peak temperature experienced by the vent and drain port seals (1410°F (766°C) at approximately 6.8 hours elapsed time), exceeds the rated long-term service temperature of the Teflon seal material.

Exceeding the long-term service temperature of the seals on the NAC LWT cask lid or vent and drain ports means that there is a potential for a release to occur. Potential releases would be limited, however, by the narrow, convoluted flow paths of the drain and vent ports and by the tight clearances of the close metal-to-metal

contact between the lid and cask body. The close contact is maintained by the pre-load created by the initial torque on the lid bolts. Because the fuel cladding remains intact, it is not expected that any radioactive material would be released from inside the fuel rods. This limits any release from the cask to CRUD particles that may flake off or spall from individual fuel rods.

The amount of releasable CRUD in the NAC LWT cask was based on contents consisting of one PWR fuel assembly containing 289 fuel rods. An estimate of the maximum "spot" CRUD activity shows that for 90% of PWR spent fuel rods the maximum activity is $20\mu Ci/cm^2$ or less [26, Table I-15]. The ratio of the peak (i.e., the maximum "spot" CRUD activity) to average concentration on the rod surface varies by a factor of two for PWR fuel rods [26, Table I-12]. The CRUD activity estimates [26] are based on newly discharged spent nuclear fuel. The CRUD activity is expected to decay by a factor of one-half for five-year cooled fuel, based on the decay rate for Co^{60}. This proves to be a good approximation because 92% of the activity for five-year cooled PWR fuel comes from Co^{60}.

Based on these data, the average CRUD activity for a PWR rod with a surface area of 1200 cm^2 is about 0.006 curies for five-year cooled fuel. The average CRUD activity for a 17 x 17 PWR assembly is about 1.73 Ci. The amount of CRUD that would flake or spall from the surface of a PWR rod due to temperatures calculated for the fuel rods in the thermal analysis is estimated to be a maximum of 15% [26, Table I-10]. Finally, a deposition factor of 0.90 was used to account for the deposition of CRUD particles on cask surfaces and fuel assemblies.

The major assumptions used to estimate CRUD release are given in Table 8.3. The potential release from the NAC LWT cask can be estimated from the same equation used for the TN-68 release estimate, as described in Section 8.2. The major driving force for material release results from the increased gas pressure inside the cask due to increases in internal temperature. The temperature change is bounded by the difference between the maximum gas temperature predicted during the fire transient and the gas temperature inside the cask at the time the cask is loaded.

For this analysis, the loading temperature is defined as 100°F (38°C), based on the temperature reported in the SAR [11]. The maximum gas temperature is assumed to be the maximum peak clad temperature predicted during the transient.

Table 8.3. Assumptions Used for Release Estimate for NAC LWT Cask

Parameter	Assumed value
Number of Assemblies in Cask	1 PWR
Rods per Assembly	289
Maximum "spot" CRUD Activity on Fuel Rod	$20\mu Ci/cm^2$
Peak to axial average variation	2
CRUD decay factor (5 yr) (based on Co^{60})	0.5
Average surface area per rod	1200 cm^2
Average CRUD Activity on PWR Fuel Rod (5 yr cooled)	0.006 Ci
Average CRUD Activity on PWR Assembly (5 yr cooled)	1.73 Ci
Fraction of CRUD released due to heating	0.15
Deposition Factor	0.90

Table 8.4 shows the results obtained when this equation is applied using the parameter values from Table 8.3 and the temperatures predicted for the NAC LWT cask in this accident scenario.

The potential release from the NAC LWT cask based on five-year cooled fuel is estimated to be approximately 0.02 curies of Co^{60}. Since the A_2 value for Co^{60} is 11 curies, the potential release is about 0.002 of an A_2 quantity (see footnote 6).

Table 8.4. Potential Release Estimate for NAC LWT Cask

Initial temperature °F (°R)	Peak temperature °F (°R)	Potential release (curies)
100 (560)	1099 (1559)	0.02

8.4 Summary of Potential Releases

The FDS model developed by NIST, as verified by the results of the NTSB investigation of the fire and the materials exposure analysis by CNWRA, has provided a detailed picture of the duration and severity of the fire that occurred in the Howard Street tunnel in Baltimore on July 18, 2001. The fire transient analyses performed with ANSYS and COBRA-SFS using the FDS simulation results as boundary conditions have shown the robust nature of the larger spent fuel transportation package designs (HI-STAR 100 and TN-68). The predicted response of the smaller LWT package, if hauled by rail and exposed to the same tunnel fire environment, indicates more component degradation.

For the TN-68 and the NAC LWT, the maximum temperatures predicted in the regions of the lid and the vent and drain ports exceed the seals' rated service temperatures, making it possible for a small release to occur, due to CRUD that might spall off the surfaces of the fuel rods. However, any release is expected to be very small due to a number of factors. These include (1) the tight clearances maintained between the lid and cask body by the closure bolts, (2) the low pressure differential between the cask interior and exterior, (3) the tendency of such small clearances to plug, and (4) the tendency of CRUD particles to settle or plate out.

USNRC staff evaluated the radiological consequences of the package responses to the Baltimore tunnel fire. The results of this evaluation strongly indicate that neither spent nuclear fuel (SNF) particles nor fission products would be released from a spent fuel shipping cask involved in a severe tunnel fire such as the Howard Street Tunnel fire in Baltimore. None of the three cask designs analyzed for the Baltimore Tunnel fire scenario (TN-68, HI-STAR 100, and NAC LWT) experienced internal temperatures that would result in rupture of the fuel cladding. Therefore, radioactive material (i.e., SNF particles or fission products) would be retained within the fuel rods. There would be no release from the HI-STAR 100, because the inner welded canister remains leak tight and all seals remain intact. The potential releases calculated for the TN-68 rail cask and the NAC LWT cask (as a consequence of exceeding seal temperature limits) indicate that any release of CRUD from either cask would be very small - less than an A_2 quantity (see footnote 6)

9 REFERENCES

1. 10 CFR 71. Jan. 1, 2003. *Packaging and Transportation of Radioactive Material.* Code of Federal Regulations, U.S. Nuclear Regulatory Commission, Washington D.C.

2. Michener TE, DR Rector, JM Cuta, RE Dodge, and CW Enderlin. 1995. *COBRA-SFS: A Thermal-Hydraulic Code for Spent Fuel Storage and Transportation Casks.* PNL-10782, Pacific Northwest National Laboratory, Richland, Washington.

3. ANSYS, Inc. 2003. "ANSYS Users Guide for Revision 8.0," ANSYS, Inc., Canonsburg, Pennsylvania.

4. McGrattan KB and A Hammins. February 2003. A. *Numerical Simulation of the Howard Street Tunnel Fire, Baltimore, Maryland, July 2001.* NUREG/CR-6793, National Institute of Standards and Technology, Washington D.C.

5. Garabedian AS, DS Dunn, and AH Chowdhury. March 2003. Center for Nuclear Waste Regulatory Analysis, *Analysis of Rail Car Components Exposed to a Tunnel Fire Environment,* NUREG/CR-6799, Center for Nuclear Waste Regulatory Analysis, Washington, D.C.

6. McGrattan KB, HR Baum, RG Rehm, GP Forney, JE Floyd, and S Hostikka. November 2001. *Fire Dynamics Simulator (Version 2), User's Guide.* NISTIR 6784, National Institute of Standards and Technology, Gaithersburg, Maryland.

7. McGrattan KB, HR Baum, RG Rehm, GP Forney, JE Floyd, and S Hostikka. November 2001. *Fire Dynamics Simulator (Version 2), Technical Reference Guide.* NISTIR 6783, National Institute of Standards and Technology, Gaithersburg, Maryland.

8. Bechtel/Parsons Brinkerhoff, Inc. November 1995. *Memorial Tunnel Fire Ventilation Test Program, Comprehensive Test Report,* Prepared for Massachusetts Highway Department and Federal Highway Administration.

9. NRC Docket Number 71-9293. May 19, 2000. *TN-68 Transport Packaging Safety Analysis Report,* Rev. 2, TransNuclear Incorporated, New York.

10. NRC Docket Number 72-1008. March 30, 2001. *Final Safety Analysis Report for Holtec International Storage Transport and Repository Cask System* (HI-STAR 100 Cask System). HI-210610, Vol. I and II. HOLTEC, Marlton, New Jersey.

11. NRC Docket Number 71-9225. *Legal Weight Truck Transport (LWT) Packaging Safety Analysis Report,* July 2000, Rev. 2; September 2001, Rev. 33; Rev. 34. Nuclear Assurance Corporation, Alanta, Georgia.

12. 49 CFR. 171–184, Subchapter C. Oct 1, 2003. *Hazardous Materials Regulations.* Code of Federal Regulations, U.S. Department of Transportation, Washington, D.C.

13. Creer JM, TE Michener, MA McKinnon, JE Tanner, ER Gilbert, and RL Goodman. 1987. *The TN-24P PWR Spent-Fuel Storage Cask: Testing and Analysis.* EPRI-NP-5128/PNL-6054, Electric Power Research Institute, Palo Alto, California.

14. Rector DR, RA McCann, UP Jenquin, CM Heeb, JM Creer, and CL Wheeler. 1986. *CASTOR-1C Spent Fuel Storage Cask Decay Heat, Heat Transfer and Shielding Analysis*. PNL-5974. Pacific Northwest Laboratory, Richland, Washington.

15. Lombardo NJ, JM Cuta, TE Michener, DR Rector, and CL Wheeler. 1986. *COBRA-SFS: A Thermal-Hydraulic Analysis Computer Code, Volume III: Validation Assessments*, PNL-6048 Vol. III. Pacific Northwest Laboratory, Richland, Washington.

16. Bahney RH III and TL Lotz. July 1996. *Spent Nuclear Fuel Effective Thermal Conductivity Report*, BBA000000-01717-5705-00010 Rev. 00. TRW Environmental Safety Systems, Inc., Fairfax, Virginia.

17. HEXCEL. 2003. HexWeb Honeycomb Attributes and Properties. Available at http://www.hexcelcomposites.com/Markets/Products/Honeycomb/Hexweb_attrib/hwp_02.htm. Hexcel, Stamford, Connecticut.

18. Guyer EC and DL Brownell, editors. 1989. *Handbook of Applied Thermal Design.* McGraw-Hill, Inc., New York, p. 1-42.

19. Kreith F and MS Bohn. 2001. *Principles of Heat Transfer, 6th Edition.* Brooks/Cole, Pacific Grove, California.

20. Holman JP. 1986. *Heat Transfer, 6th Edition.* McGraw-Hill, Inc., New York.

21. Kreith F. 1976. *Principles of Heat Transfer, 3rd Edition.* Intext Education Publishers, New York.

22. Bucholz JA. January 1983. *Scoping Design Analyses for Optimized Shipping Casks Containing 1-, 2-, 3-, 5-, 7-, or 10-year old PWR Spent Fuel.* ORNL/CSD/TM-149. Oak Ridge National Laboratory, Oak Ridge, Tennessee.

23. U.S. Nuclear Regulatory Commission. January 1997. "Standard Review Plan for Dry Cask Storage Systems." NUREG-1536, USNRC, Washington, DC.

24. Johnson AB and ER Gilbert. September 1983. *Technical Basis for Storage of Zircaloy-Clad Spent Fuel in Inert Gases*, PNL-4835. Pacific Northwest Laboratory, Richland, Washington.

25. Sprung JL, DJ Ammerman, NL Breivik, RJ Dukart, and FL Kanipe. March 2000. *Reexamination of Spent Fuel Shipment Risk Estimates*, NUREG/CR-6672, Vol. 1 (SAND2000-0234). Sandia National Laboratories, Albuquerque, New Mexico.

26. Sandoval RP, RE Einziger, H Jordan, AP Malinauskas, and WJ Mings. January 1991. *Estimate of CRUD Contribution to Shipping Cask Containment Requirements*, SAND88-1358. Sandia National Laboratories, Albuquerque, New Mexico.

Appendix A

Material Properties for COBRA-SFS Model of TN-68 Package

Table A.1. Internal Fill Gas—Helium at Atmospheric Pressure

Temperature (°F)	Enthalpy (Btu/lbm)	Thermal Conductivity (Btu/hr-ft-°F)	Specific Heat (Btu/lbm-°F)	Specific Volume (ft^3/lbm)	Viscosity (lbm/hr-ft)
0	100	0.078	1.24	83.33	0.0410
200	348	0.097	1.24	119.76	0.0533
400	596	0.115	1.24	156.25	0.0641
600	844	0.129	1.24	192.31	0.0727
800	1092	0.138	1.24	229.36	0.0823
1000	1340	0.138	1.24	265.25	0.0907
2552	3264	0.138	1.24	549.00	0.1138

Table A.2. External Ambient Air at Atmospheric Pressure

Temperature (°F)	Enthalpy (Btu/lbm)	Thermal Conductivity (Btu/hr-ft-°F)	Specific Heat (Btu/lbm-°F)	Specific Volume (ft^3/lbm)	Viscosity (lbm/hr-ft)
60	124.5	0.0146	0.24	13.5669	0.0434
300	182.1	0.0193	0.243	19.8325	0.058
400	206.5	0.0212	0.245	22.4432	0.063
500	231.1	0.0231	0.247	25.0539	0.068
600	256	0.025	0.25	27.6645	0.072
700	281.1	0.0268	0.253	30.2752	0.077
800	306.7	0.0286	0.256	32.8859	0.081
900	332.5	0.0303	0.259	35.4966	0.085
1000	358.6	0.0319	0.262	38.1072	0.0889
2000	617.2	0.0471	0.2586	64.214	0.1242
4000	1522	0.0671	0.4524	116.428	0.1242

Table A.3. Summary of All Solid Material Properties Pre-Fire

Specific Heat (Btu/lbm-°F)	Density (lbm/ft^3)	Thermal Conductivity (Btu/hr-ft-°F)	Emissivity	Description
0.129	483.8	22.92	0.3	gamma shielding (SA-517 grade 70 carbon steel)
0.13	499.4	10.44	0.3	fuel tubes (SA-240 stainless steel)
0.214	165.9	41.72	0.3	borated aluminum poison plates
0.311	98.5	4.34	N/A	neutron shield (borated polyester)
0.228	165.9	99.84	0.3	Aluminum alloy basket rails
0.118	483.8	22.92	0.3	cask outer shell[a]
0.228	165.9	84.00	N/A	aluminum in neutron shield and thermal shield between cask and bottom impact limiter
0.420	23.1	0.064	N/A	wooden impact limiters (covered with sheet steel)
0.420	11.0	0.053	N/A	thin top layer of wood on impact limiter ends (covered with sheet steel)

[a]Based on nominal emissivity for carbon steel. SAR analyses use emissivity of 0.9 for painted cask surface, but cask specifications allow option for unpainted outer surface.

Table A.4. Summary of All Solid Material Properties Post-Fire

Specific Heat (Btu/lbm-°F)	Density (lbm/ft^3)	Thermal Conductivity (Btu/hr-ft-°F)	Emissivity	Description
0.129	483.8	22.92	0.3	gamma shielding (SA-517 grade 70 carbon steel)
0.13	499.4	10.44	0.3	fuel tubes (SA-240 stainless steel)
0.214	165.9	41.72	0.3	borated aluminum poison plates
0.26	0.027	0.03	N/A	hot air (replaces polyresin neutron shield vaporized in fire)
0.228	165.9	99.84	0.3	aluminum alloy basket rails
0.118	483.8	22.92	0.8	steel shell (SAR value post-fire is 0.95 for charred cask surface emissivity)
0.228	165.9	84.00	0.9	aluminum in neutron shield; inner and outer ring after polyresin evaporates
1020.0	134.8	0.00735	0.8	charcoal (impact limiters after the fire)
			0.9	tunnel wall

COBRA-SFS Material Properties Compared with Published SAR Values

Table A.5. BWR Spent Fuel Assemblies

SAR values determined using k-effective model for homogeneous representation of fuel rods and helium gas within fuel tube.

Temperature (°F)	Transverse Thermal Conductivity (Btu/hr-ft-°F)	Axial Thermal Conductivity (Btu/hr-ft-°F)	Specific Heat (Btu/lbm-°F)	Density (lbm/ft^3)
195.8	0.0157		0.055	257.5
200.0		0.058		
268.4	0.0178			
365.9	0.0206			
400.0		0.0646		
463.7	0.0239			
561.8	0.0277			
600.0		0.0709		
660.3	0.0319			
758.9	0.0367			
800.0		0.0769	0.055	257.5

COBRA-SFS input— BWR fuel rods; conservative values at nominal operating temperature and above.

Component	Thermal Conductivity (Btu/hr-ft-°F)	Specific Heat (Btu/lbm-°F)	Density (lbm/ft^3)
fuel pellet:	3.0	0.059	655.0
cladding:	10.0	0.1	409.0

Table A.6. Stainless Steel Type 304/304L (for fuel tubes)

SAR values			
Temperature (°F)	**Thermal Conductivity (Btu/hr-ft-°F)**	**Specific Heat (Btu/lbm-°F)**	**Density (lbm/ft^3)**
70	7.56	0.111	499.4
100	8.76		
200	9.36	0.124	
400	10.44	0.130	
600	11.28	0.134	
800	12.24	0.140	
1000	13.2		499.4
COBRA-SFS input—selected conservative representative values at nominal operating temperature and above			
all	10.44	0.13	499.4

Table A.7. Poison Plates (borated aluminum or boron carbide/aluminum matrix)

SAR values			
Temperature (°F)	**Thermal Conductivity (Btu/hr-ft-°F)**	**Specific Heat (Btu/lbm-°F)**	**Density (lbm/ft^3)**
68	69.36	0.214	169.3
212	83.76		
482	86.64		
571	86.64	0.214	169.3
COBRA-SFS input—selected conservative values based on range of allowable fabrication variations, as described for cask specifications in SAR.			
all	41.72	0.214	165.9

Table A.8. Aluminum Type 6060 (for basket support rails and shims)

SAR values			
Temperature (°F)	**Thermal Conductivity (Btu/hr-ft-°F)**	**Specific Heat (Btu/lbm-°F)**	**Density (lbm/ft^3)**
70	96.12	0.218	165.9
100	96.96	0.219	
150	98.04	0.223	
200	99	0.225	
250	99.84	0.228	
300	100.56	0.23	
350	101.28	0.233	
400	101.88	0.234	165.9
COBRA-SFS input—selected conservative representative values at nominal operating temperature and above.			
all	99.84	0.228	165.9

Table A.9. Carbon Steel SA-516 Grade 70 (for inner and outer gamma shield and lid)

SAR values			
Temperature (°F)	**Thermal Conductivity (Btu/hr-ft-°F)**	**Specific Heat (Btu/lbm-°F)**	**Density (lbm/ft^3)**
70	22.92	0.109	483.8
200	23.76	0.118	
400	23.88	0.129	
600	22.92	0.139	
800	21.6	0.152	
1000	20.16	0.169	
1200	18.24	0.206	
1400	15.48	0.184	483.8
COBRA-SFS input—selected conservative representative values at nominal operating temperature and above.			
all	22.92	0.129	483.8

Table A.10. Neutron Shield (polyester resin with aluminum boxes)

SAR values—properties are composite values for polyester resin and aluminum boxes modeled as single homogeneous material.			
Temperature (°F)	**Thermal Conductivity (Btu/hr-ft-°F)**	**Specific Heat (Btu/lbm-°F)**	**Density (lbm/ft^3)**
all	0.0996	0.311	98.5
COBRA-SFS input—selected conservative representative values at nominal operating temperature and above.			
borated polyester	4.34	0.311	98.5
aluminum	84.00	0.228	165.9

Table A.11. Carbon Steel SA-350 grade LF3 (for cask outer shell)

SAR values			
Temperature (°F)	**Thermal Conductivity (Btu/hr-ft-°F)**	**Specific Heat (Btu/lbm-°F)**	**Density (lbm/ft^3)**
70	23.64	0.106	489.0
100	23.88	0.11	
200	24.36	0.118	
400	24.24	0.128	
600	23.16	0.137	
800	21.72	0.149	
1000	20.04	0.165	
1200	18.24	0.189	
1400	15.36	0.406	489.0
COBRA-SFS input—typical values for carbon steel at nominal operating temperature and above, based on range of allowable fabrication variations described for cask specifications in SAR.			
all	22.92	0.118	483.8

Table A.12. Impact Limiters (wood covered with sheet steel)

SAR values—none provided; SAR analyses assume impact limiters act as perfect insulators on cask ends for normal, off-normal, and fire accident conditions.			
COBRA-SFS input—selected conservative representative values at nominal operating temperature and above.			
Material	**Thermal Conductivity (Btu/hr-ft-°F)**	**Specific Heat (Btu/lbm-°F)**	**Density (lbm/ft^3)**
redwood	0.064	0.311	98.5
balsa	0.053	0.228	165.9
carbon steel	22.92	0.118	483.8
charcoal	0.00735	1020.0	134.8

Table A.13. Air (replacing neutron shield polyethylene after fire)

SAR values			
Temperature (°F)	**Thermal Conductivity (Btu/hr-ft-°F)**	**Specific Heat (Btu/lbm-°F)**	**Density (lbm/ft^3)**
81	0.0156	0.231	0.0734
261	0.0192	0.237	0.0551
441	0.0228	0.239	0.0440
621	0.0264	0.246	0.0367
981	0.0336	0.264	0.0275
COBRA-SFS input—selected representative values at immediate post-fire temperature and above.			
all	0.03	0.26	0.0270

Appendix B

Material Properties for ANSYS Model of HI-STAR 100 Package

Table B.14. Homogeneous Fuel Region for Westinghouse 17x17 OFA

Temperature (°F)	Thermal Conductivity (Btu/hr-in-°F) (x)	Thermal Conductivity (Btu/hr-in-°F) (y)	Thermal Conductivity (Btu/hr-in-°F) (z)	Density (lbm/in^3)	Specific Heat (Btu/lbm-°F)	Description
0	0.04412	0.04412	0.06256	0.14353	0.05869	Fuel Region (2.25 multiplier against helium contribution to account for limited convection and pressurization enhancement)
100	0.04412	0.04412	0.06256	0.14353	0.05869	
200	0.04412	0.04412	0.06256	0.14352	0.05869	
300	0.05078	0.05078	0.06509	0.14352	0.05869	
400	0.05895	0.05895	0.06797	0.14352	0.05869	
500	0.06837	0.06837	0.07082	0.14352	0.05869	
600	0.07834	0.07834	0.07391	0.14352	0.05869	
700	0.08920	0.08920	0.07756	0.14352	0.05869	
800	0.09508	0.09508	0.08121	0.15352	0.05869	
900	0.09508	0.09508	0.08484	0.15352	0.05869	
1000	0.09508	0.09508	0.08600	0.15352	0.05869	

Table B.15. Alloy-X

Temperature (°F)	Thermal Conductivity (Btu/hr-in-°F) (x)	Thermal Conductivity (Btu/hr-in-°F) (y)	Thermal Conductivity (Btu/hr-in-°F) (z)	Density (lbm/in^3)	Specific Heat (Btu/lbm-°F)	Description
200	0.70000	*	*	0.28993	0.12000	Basket Plates, Basket Supports, Boral Plate Sheathing, MPC shell, impact limiter skin shell
450	0.81667	*	*			
700	0.91667	*	*			
1400	1.19670	*	*			

Table B.16. Helium

Temperature (°F)	Thermal Conductivity (Btu/hr-in-°F) (x)	Thermal Conductivity (Btu/hr-in-°F) (y)	Thermal Conductivity (Btu/hr-in-°F) (z)	Density (lbm/in^3)	Specific Heat (Btu/lbm-°F)	Description
0	0.00650	*	*	6.90E-06	1.24000	gas conduction between MPC and cask
200	0.00808	*	*	4.81E-06		
400	0.00958	*	*	3.69E-06		
600	0.01075	*	*	2.99E-06		
800	0.01150	*	*	2.52E-06		
1400	0.01370	*	*	1.71E-06		

Table B.17. Helium (2.25 multiplier to account for limited convection and pressurization enhancement)

Temperature (°F)	Thermal Conductivity (Btu/hr-in-°F) (x)	Thermal Conductivity (Btu/hr-in-°F) (y)	Thermal Conductivity (Btu/hr-in-°F) (z)	Density (lbm/in^3)	Specific Heat (Btu/lbm-°F)	Description
0	0.01400	*	*	6.90E-06	1.24000	Conduction in: central core region, between guide tubes and basket plates, between fuel and compartments, and between basket and MPC Shell
200	0.01740	*	*	4.81E-06		
400	0.02063	*	*	3.69E-06		
600	0.02315	*	*	2.99E-06		
800	0.02476	*	*	2.52E-06		
1400	0.02950	*	*	1.71E-06		

Table B.18. Boral Plates (includes 0.004" helium gap and gap radiation on both sides of Boral)

Temperature (°F)	Thermal Conductivity (Btu/hr-in-°F) (x)	Thermal Conductivity (Btu/hr-in-°F) (y)	Thermal Conductivity (Btu/hr-in-°F) (z)	Density (lbm/in^3)	Specific Heat (Btu/lbm-°F)	Description
0	0.30836	4.62020	4.62020	0.08390	0.24762	parallel to thickness (switch x & y to define cross-width)
100	0.34331	4.62550	4.62550	0.08390		
200	0.37738	4.64850	4.64850	0.08390		
300	0.40969	4.69040	4.69040	0.08390		
400	0.44166	4.73250	4.73250	0.08390		
500	0.46611	4.74620	4.74620	0.08390		
600	0.49024	4.75200	4.75200	0.08390		
700	0.50544	4.73700	4.73700	0.08390		
800	0.52053	4.72210	4.72210	0.08390		
900	0.53517	4.70710	4.70710	0.08390		
1000	0.54970	4.69220	4.69220	0.08390		
1100	0.56438	4.68350	4.68350	0.08390		

Table B.19. Carbon Steel (SA-516, Gr. 70)

Temperature (°F)	Thermal Conductivity (Btu/hr-in-°F) (radial)	Thermal Conductivity (Btu/hr-in-°F) (circumferential)	Thermal Conductivity (Btu/hr-in-°F) (axial)	Density (lbm/in^3)	Specific Heat (Btu/lbm-°F)	Description
200	0.17409	2.03330	2.03330	0.28299	0.10000	Gamma Shield with 0.01" air gaps between plates
450	0.22634	1.99170	1.99170			
700	0.28273	1.86670	1.86670			
1400	0.44136	1.46670	1.46670			

Table B.20. Carbon Steel (SA-515, Gr. 70)

Temperature (°F)	Thermal Conductivity (Btu/hr-in-°F) (x)	Thermal Conductivity (Btu/hr-in-°F) (y)	Thermal Conductivity (Btu/hr-in-°F) (z)	Density (lbm/in^3)	Specific Heat (Btu/lbm-°F)	Description
200	2.43330	*	*	0.28299	0.10000	For radial channels of overpack and enclosure of shells of overpack (Fins)
450	2.25830	*	*			
700	2.05000	*	*			
1400	1.46670	*	*			

Table B.21. Holtite-A

Temperature (°F)	Thermal Conductivity (Btu/hr-in-°F) (x)	Thermal Conductivity (Btu/hr-in-°F) (y)	Thermal Conductivity (Btu/hr-in-°F) (z)	Density (lbm/in^3)	Specific Heat (Btu/lbm-°F)	Description
*	0.03108	*	*	0.06076	0.39000	Neutron Shield/In impact limiter

Table B.22. HT-870

Temperature (°F)	Thermal Conductivity (Btu/hr-in-°F) (x)	Thermal Conductivity (Btu/hr-in-°F) (y)	Thermal Conductivity (Btu/hr-in-°F) (z)	Density (lbm/in^3)	Specific Heat (Btu/lbm-°F)	Description
*	0.00340	*	*	0.00868	0.39000	Foam on back side of fins

Table B.23. Air Properties Representing Degraded Materials

Temperature (°F)	Thermal Conductivity (Btu/hr-in-°F) (x)	Thermal Conductivity (Btu/hr-in-°F) (y)	Thermal Conductivity (Btu/hr-in-°F) (z)	Density (lbm/in³)	Specific Heat (Btu/lbm-°F)	Description
200	0.00148	*	*	3.48E-05	0.24110	For degraded Holtite-A, HT-870, and Honeycomb after fire
450	0.00188	*	*	2.53E-05	0.24605	
700	0.00227	*	*	1.99E-05	0.25355	
1400	0.00336	*	*	1.31E-05	0.27445	

Table B.24. One-Quarter-Inch Fillet Weld - Carbon Steel (SA-515, Gr. 70)

Temperature (°F)	Thermal Conductivity (Btu/hr-in-°F) (x)	Thermal Conductivity (Btu/hr-in-°F) (y)	Thermal Conductivity (Btu/hr-in-°F) (z)	Density (lbm/in³)	Specific Heat (Btu/lbm-°F)	Description
200	1.21670	2.43330	2.43330	0.28299	0.10000	Reduced radial channel conductivity (Fin Fillet Weld Root)
450	1.12920	2.25830	2.25830			
700	1.02500	2.05000	2.05000			
1400	0.73333	1.46670	1.46670			

Table B.25. Carbon Steel (SA-516, Gr. 70)

Temperature (°F)	Thermal Conductivity (Btu/hr-in-°F) (x)	Thermal Conductivity (Btu/hr-in-°F) (y)	Thermal Conductivity (Btu/hr-in-°F) (z)	Density (lbm/in³)	Specific Heat (Btu/lbm-°F)	Description
200	2.03330	*	*	0.28299	0.10000	Gamma Shield (intimate contact) and impact limiter base structure
450	1.99170	*	*			
700	1.86670	*	*			
1400	1.46670	*	*			

Table B.26. Aluminum Honeycomb (700 psi unidirectional w/1700 psi cross-core backing)

Temperature (°F)	Thermal Conductivity (Btu/hr-in-°F) (x)	Thermal Conductivity (Btu/hr-in-°F) (y)	Thermal Conductivity (Btu/hr-in-°F) (z)	Density (lbm/in³)	Specific Heat (Btu/lbm-°F)	Description
68	1.11710	0.47427	1.11710	0.01406	0.20800 (assumed)	Type 1: Aluminum Honeycomb
212	1.15270	0.48944	1.15270	0.01406		
752	1.42620	0.59537	1.42620	0.01406		
1400	1.75440	0.72248	1.75440	0.01406		

Table B.27. Aluminum Honeycomb (700 psi unidirectional and 2300 psi cross-core)

Temperature (°F)	Thermal Conductivity (Btu/hr-in-°F) (x)	Thermal Conductivity (Btu/hr-in-°F) (y)	Thermal Conductivity (Btu/hr-in-°F) (z)	Density (lbm/in³)	Specific Heat (Btu/lbm-°F)	Description
68	0.82721	0.31682	0.82721	0.00579	0.20800 (assumed)	Type 2&5: Aluminum Honeycomb
212	0.85369	0.32693	0.85369	0.00579		
752	1.03810	0.39771	1.03810	0.00579		
1400	1.25940	0.48265	1.25940	0.00579		

Table B.28. Aluminum Honeycomb (2300 psi cross-core)

Temperature (°F)	Thermal Conductivity (Btu/hr-in-°F) (x)	Thermal Conductivity (Btu/hr-in-°F) (y)	Thermal Conductivity (Btu/hr-in-°F) (z)	Density (lbm/in^3)	Specific Heat (Btu/lbm-°F)	Description
68	1.40690	0.63172	1.40690	0.01684	0.20800 (assumed)	Type 3: Aluminum Honeycomb
212	1.45170	0.65194	1.45170	0.01684		
752	1.81430	0.79302	1.81430	0.01684		
1400	2.24930	0.96231	2.24930	0.01684		

Table B.29. Aluminum Honeycomb (1100 psi unidirectional and 2300 psi cross-core)

Temperature (°F)	Thermal Conductivity (Btu/hr-in-°F) (x)	Thermal Conductivity (Btu/hr-in-°F) (y)	Thermal Conductivity (Btu/hr-in-°F) (z)	Density (lbm/in^3)	Specific Heat (Btu/lbm-°F)	Description
68	1.40690	0.63172	1.40690	1.40630	0.20800 (assumed)	Type 4: Aluminum Honeycomb
212	1.45170	0.65194	1.45170	1.40630		
752	1.81430	0.79302	1.81430	1.40630		
1400	2.24930	0.96231	2.24930	1.40630		

Table B.30. Emissivity Values for Radiation Heat Transfer

Component	Material	Emissivity
Fuel	Zircaloy	0.80
Basket	Alloy-X	0.36
Support Bracket	Alloy-X	0.36
MPC Wall	Alloy-X	0.36
Borated Aluminum Plate	Boral	0.55
Bare Carbon Steel	Carbon Steel	0.65
Painted Surfaces		0.90
Cask and Impact Limiter Surfaces	Alloy-X	0.36
Tunnel Surface		0.90
Soot Surfaces		0.90

Appendix C

Material Properties for ANSYS Model of Legal Weight Truck Package

Table C.1. 304 Stainless Steel

Temperature (°F)	Thermal Conductivity (Btu/hr-in-°F)	Density (lbm/in^3)	Specific Heat (Btu/lbm-°F)	Description
70	0.7143	-	0.1141	Used for cask body, cask lid, spokes
212	0.7800	0.2888	0.1207	
392	0.8592	0.2872	0.1272	
572	0.9333	0.2855	0.1320	
752	1.0042	0.2839	0.1356	
932	1.0717	0.2822	0.1385	
1112	1.1375	0.2805	0.1412	

Table C.2. 6061-T6 Aluminum

Temperature (°F)	Thermal Conductivity (Btu/hr-in-°F)	Density (lbm/in^3)	Specific Heat (Btu/lbm-°F)	Description
32	9.7500	0.0984	0.2140	Used for basket, IL 1, 2 skin
212	9.9167			
572	11.0833			
932	12.9167			

Table C.3. 6061-T6 Aluminum Honeycomb

Temperature (°F)	Thermal Conductivity (Btu/hr-in-°F)	Density (lbm/in^3)	Specific Heat (Btu/lbm-°F)	Description
32	1.6965	0.017118056	0.214	Used for IL 1 (Honeycomb)
212	1.7255			
572	1.9285			
932	2.2475			

Table C.4. 6061-T6 Aluminum Honeycomb

Temperature (°F)	Thermal Conductivity (Btu/hr-in-°F)	Density (lbm/in^3)	Specific Heat (Btu/lbm-°F)	Description
32	1.4235	0.0144	0.214	Used for IL 2 (Honeycomb)
212	1.4478			
572	1.6182			
932	1.8858			

Table C.5. Helium

Temperature (°F)	Thermal Conductivity (Btu/hr-in-°F)	Density (lbm/in^3)	Specific Heat (Btu/lbm-°F)	Description
200	0.00808	4.83E-06	1.24	Used for cask gap and fuel gap
400	0.00942	3.70E-06		
600	0.01075	3.01E-06		
800	0.0115	2.52E-06		

Table C.6. Chemical Copper Lead

Temperature (°F)	Thermal Conductivity (Btu/hr-in-°F)	Density (lbm/in^3)	Specific Heat (Btu/lbm-°F)	Description
68	1.6651	0.3	0.06	Used for lead regions
209	1.6308			
400	1.526			
499	1.4111			
581	1.2096			
630	1.0079			

Table C.7. 56% Ethylene Glycol Solution

Avg. Temperature (°F)	Thermal Conductivity (Btu/hr-in-°F)	Specific Heat (Btu/lbm-°F)	Density (lbm/in^3)
50	0.0188	0.7405	0.0391
70	0.0187	0.7522	0.0389
100	0.0185	0.7696	0.0385
150	0.0182	0.7979	0.0378
200	0.0179	0.8255	0.0370
250	0.0177	0.8522	0.0362
260	0.0176	0.8575	0.0360
270	0.0176	0.8627	0.0358
280	0.0175	0.8679	0.0357
290	0.0175	0.8731	0.0355
300	0.0174	0.8782	0.0353
310	0.0174	0.8833	0.0351
320	0.0173	0.8884	0.0349
330	0.0173	0.8934	0.0347
340	0.0172	0.8984	0.0345
350	0.0172	0.9034	0.0343

Table C.8. Air

Avg. Temperature (°F)	Thermal Conductivity (Btu/hr-in-°F)	Specific Heat (Btu/lbm-°F)	Density (lbm/in^3)
350	0.0017	0.2467	0.0000283
450	0.0018	0.2494	0.0000252
550	0.0020	0.2516	0.0000227
650	0.0022	0.2533	0.0000206
750	0.0023	0.2546	0.0000189
850	0.0025	0.2556	0.0000175
950	0.0026	0.2562	0.0000162
1050	0.0027	0.2566	0.0000152
1150	0.0029	0.2568	0.0000142

Table C.8. Air

Avg. Temperature (°F)	Thermal Conductivity (Btu/hr-in-°F)	Specific Heat (Btu/lbm-°F)	Density (lbm/in^3)
1250	0.0030	0.2570	0.0000134
1350	0.0031	0.2571	0.0000126
1450	0.0033	0.2571	0.0000120
1550	0.0034	0.2573	0.0000114
1650	0.0035	0.2576	0.0000108
1750	0.0036	0.2581	0.0000104
1850	0.0038	0.2589	0.0000099
1950	0.0039	0.2599	0.0000095
2050	0.0040	0.2614	0.0000091

Table C.9. Effective Conductivity for Liquid Neutron Shield with 1°F Temperature Gradient

Avg. Temperature (°F)	56% Ethylene Glycol		Air	
	Effective Conductivity Neutron Shield (Btu/hr-in-°F)	Effective Conductivity Expansion Tank (Btu/hr-in-°F)	Effective Conductivity Neutron Shield (Btu/hr-in-°F)	Effective Conductivity Expansion Tank (Btu/hr-in-°F)
250	0.364	0.149	0.003	0.002
260	0.374	0.153	0.003	0.002
270	0.384	0.157	0.003	0.002
280	0.393	0.161	0.003	0.002
290	0.398	0.163	0.003	0.002
300	0.396	0.162	0.003	0.002
310	0.395	0.162	0.003	0.002
320	0.394	0.161	0.003	0.002
330	0.393	0.161	0.003	0.002
340	0.391	0.160	0.003	0.002
350	0.390	0.160	0.003	0.002
351	*	*	0.003	0.002
400	*	*	0.003	0.002
500	*	*	0.003	0.002
600	*	*	0.003	0.002
700	*	*	0.003	0.002
800	*	*	0.003	0.002
1000	*	*	0.003	0.003
1200	*	*	0.003	0.003
1500	*	*	0.003	0.003
2000	*	*	0.004	0.004
2500	*	*	0.004	0.004

Table C.10. Effective Conductivity for Liquid Neutron Shield with 10°F Temperature Gradient

Avg. Temperature (°F)	56% Ethylene Glycol		Air	
	Effective Conductivity Neutron Shield (Btu/hr-in-°F)	Effective Conductivity Expansion Tank (Btu/hr-in-°F)	Effective Conductivity Neutron Shield (Btu/hr-in-°F)	Effective Conductivity Expansion Tank (Btu/hr-in-°F)
250	0.654	0.268	0.006	0.002
260	0.673	0.276	0.006	0.002
270	0.691	0.283	0.006	0.002
280	0.704	0.288	0.006	0.002
290	0.705	0.289	0.006	0.002
300	0.703	0.288	0.006	0.002
310	0.701	0.287	0.006	0.002
320	0.699	0.286	0.006	0.002
330	0.697	0.286	0.006	0.002
340	0.695	0.285	0.006	0.002
350	*	*	0.006	0.002
351	*	*	0.006	0.002
400	*	*	0.006	0.002
500	*	*	0.006	0.002
600	*	*	0.005	0.002
700	*	*	0.005	0.002
800	*	*	0.005	0.002
1000	*	*	0.005	0.003
1200	*	*	0.005	0.003
1500	*	*	0.004	0.003
2000	*	*	0.004	0.004
2500	*	*	0.004	0.004

Table C.11. Effective Conductivity for Liquid Neutron Shield with 25°F Temperature Gradient

Avg. Temperature (°F)	56% Ethylene Glycol		Air	
	Effective Conductivity Neutron Shield (Btu/hr-in-°F)	Effective Conductivity Expansion Tank (Btu/hr-in-°F)	Effective Conductivity Neutron Shield (Btu/hr-in-°F)	Effective Conductivity Expansion Tank (Btu/hr-in-°F)
250	0.840	0.344	0.008	0.003
260	0.863	0.353	0.008	0.003
270	0.882	0.361	0.008	0.003
280	0.888	0.364	0.008	0.003
290	0.885	0.363	0.007	0.003
300	0.883	0.361	0.007	0.003
310	0.880	0.360	0.007	0.003
320	0.877	0.359	0.007	0.003
330	0.875	0.358	0.007	0.003
340	0.872	0.357	0.007	0.003
350	*	*	0.007	0.003
351	*	*	0.007	0.003
400	*	*	0.007	0.003
500	*	*	0.007	0.003
600	*	*	0.007	0.003
700	*	*	0.007	0.003
800	*	*	0.006	0.003
1000	*	*	0.006	0.003
1200	*	*	0.006	0.003
1500	*	*	0.005	0.003
2000	*	*	0.005	0.004
2500	*	*	0.005	0.004

Table C.12. Effective Conductivity for Liquid Neutron Shield with 50°F Temperature Gradient

Avg. Temperature (°F)	56% Ethylene Glycol		Air	
	Effective Conductivity Neutron Shield (Btu/hr-in-°F)	Effective Conductivity Expansion Tank (Btu/hr-in-°F)	Effective Conductivity Neutron Shield (Btu/hr-in-°F)	Effective Conductivity Expansion Tank (Btu/hr-in-°F)
250	1.061	0.434	0.009	0.004
260	1.058	0.433	0.009	0.004
270	1.055	0.432	0.009	0.004
280	1.052	0.431	0.009	0.004
290	1.049	0.430	0.009	0.004
300	1.046	0.428	0.009	0.004
310	1.043	0.427	0.009	0.004
320	1.039	0.426	0.009	0.004
330	*	*	0.009	0.004
340	*	*	0.009	0.004
350	*	*	0.009	0.004
351	*	*	0.009	0.004
400	*	*	0.009	0.003
500	*	*	0.008	0.003
600	*	*	0.008	0.003
700	*	*	0.008	0.003
800	*	*	0.008	0.003
1000	*	*	0.007	0.003
1200	*	*	0.007	0.003
1500	*	*	0.006	0.003
2000	*	*	0.006	0.004
2500	*	*	0.006	0.004

Table C.13. Effective Conductivity for Liquid Neutron Shield with 70°F Temperature Gradient

Avg. Temperature (°F)	56% Ethylene Glycol		Air	
	Effective Conductivity Neutron Shield (Btu/hr-in-°F)	Effective Conductivity Expansion Tank (Btu/hr-in-°F)	Effective Conductivity Neutron Shield (Btu/hr-in-°F)	Effective Conductivity Expansion Tank (Btu/hr-in-°F)
250	1.151	0.471	0.010	0.004
260	1.148	0.470	0.010	0.004
270	1.144	0.469	0.010	0.004
280	1.141	0.467	0.010	0.004
290	1.138	0.466	0.010	0.004
300	1.134	0.464	0.010	0.004
310	1.131	0.463	0.010	0.004
320	*	*	0.010	0.004
330	*	*	0.010	0.004
340	*	*	0.009	0.004
350	*	*	0.009	0.004
351	*	*	0.009	0.004
400	*	*	0.009	0.004
500	*	*	0.009	0.004
600	*	*	0.009	0.004
700	*	*	0.008	0.003
800	*	*	0.008	0.003
1000	*	*	0.008	0.003
1200	*	*	0.007	0.003
1500	*	*	0.007	0.003
2000	*	*	0.006	0.004
2500	*	*	0.006	0.004

Table C.14. Effective Conductivity for Liquid Neutron Shield with 100°F Temperature Gradient

Avg. Temperature (°F)	56% Ethylene Glycol		Air	
	Effective Conductivity Neutron Shield (Btu/hr-in-°F)	Effective Conductivity Expansion Tank (Btu/hr-in-°F)	Effective Conductivity Neutron Shield (Btu/hr-in-°F)	Effective Conductivity Expansion Tank (Btu/hr-in-°F)
250	1.253	0.513	0.011	0.004
260	1.249	0.512	0.011	0.004
270	1.245	0.510	0.011	0.004
280	1.242	0.509	0.011	0.004
290	1.238	0.507	0.011	0.004
300	1.234	0.505	0.011	0.004
310	*	*	0.010	0.004
320	*	*	0.010	0.004
330	*	*	0.010	0.004
340	*	*	0.010	0.004
350	*	*	0.010	0.004
351	*	*	0.010	0.004
400	*	*	0.010	0.004
500	*	*	0.010	0.004
600	*	*	0.009	0.004
700	*	*	0.009	0.004
800	*	*	0.009	0.004
1000	*	*	0.008	0.003
1200	*	*	0.008	0.003
1500	*	*	0.008	0.003
2000	*	*	0.007	0.004
2500	*	*	0.007	0.004

Table C.15. Effective Conductivity for Liquid Neutron Shield with 200°F Temperature Gradient

Avg. Temperature (°F)	56% Ethylene Glycol		Air	
	Effective Conductivity Neutron Shield (Btu/hr-in-°F)	Effective Conductivity Expansion Tank (Btu/hr-in-°F)	Effective Conductivity Neutron Shield (Btu/hr-in-°F)	Effective Conductivity Expansion Tank (Btu/hr-in-°F)
250	1.468	0.601	0.013	0.005
260	*	*	0.013	0.005
270	*	*	0.013	0.005
280	*	*	0.013	0.005
290	*	*	0.013	0.005
300	*	*	0.012	0.005
310	*	*	0.012	0.005
320	*	*	0.012	0.005
330	*	*	0.012	0.005
340	*	*	0.012	0.005
350	*	*	0.012	0.005
351	*	*	0.012	0.005
400	*	*	0.012	0.005
500	*	*	0.012	0.005
600	*	*	0.011	0.004
700	*	*	0.011	0.004
800	*	*	0.011	0.004
1000	*	*	0.010	0.004
1200	*	*	0.010	0.004
1500	*	*	0.009	0.004
2000	*	*	0.008	0.004
2500	*	*	0.008	0.005

Table C.16. Effective Conductivity for Liquid Neutron Shield with 300°F Temperature Gradient

Avg. Temperature (°F)	56% Ethylene Glycol		Air	
	Effective Conductivity Neutron Shield (Btu/hr-in-°F)	Effective Conductivity Expansion Tank (Btu/hr-in-°F)	Effective Conductivity Neutron Shield (Btu/hr-in-°F)	Effective Conductivity Expansion Tank (Btu/hr-in-°F)
250	*	*	0.014	0.005
260	*	*	0.014	0.005
270	*	*	0.014	0.005
280	*	*	0.014	0.005
290	*	*	0.014	0.005
300	*	*	0.014	0.005
310	*	*	0.014	0.005
320	*	*	0.014	0.005
330	*	*	0.014	0.005
340	*	*	0.014	0.005
350	*	*	0.013	0.005
351	*	*	0.013	0.005
400	*	*	0.013	0.005
500	*	*	0.013	0.005
600	*	*	0.012	0.005
700	*	*	0.012	0.005
800	*	*	0.012	0.005
1000	*	*	0.011	0.004
1200	*	*	0.011	0.004
1500	*	*	0.010	0.004
2000	*	*	0.009	0.004
2500	*	*	0.009	0.005

Table C.17. Effective Conductivity for Liquid Neutron Shield with 500°F Temperature Gradient

Avg. Temperature (°F)	56% Ethylene Glycol		Air	
	Effective Conductivity Neutron Shield (Btu/hr-in-°F)	Effective Conductivity Expansion Tank (Btu/hr-in-°F)	Effective Conductivity Neutron Shield (Btu/hr-in-°F)	Effective Conductivity Expansion Tank (Btu/hr-in-°F)
250	*	*	0.016	0.006
260	*	*	0.016	0.006
270	*	*	0.016	0.006
280	*	*	0.016	0.006
290	*	*	0.016	0.006
300	*	*	0.015	0.006
310	*	*	0.015	0.006
320	*	*	0.015	0.006
330	*	*	0.015	0.006
340	*	*	0.015	0.006
350	*	*	0.015	0.006
351	*	*	0.015	0.006
400	*	*	0.015	0.006
500	*	*	0.014	0.006
600	*	*	0.014	0.005
700	*	*	0.014	0.005
800	*	*	0.013	0.005
1000	*	*	0.013	0.005
1200	*	*	0.012	0.005
1500	*	*	0.011	0.005
2000	*	*	0.011	0.004
2500	*	*	0.010	0.005

Table C.18. Emissivity Values for Radiation Heat Transfer

Component	Material	Emissivity Before Fire	Emissivity During/After Fire
Canister	stainless steel	0.36	0.36
Cask	stainless steel	0.36	0.36
Outer Neutron Shield		0.34	0.34
Inner Neutron Shield		0.34	0.34
Basket	stainless steel	0.36	0.36
Fuel Clad	zircaloy	0.8	0.8
Boral Plate	aluminum clad	0.55	0.55
Shell Interior	stainless steel	0.36	0.36
Cask Exterior	stainless steel	0.85	0.9
Tunnel/ISO	various		0.9

Appendix D

Blackbody Viewfactors for COBRA-SFS Model of TN-68 Package

C TUNNEL.1=TOP TUNNEL.2=SIDE TUNNEL.3=BOTTOM

Cnode_1	node_2	Area*e*Bij	$	Bij	Bji
CASK.101,	TUNNEL.1,	137.54	$	0.79418,0.00045040	
CASK.101,	TUNNEL.2,	25.477	$	0.14711,7.5761e-005	
CASK.101,	TUNNEL.3,	6.3683	$	0.036772,2.1839e-005	
CASK.102,	TUNNEL.1,	67.819	$	0.39161,0.00022209	
CASK.102,	TUNNEL.2,	87.635	$	0.50603,0.00026060	
CASK.102,	TUNNEL.3,	13.723	$	0.079241,4.7061e-005	
CASK.103,	TUNNEL.1,	12.951	$	0.074781,4.2410e-005	
CASK.103,	TUNNEL.2,	90.996	$	0.52544,0.00027059	
CASK.103,	TUNNEL.3,	65.443	$	0.37789,0.00022443	
CASK.104,	TUNNEL.1,	6.2714	$	0.036213,2.0538e-005	
CASK.104,	TUNNEL.2,	31.022	$	0.17913,9.2251e-005	
CASK.104,	TUNNEL.3,	132.32	$	0.76404,0.00045376	
CASK.201,	TUNNEL.1,	138.22	$	0.79812,0.00045264	
CASK.201,	TUNNEL.2,	24.978	$	0.14423,7.4277e-005	
CASK.201,	TUNNEL.3,	6.3135	$	0.036456,2.1651e-005	
CASK.202,	TUNNEL.1,	68.135	$	0.39343,0.00022313	
CASK.202,	TUNNEL.2,	87.392	$	0.50463,0.00025988	
CASK.202,	TUNNEL.3,	13.599	$	0.078527,4.6637e-005	
CASK.203,	TUNNEL.1,	12.937	$	0.074702,4.2365e-005	
CASK.203,	TUNNEL.2,	90.689	$	0.52367,0.00026968	
CASK.203,	TUNNEL.3,	65.701	$	0.37938,0.00022531	
CASK.204,	TUNNEL.1,	6.1691	$	0.035622,2.0203e-005	
CASK.204,	TUNNEL.2,	31.104	$	0.17961,9.2494e-005	
CASK.204,	TUNNEL.3,	132.31	$	0.76399,0.00045373	
CASK.301,	TUNNEL.1,	137.98	$	0.79676,0.00045187	
CASK.301,	TUNNEL.2,	25.169	$	0.14533,7.4844e-005	
CASK.301,	TUNNEL.3,	6.3354	$	0.036583,2.1726e-005	
CASK.302,	TUNNEL.1,	68.192	$	0.39376,0.00022331	
CASK.302,	TUNNEL.2,	87.312	$	0.50417,0.00025964	
CASK.302,	TUNNEL.3,	13.687	$	0.079031,4.6936e-005	
CASK.303,	TUNNEL.1,	12.880	$	0.074375,4.2180e-005	
CASK.303,	TUNNEL.2,	91.267	$	0.52700,0.00027140	
CASK.303,	TUNNEL.3,	65.225	$	0.37663,0.00022368	
CASK.304,	TUNNEL.1,	6.1435	$	0.035475,2.0119e-005	
CASK.304,	TUNNEL.2,	31.213	$	0.18024,9.2819e-005	
CASK.304,	TUNNEL.3,	132.07	$	0.76261,0.00045291	
CASK.401,	TUNNEL.1,	138.03	$	0.79704,0.00045202	
CASK.401,	TUNNEL.2,	25.096	$	0.14491,7.4627e-005	
CASK.401,	TUNNEL.3,	6.3204	$	0.036496,2.1675e-005	
CASK.402,	TUNNEL.1,	68.295	$	0.39436,0.00022365	
CASK.402,	TUNNEL.2,	87.210	$	0.50358,0.00025934	
CASK.402,	TUNNEL.3,	13.632	$	0.078717,4.6750e-005	
CASK.403,	TUNNEL.1,	13.054	$	0.075376,4.2748e-005	
CASK.403,	TUNNEL.2,	90.720	$	0.52385,0.00026977	
CASK.403,	TUNNEL.3,	65.460	$	0.37799,0.00022448	
CASK.404,	TUNNEL.1,	6.0468	$	0.034916,1.9802e-005	
CASK.404,	TUNNEL.2,	30.945	$	0.17868,9.2020e-005	
CASK.404,	TUNNEL.3,	132.46	$	0.76484,0.00045424	
CASK.501,	TUNNEL.1,	138.12	$	0.79752,0.00045230	
CASK.501,	TUNNEL.2,	25.031	$	0.14454,7.4434e-005	
CASK.501,	TUNNEL.3,	6.3279	$	0.036539,2.1701e-005	
CASK.502,	TUNNEL.1,	68.608	$	0.39616,0.00022468	
CASK.502,	TUNNEL.2,	86.890	$	0.50173,0.00025838	
CASK.502,	TUNNEL.3,	13.693	$	0.079069,4.6959e-005	
CASK.503,	TUNNEL.1,	12.946	$	0.074757,4.2397e-005	
CASK.503,	TUNNEL.2,	91.115	$	0.52613,0.00027095	
CASK.503,	TUNNEL.3,	65.179	$	0.37636,0.00022352	
CASK.504,	TUNNEL.1,	5.9701	$	0.034474,1.9551e-005	
CASK.504,	TUNNEL.2,	30.931	$	0.17860,9.1979e-005	
CASK.504,	TUNNEL.3,	132.45	$	0.76480,0.00045422	
CASK.601,	TUNNEL.1,	138.18	$	0.79788,0.00045250	
CASK.601,	TUNNEL.2,	24.944	$	0.14403,7.4176e-005	
CASK.601,	TUNNEL.3,	6.2188	$	0.035909,2.1326e-005	
CASK.602,	TUNNEL.1,	68.688	$	0.39663,0.00022494	
CASK.602,	TUNNEL.2,	86.987	$	0.50229,0.00025867	
CASK.602,	TUNNEL.3,	13.491	$	0.077899,4.6264e-005	
CASK.603,	TUNNEL.1,	13.037	$	0.075278,4.2692e-005	
CASK.603,	TUNNEL.2,	91.088	$	0.52597,0.00027087	
CASK.603,	TUNNEL.3,	65.088	$	0.37584,0.00022321	
CASK.604,	TUNNEL.1,	5.9256	$	0.034216,1.9405e-005	
CASK.604,	TUNNEL.2,	31.061	$	0.17936,9.2367e-005	
CASK.604,	TUNNEL.3,	132.28	$	0.76385,0.00045365	
CASK.701,	TUNNEL.1,	138.29	$	0.79854,0.00045288	
CASK.701,	TUNNEL.2,	24.847	$	0.14347,7.3886e-005	
CASK.701,	TUNNEL.3,	6.2483	$	0.036080,2.1428e-005	
CASK.702,	TUNNEL.1,	68.225	$	0.39395,0.00022342	
CASK.702,	TUNNEL.2,	87.042	$	0.50261,0.00025884	
CASK.702,	TUNNEL.3,	13.824	$	0.079826,4.7408e-005	
CASK.703,	TUNNEL.1,	13.006	$	0.075103,4.2593e-005	
CASK.703,	TUNNEL.2,	90.921	$	0.52501,0.00027037	
CASK.703,	TUNNEL.3,	65.304	$	0.37709,0.00022395	
CASK.704,	TUNNEL.1,	5.8582	$	0.033827,1.9184e-005	
CASK.704,	TUNNEL.2,	31.026	$	0.17916,9.2263e-005	
CASK.704,	TUNNEL.3,	132.40	$	0.76454,0.00045406	
CASK.801,	TUNNEL.1,	138.10	$	0.79744,0.00045225	
CASK.801,	TUNNEL.2,	25.102	$	0.14495,7.4647e-005	
CASK.801,	TUNNEL.3,	6.2315	$	0.035983,2.1370e-005	
CASK.802,	TUNNEL.1,	67.889	$	0.39201,0.00022232	
CASK.802,	TUNNEL.2,	87.307	$	0.50414,0.00025963	
CASK.802,	TUNNEL.3,	13.869	$	0.080083,4.7561e-005	
CASK.803,	TUNNEL.1,	12.847	$	0.074182,4.2071e-005	
CASK.803,	TUNNEL.2,	90.805	$	0.52434,0.00027003	
CASK.803,	TUNNEL.3,	65.535	$	0.37842,0.00022474	
CASK.804,	TUNNEL.1,	5.7617	$	0.033270,1.8868e-005	
CASK.804,	TUNNEL.2,	31.064	$	0.17937,9.2374e-005	
CASK.804,	TUNNEL.3,	132.36	$	0.76430,0.00045391	
CASK.901,	TUNNEL.1,	138.13	$	0.79764,0.00045236	
CASK.901,	TUNNEL.2,	25.128	$	0.14510,7.4724e-005	
CASK.901,	TUNNEL.3,	6.2207	$	0.035921,2.1333e-005	
CASK.902,	TUNNEL.1,	68.091	$	0.39318,0.00022298	
CASK.902,	TUNNEL.2,	87.277	$	0.50396,0.00025953	
CASK.902,	TUNNEL.3,	13.700	$	0.079107,4.6981e-005	
CASK.903,	TUNNEL.1,	12.952	$	0.074789,4.2415e-005	
CASK.903,	TUNNEL.2,	90.982	$	0.52536,0.00027055	
CASK.903,	TUNNEL.3,	65.132	$	0.37609,0.00022336	
CASK.904,	TUNNEL.1,	5.7522	$	0.033215,1.8837e-005	
CASK.904,	TUNNEL.2,	31.124	$	0.17972,9.2553e-005	
CASK.904,	TUNNEL.3,	132.31	$	0.76400,0.00045374	
CASK.1001,	TUNNEL.1,	137.84	$	0.79593,0.00045139	
CASK.1001,	TUNNEL.2,	25.412	$	0.14674,7.5569e-005	
CASK.1001,	TUNNEL.3,	6.2311	$	0.035981,2.1369e-005	
CASK.1002,	TUNNEL.1,	68.564	$	0.39591,0.00022453	
CASK.1002,	TUNNEL.2,	86.856	$	0.50153,0.00025828	
CASK.1002,	TUNNEL.3,	13.655	$	0.078849,4.6828e-005	
CASK.1003,	TUNNEL.1,	12.716	$	0.073426,4.1642e-005	
CASK.1003,	TUNNEL.2,	90.924	$	0.52502,0.00027038	
CASK.1003,	TUNNEL.3,	65.500	$	0.37822,0.00022462	
CASK.1004,	TUNNEL.1,	5.6573	$	0.032667,1.8526e-005	
CASK.1004,	TUNNEL.2,	31.197	$	0.18014,9.2770e-005	
CASK.1004,	TUNNEL.3,	132.27	$	0.76378,0.00045361	
CASK.1101,	TUNNEL.1,	138.17	$	0.79782,0.00045247	
CASK.1101,	TUNNEL.2,	25.006	$	0.14440,7.4362e-005	
CASK.1101,	TUNNEL.3,	6.1872	$	0.035727,2.1218e-005	
CASK.1102,	TUNNEL.1,	68.446	$	0.39523,0.00022415	
CASK.1102,	TUNNEL.2,	87.049	$	0.50265,0.00025886	
CASK.1102,	TUNNEL.3,	13.505	$	0.077980,4.6312e-005	
CASK.1103,	TUNNEL.1,	12.985	$	0.074982,4.2524e-005	
CASK.1103,	TUNNEL.2,	91.145	$	0.52630,0.00027104	
CASK.1103,	TUNNEL.3,	65.061	$	0.37568,0.00022312	
CASK.1104,	TUNNEL.1,	5.6898	$	0.032855,1.8633e-005	
CASK.1104,	TUNNEL.2,	30.943	$	0.17868,9.2016e-005	
CASK.1104,	TUNNEL.3,	132.40	$	0.76453,0.00045405	
CASK.1201,	TUNNEL.1,	137.88	$	0.79616,0.00045153	
CASK.1201,	TUNNEL.2,	25.412	$	0.14674,7.5567e-005	
CASK.1201,	TUNNEL.3,	6.1750	$	0.035657,2.1176e-005	
CASK.1202,	TUNNEL.1,	67.908	$	0.39212,0.00022238	
CASK.1202,	TUNNEL.2,	87.439	$	0.50490,0.00026002	
CASK.1202,	TUNNEL.3,	13.717	$	0.079208,4.7041e-005	
CASK.1203,	TUNNEL.1,	12.998	$	0.075055,4.2566e-005	
CASK.1203,	TUNNEL.2,	90.706	$	0.52377,0.00026973	
CASK.1203,	TUNNEL.3,	65.409	$	0.37769,0.00022431	
CASK.1204,	TUNNEL.1,	5.5919	$	0.032289,1.8312e-005	
CASK.1204,	TUNNEL.2,	31.129	$	0.17975,9.2567e-005	
CASK.1204,	TUNNEL.3,	132.27	$	0.76380,0.00045362	
CASK.1301,	TUNNEL.1,	138.25	$	0.79830,0.00045274	
CASK.1301,	TUNNEL.2,	24.993	$	0.14432,7.4320e-005	

CASK.1301,	TUNNEL.3,	6.1782	$	0.035675,2.1187e-005	CASK.1902,	TUNNEL.3,	13.637	$	0.078746,4.6767e-005
CASK.1302,	TUNNEL.1,	68.155	$	0.39355,0.00022319	CASK.1903,	TUNNEL.1,	12.841	$	0.074146,4.2051e-005
CASK.1302,	TUNNEL.2,	87.155	$	0.50326,0.00025917	CASK.1903,	TUNNEL.2,	91.151	$	0.52633,0.00027105
CASK.1302,	TUNNEL.3,	13.671	$	0.078943,4.6884e-005	CASK.1903,	TUNNEL.3,	65.209	$	0.37654,0.00022362
CASK.1303,	TUNNEL.1,	12.737	$	0.073546,4.1710e-005	CASK.1904,	TUNNEL.1,	5.6276	$	0.032496,1.8429e-005
CASK.1303,	TUNNEL.2,	91.130	$	0.52622,0.00027099	CASK.1904,	TUNNEL.2,	30.798	$	0.17784,9.1584e-005
CASK.1303,	TUNNEL.3,	65.245	$	0.37674,0.00022375	CASK.1904,	TUNNEL.3,	132.57	$	0.76549,0.00045462
CASK.1304,	TUNNEL.1,	5.6600	$	0.032683,1.8535e-005	CASK.2001,	TUNNEL.1,	138.26	$	0.79837,0.00045278
CASK.1304,	TUNNEL.2,	31.047	$	0.17928,9.2325e-005	CASK.2001,	TUNNEL.2,	24.969	$	0.14418,7.4252e-005
CASK.1304,	TUNNEL.3,	132.30	$	0.76396,0.00045372	CASK.2001,	TUNNEL.3,	6.1633	$	0.035589,2.1136e-005
CASK.1401,	TUNNEL.1,	138.04	$	0.79707,0.00045204	CASK.2002,	TUNNEL.1,	67.893	$	0.39204,0.00022234
CASK.1401,	TUNNEL.2,	25.121	$	0.14506,7.4703e-005	CASK.2002,	TUNNEL.2,	87.430	$	0.50485,0.00025999
CASK.1401,	TUNNEL.3,	6.2019	$	0.035812,2.1269e-005	CASK.2002,	TUNNEL.3,	13.778	$	0.079561,4.7251e-005
CASK.1402,	TUNNEL.1,	68.195	$	0.39378,0.00022332	CASK.2003,	TUNNEL.1,	12.702	$	0.073347,4.1597e-005
CASK.1402,	TUNNEL.2,	87.073	$	0.50279,0.00025893	CASK.2003,	TUNNEL.2,	90.326	$	0.52157,0.00026860
CASK.1402,	TUNNEL.3,	13.807	$	0.079729,4.7351e-005	CASK.2003,	TUNNEL.3,	66.063	$	0.38147,0.00022655
CASK.1403,	TUNNEL.1,	12.669	$	0.073153,4.1487e-005	CASK.2004,	TUNNEL.1,	5.6088	$	0.032387,1.8368e-005
CASK.1403,	TUNNEL.2,	91.365	$	0.52757,0.00027169	CASK.2004,	TUNNEL.2,	30.836	$	0.17806,9.1696e-005
CASK.1403,	TUNNEL.3,	65.069	$	0.37573,0.00022314	CASK.2004,	TUNNEL.3,	132.54	$	0.76530,0.00045451
CASK.1404,	TUNNEL.1,	5.5888	$	0.032272,1.8302e-005	CASK.2101,	TUNNEL.1,	137.99	$	0.79682,0.00045190
CASK.1404,	TUNNEL.2,	31.163	$	0.17994,9.2668e-005	CASK.2101,	TUNNEL.2,	25.223	$	0.14564,7.5005e-005
CASK.1404,	TUNNEL.3,	132.22	$	0.76345,0.00045341	CASK.2101,	TUNNEL.3,	6.2208	$	0.035921,2.1333e-005
CASK.1501,	TUNNEL.1,	138.17	$	0.79785,0.00045249	CASK.2102,	TUNNEL.1,	68.122	$	0.39336,0.00022308
CASK.1501,	TUNNEL.2,	25.075	$	0.14479,7.4565e-005	CASK.2102,	TUNNEL.2,	87.248	$	0.50380,0.00025945
CASK.1501,	TUNNEL.3,	6.1911	$	0.035749,2.1231e-005	CASK.2102,	TUNNEL.3,	13.695	$	0.079082,4.6967e-005
CASK.1502,	TUNNEL.1,	68.139	$	0.39346,0.00022314	CASK.2103,	TUNNEL.1,	12.623	$	0.072889,4.1338e-005
CASK.1502,	TUNNEL.2,	87.197	$	0.50350,0.00025930	CASK.2103,	TUNNEL.2,	91.084	$	0.52595,0.00027086
CASK.1502,	TUNNEL.3,	13.646	$	0.078797,4.6798e-005	CASK.2103,	TUNNEL.3,	65.444	$	0.37790,0.00022443
CASK.1503,	TUNNEL.1,	12.784	$	0.073818,4.1864e-005	CASK.2104,	TUNNEL.1,	5.6251	$	0.032481,1.8421e-005
CASK.1503,	TUNNEL.2,	91.009	$	0.52552,0.00027063	CASK.2104,	TUNNEL.2,	30.935	$	0.17863,9.1992e-005
CASK.1503,	TUNNEL.3,	65.230	$	0.37666,0.00022370	CASK.2104,	TUNNEL.3,	132.48	$	0.76497,0.00045431
CASK.1504,	TUNNEL.1,	5.6144	$	0.032419,1.8386e-005	CASK.2201,	TUNNEL.1,	138.00	$	0.79686,0.00045192
CASK.1504,	TUNNEL.2,	31.011	$	0.17907,9.2217e-005	CASK.2201,	TUNNEL.2,	25.240	$	0.14575,7.5057e-005
CASK.1504,	TUNNEL.3,	132.37	$	0.76434,0.00045394	CASK.2201,	TUNNEL.3,	6.1738	$	0.035650,2.1172e-005
CASK.1601,	TUNNEL.1,	138.38	$	0.79906,0.00045317	CASK.2202,	TUNNEL.1,	68.741	$	0.39693,0.00022511
CASK.1601,	TUNNEL.2,	24.861	$	0.14355,7.3928e-005	CASK.2202,	TUNNEL.2,	86.917	$	0.50189,0.00025847
CASK.1601,	TUNNEL.3,	6.1468	$	0.035493,2.1079e-005	CASK.2202,	TUNNEL.3,	13.480	$	0.077838,4.6228e-005
CASK.1602,	TUNNEL.1,	68.267	$	0.39420,0.00022356	CASK.2203,	TUNNEL.1,	12.900	$	0.074490,4.2246e-005
CASK.1602,	TUNNEL.2,	87.153	$	0.50325,0.00025917	CASK.2203,	TUNNEL.2,	91.269	$	0.52702,0.00027141
CASK.1602,	TUNNEL.3,	13.587	$	0.078457,4.6595e-005	CASK.2203,	TUNNEL.3,	64.953	$	0.37506,0.00022275
CASK.1603,	TUNNEL.1,	12.646	$	0.073025,4.1414e-005	CASK.2204,	TUNNEL.1,	5.6790	$	0.032793,1.8598e-005
CASK.1603,	TUNNEL.2,	90.521	$	0.52270,0.00026918	CASK.2204,	TUNNEL.2,	30.883	$	0.17833,9.1837e-005
CASK.1603,	TUNNEL.3,	65.886	$	0.38045,0.00022595	CASK.2204,	TUNNEL.3,	132.53	$	0.76527,0.00045449
CASK.1604,	TUNNEL.1,	5.5843	$	0.032245,1.8287e-005	CASK.2301,	TUNNEL.1,	137.99	$	0.79683,0.00045190
CASK.1604,	TUNNEL.2,	30.824	$	0.17799,9.1661e-005	CASK.2301,	TUNNEL.2,	25.190	$	0.14546,7.4909e-005
CASK.1604,	TUNNEL.3,	132.56	$	0.76547,0.00045461	CASK.2301,	TUNNEL.3,	6.2267	$	0.035955,2.1354e-005
CASK.1701,	TUNNEL.1,	137.89	$	0.79623,0.00045156	CASK.2302,	TUNNEL.1,	68.414	$	0.39504,0.00022404
CASK.1701,	TUNNEL.2,	25.339	$	0.14632,7.5351e-005	CASK.2302,	TUNNEL.2,	86.942	$	0.50203,0.00025854
CASK.1701,	TUNNEL.3,	6.1499	$	0.035511,2.1090e-005	CASK.2302,	TUNNEL.3,	13.674	$	0.078957,4.6892e-005
CASK.1702,	TUNNEL.1,	68.793	$	0.39723,0.00022528	CASK.2303,	TUNNEL.1,	12.930	$	0.074664,4.2344e-005
CASK.1702,	TUNNEL.2,	86.707	$	0.50067,0.00025784	CASK.2303,	TUNNEL.2,	90.672	$	0.52357,0.00026963
CASK.1702,	TUNNEL.3,	13.529	$	0.078123,4.6397e-005	CASK.2303,	TUNNEL.3,	65.491	$	0.37816,0.00022459
CASK.1703,	TUNNEL.1,	12.704	$	0.073359,4.1604e-005	CASK.2304,	TUNNEL.1,	5.6849	$	0.032826,1.8617e-005
CASK.1703,	TUNNEL.2,	91.173	$	0.52646,0.00027112	CASK.2304,	TUNNEL.2,	31.044	$	0.17926,9.2315e-005
CASK.1703,	TUNNEL.3,	65.193	$	0.37645,0.00022357	CASK.2304,	TUNNEL.3,	132.32	$	0.76406,0.00045377
CASK.1704,	TUNNEL.1,	5.5697	$	0.032161,1.8240e-005	CASK.2401,	TUNNEL.1,	137.91	$	0.79636,0.00045164
CASK.1704,	TUNNEL.2,	31.366	$	0.18112,9.3274e-005	CASK.2401,	TUNNEL.2,	25.207	$	0.14555,7.4957e-005
CASK.1704,	TUNNEL.3,	132.07	$	0.76260,0.00045290	CASK.2401,	TUNNEL.3,	6.2003	$	0.035803,2.1263e-005
CASK.1801,	TUNNEL.1,	138.30	$	0.79856,0.00045289	CASK.2402,	TUNNEL.1,	68.065	$	0.39303,0.00022290
CASK.1801,	TUNNEL.2,	24.981	$	0.14425,7.4286e-005	CASK.2402,	TUNNEL.2,	87.281	$	0.50399,0.00025955
CASK.1801,	TUNNEL.3,	6.1334	$	0.035416,2.1034e-005	CASK.2402,	TUNNEL.3,	13.655	$	0.078847,4.6827e-005
CASK.1802,	TUNNEL.1,	68.068	$	0.39304,0.00022291	CASK.2403,	TUNNEL.1,	12.813	$	0.073989,4.1961e-005
CASK.1802,	TUNNEL.2,	87.271	$	0.50393,0.00025952	CASK.2403,	TUNNEL.2,	90.843	$	0.52456,0.00027014
CASK.1802,	TUNNEL.3,	13.649	$	0.078815,4.6808e-005	CASK.2403,	TUNNEL.3,	65.521	$	0.37834,0.00022470
CASK.1803,	TUNNEL.1,	12.694	$	0.073297,4.1569e-005	CASK.2404,	TUNNEL.1,	5.7547	$	0.033229,1.8845e-005
CASK.1803,	TUNNEL.2,	91.352	$	0.52750,0.00027165	CASK.2404,	TUNNEL.2,	31.095	$	0.17955,9.2466e-005
CASK.1803,	TUNNEL.3,	65.097	$	0.37589,0.00022324	CASK.2404,	TUNNEL.3,	132.32	$	0.76405,0.00045377
CASK.1804,	TUNNEL.1,	5.5500	$	0.032047,1.8175e-005	CASK.2501,	TUNNEL.1,	138.26	$	0.79836,0.00045277
CASK.1804,	TUNNEL.2,	31.344	$	0.18099,9.3208e-005	CASK.2501,	TUNNEL.2,	25.000	$	0.14436,7.4342e-005
CASK.1804,	TUNNEL.3,	132.06	$	0.76255,0.00045287	CASK.2501,	TUNNEL.3,	6.1776	$	0.035672,2.1185e-005
CASK.1901,	TUNNEL.1,	138.28	$	0.79848,0.00045284	CASK.2502,	TUNNEL.1,	68.473	$	0.39539,0.00022424
CASK.1901,	TUNNEL.2,	24.841	$	0.14344,7.3870e-005	CASK.2502,	TUNNEL.2,	87.067	$	0.50275,0.00025891
CASK.1901,	TUNNEL.3,	6.1732	$	0.035646,2.1170e-005	CASK.2502,	TUNNEL.3,	13.573	$	0.078375,4.6547e-005
CASK.1902,	TUNNEL.1,	68.778	$	0.39714,0.00022523	CASK.2503,	TUNNEL.1,	12.768	$	0.073729,4.1814e-005
CASK.1902,	TUNNEL.2,	86.557	$	0.49981,0.00025739	CASK.2503,	TUNNEL.2,	91.066	$	0.52584,0.00027080

CASK.2503,	TUNNEL.3,	65.294	$	0.37703,0.00022391	CASK.2902,	TUNNEL.2,	87.286	$	0.50402,0.00025956
CASK.2504,	TUNNEL.1,	5.8355	$	0.033696,1.9110e-005	CASK.2902,	TUNNEL.3,	13.756	$	0.079430,4.7173e-005
CASK.2504,	TUNNEL.2,	30.930	$	0.17860,9.1976e-005	CASK.2903,	TUNNEL.1,	12.735	$	0.073535,4.1704e-005
CASK.2504,	TUNNEL.3,	132.43	$	0.76468,0.00045414	CASK.2903,	TUNNEL.2,	91.049	$	0.52575,0.00027075
CASK.2601,	TUNNEL.1,	138.10	$	0.79746,0.00045226	CASK.2903,	TUNNEL.3,	65.491	$	0.37817,0.00022459
CASK.2601,	TUNNEL.2,	25.102	$	0.14495,7.4647e-005	CASK.2904,	TUNNEL.1,	6.0330	$	0.034837,1.9757e-005
CASK.2601,	TUNNEL.3,	6.2378	$	0.036019,2.1392e-005	CASK.2904,	TUNNEL.2,	31.507	$	0.18193,9.3691e-005
CASK.2602,	TUNNEL.1,	68.554	$	0.39585,0.00022450	CASK.2904,	TUNNEL.3,	131.85	$	0.76133,0.00045215
CASK.2602,	TUNNEL.2,	86.943	$	0.50203,0.00025854	CASK.3001,	TUNNEL.1,	137.97	$	0.79670,0.00045183
CASK.2602,	TUNNEL.3,	13.613	$	0.078605,4.6684e-005	CASK.3001,	TUNNEL.2,	25.049	$	0.14464,7.4489e-005
CASK.2603,	TUNNEL.1,	12.843	$	0.074160,4.2058e-005	CASK.3001,	TUNNEL.3,	6.3339	$	0.036574,2.1721e-005
CASK.2603,	TUNNEL.2,	91.332	$	0.52738,0.00027160	CASK.3002,	TUNNEL.1,	68.734	$	0.39689,0.00022509
CASK.2603,	TUNNEL.3,	64.991	$	0.37528,0.00022288	CASK.3002,	TUNNEL.2,	86.655	$	0.50038,0.00025769
CASK.2604,	TUNNEL.1,	5.8796	$	0.033951,1.9254e-005	CASK.3002,	TUNNEL.3,	13.815	$	0.079771,4.7376e-005
CASK.2604,	TUNNEL.2,	31.149	$	0.17987,9.2628e-005	CASK.3003,	TUNNEL.1,	12.791	$	0.073857,4.1886e-005
CASK.2604,	TUNNEL.3,	132.23	$	0.76355,0.00045347	CASK.3003,	TUNNEL.2,	91.080	$	0.52592,0.00027084
CASK.2701,	TUNNEL.1,	138.10	$	0.79741,0.00045224	CASK.3003,	TUNNEL.3,	65.432	$	0.37783,0.00022439
CASK.2701,	TUNNEL.2,	25.040	$	0.14459,7.4462e-005	CASK.3004,	TUNNEL.1,	6.1398	$	0.035453,2.0106e-005
CASK.2701,	TUNNEL.3,	6.3016	$	0.036387,2.1610e-005	CASK.3004,	TUNNEL.2,	31.115	$	0.17967,9.2525e-005
CASK.2702,	TUNNEL.1,	68.016	$	0.39275,0.00022274	CASK.3004,	TUNNEL.3,	132.27	$	0.76378,0.00045361
CASK.2702,	TUNNEL.2,	87.294	$	0.50407,0.00025959	CASK.3101,	TUNNEL.1,	137.70	$	0.79510,0.00045093
CASK.2702,	TUNNEL.3,	13.821	$	0.079805,4.7396e-005	CASK.3101,	TUNNEL.2,	25.393	$	0.14663,7.5511e-005
CASK.2703,	TUNNEL.1,	12.778	$	0.073785,4.1846e-005	CASK.3101,	TUNNEL.3,	6.3698	$	0.036781,2.1844e-005
CASK.2703,	TUNNEL.2,	90.618	$	0.52326,0.00026947	CASK.3102,	TUNNEL.1,	68.267	$	0.39420,0.00022356
CASK.2703,	TUNNEL.3,	65.768	$	0.37977,0.00022554	CASK.3102,	TUNNEL.2,	87.177	$	0.50339,0.00025924
CASK.2704,	TUNNEL.1,	5.8947	$	0.034038,1.9304e-005	CASK.3102,	TUNNEL.3,	13.703	$	0.079126,4.6993e-005
CASK.2704,	TUNNEL.2,	31.135	$	0.17978,9.2585e-005	CASK.3103,	TUNNEL.1,	12.902	$	0.074502,4.2252e-005
CASK.2704,	TUNNEL.3,	132.22	$	0.76350,0.00045344	CASK.3103,	TUNNEL.2,	91.407	$	0.52781,0.00027182
CASK.2801,	TUNNEL.1,	137.92	$	0.79641,0.00045167	CASK.3103,	TUNNEL.3,	65.078	$	0.37578,0.00022317
CASK.2801,	TUNNEL.2,	25.255	$	0.14583,7.5100e-005	CASK.3104,	TUNNEL.1,	6.2118	$	0.035869,2.0342e-005
CASK.2801,	TUNNEL.3,	6.2785	$	0.036254,2.1531e-005	CASK.3104,	TUNNEL.2,	30.914	$	0.17851,9.1928e-005
CASK.2802,	TUNNEL.1,	68.305	$	0.39442,0.00022369	CASK.3104,	TUNNEL.3,	132.43	$	0.76470,0.00045415
CASK.2802,	TUNNEL.2,	87.253	$	0.50383,0.00025946	CASK.3201,	TUNNEL.1,	138.23	$	0.79819,0.00045268
CASK.2802,	TUNNEL.3,	13.602	$	0.078545,4.6648e-005	CASK.3201,	TUNNEL.2,	24.820	$	0.14332,7.3808e-005
CASK.2803,	TUNNEL.1,	12.785	$	0.073827,4.1869e-005	CASK.3201,	TUNNEL.3,	6.3863	$	0.036877,2.1901e-005
CASK.2803,	TUNNEL.2,	91.110	$	0.52610,0.00027094	CASK.3202,	TUNNEL.1,	67.949	$	0.39236,0.00022252
CASK.2803,	TUNNEL.3,	65.358	$	0.37740,0.00022414	CASK.3202,	TUNNEL.2,	87.413	$	0.50475,0.00025994
CASK.2804,	TUNNEL.1,	6.0104	$	0.034706,1.9683e-005	CASK.3202,	TUNNEL.3,	13.866	$	0.080068,4.7552e-005
CASK.2804,	TUNNEL.2,	31.037	$	0.17922,9.2294e-005	CASK.3203,	TUNNEL.1,	13.070	$	0.075471,4.2802e-005
CASK.2804,	TUNNEL.3,	132.37	$	0.76435,0.00045394	CASK.3203,	TUNNEL.2,	90.901	$	0.52489,0.00027031
CASK.2901,	TUNNEL.1,	137.95	$	0.79655,0.00045175	CASK.3203,	TUNNEL.3,	65.388	$	0.37757,0.00022424
CASK.2901,	TUNNEL.2,	25.208	$	0.14556,7.4961e-005	CASK.3204,	TUNNEL.1,	6.2751	$	0.036235,2.0550e-005
CASK.2901,	TUNNEL.3,	6.3047	$	0.036405,2.1621e-005	CASK.3204,	TUNNEL.2,	31.217	$	0.18026,9.2829e-005
CASK.2902,	TUNNEL.1,	68.094	$	0.39320,0.00022299	CASK.3204,	TUNNEL.3,	132.12	$	0.76292,0.00045309

Appendix E

HOLTEC HI-STAR 100 Component Temperature Distributions

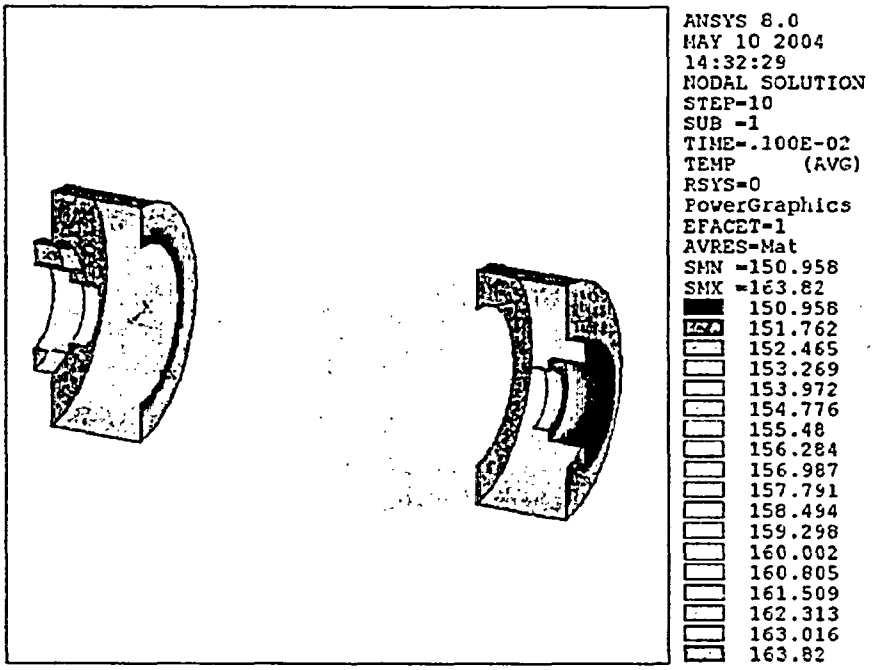

Figure E.1. Impact Limiter Skin Temperature Distribution - Normal Transport Conditions.

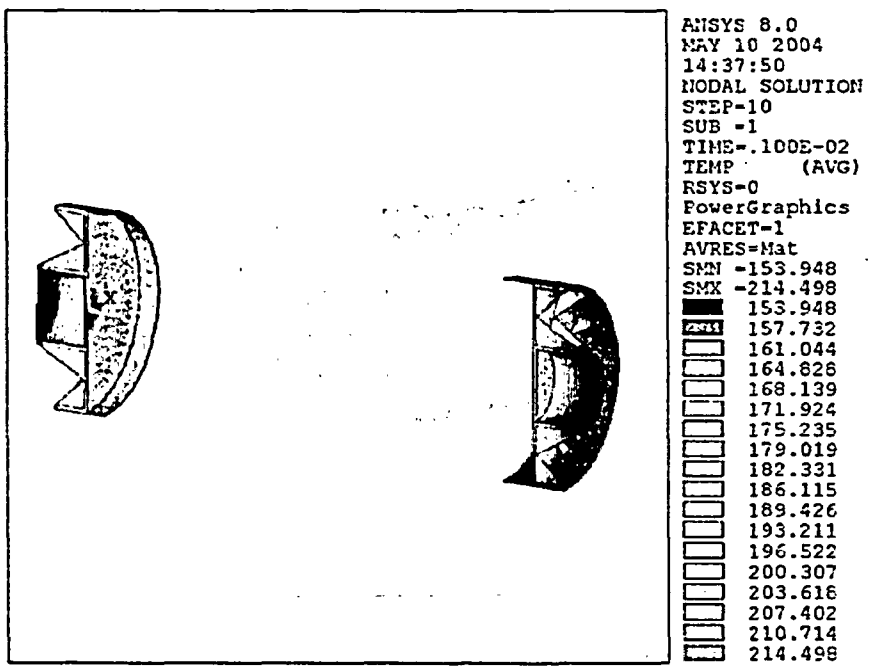

Figure E.2. Impact Limiter Structure Temperature Distribution - Normal Transport Conditions.

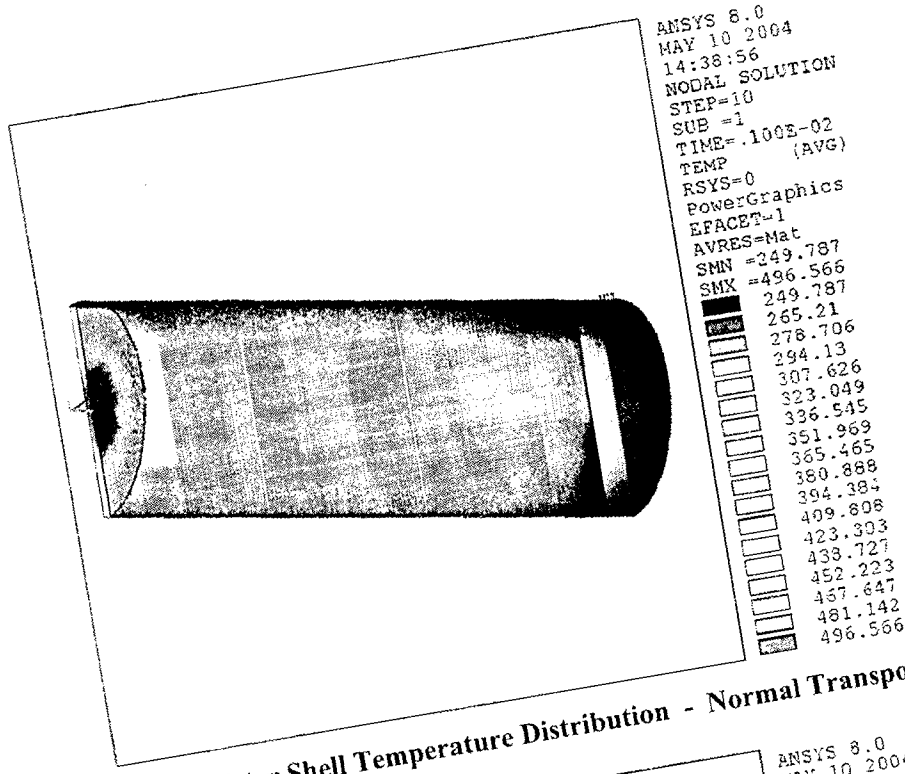

Figure E.3. Canister Shell Temperature Distribution - Normal Transport Conditions.

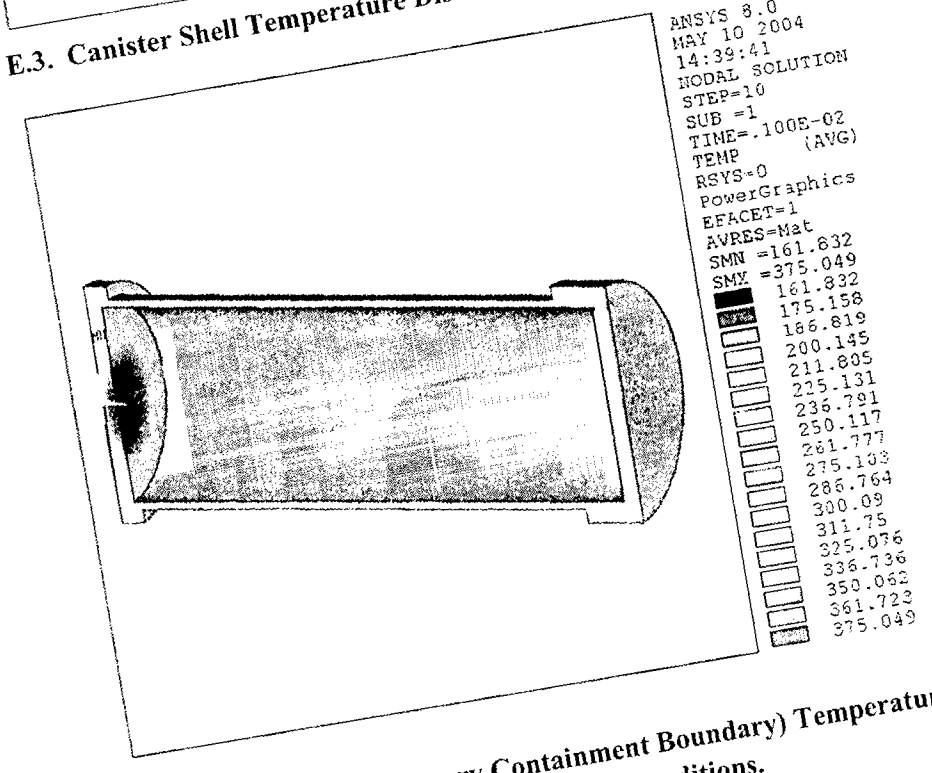

Figure E.4. Cask Inner Shell (Primary Containment Boundary) Temperature Distribution - Normal Transport Conditions.

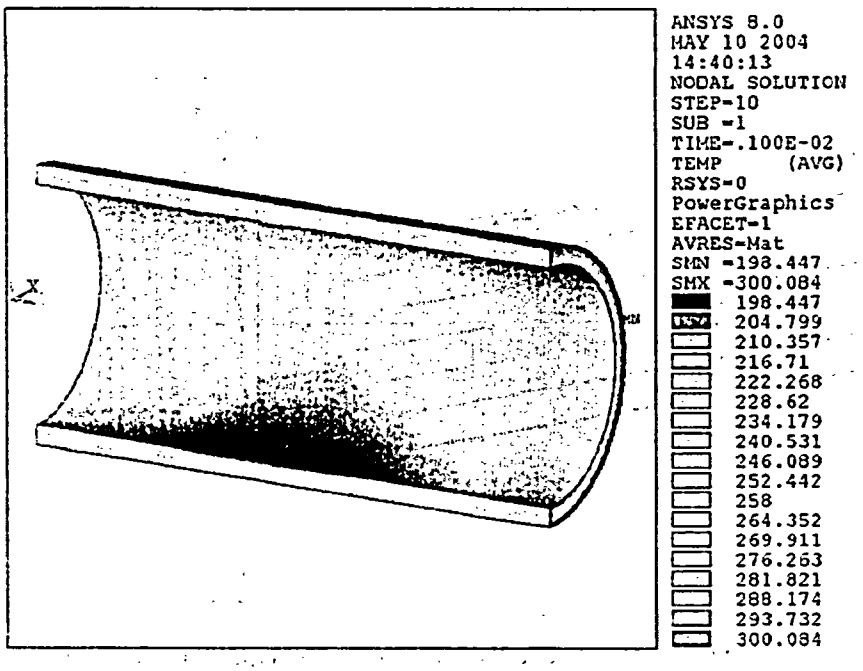

Figure E.5. Gamma Shield Temperature Distribution - Normal Transport Conditions.

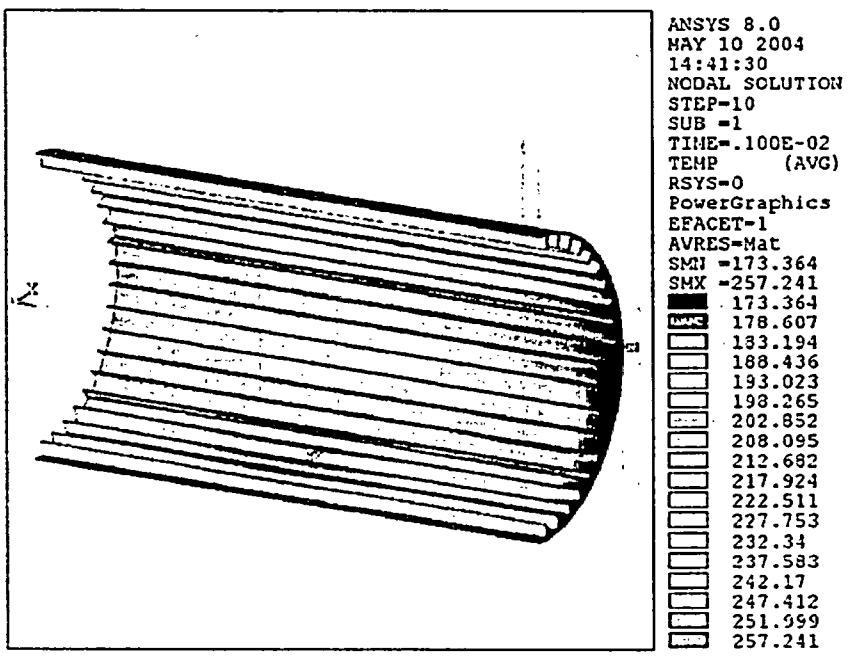

Figure E.6. Fin Structure Temperature Distribution - Normal Transport Conditions.

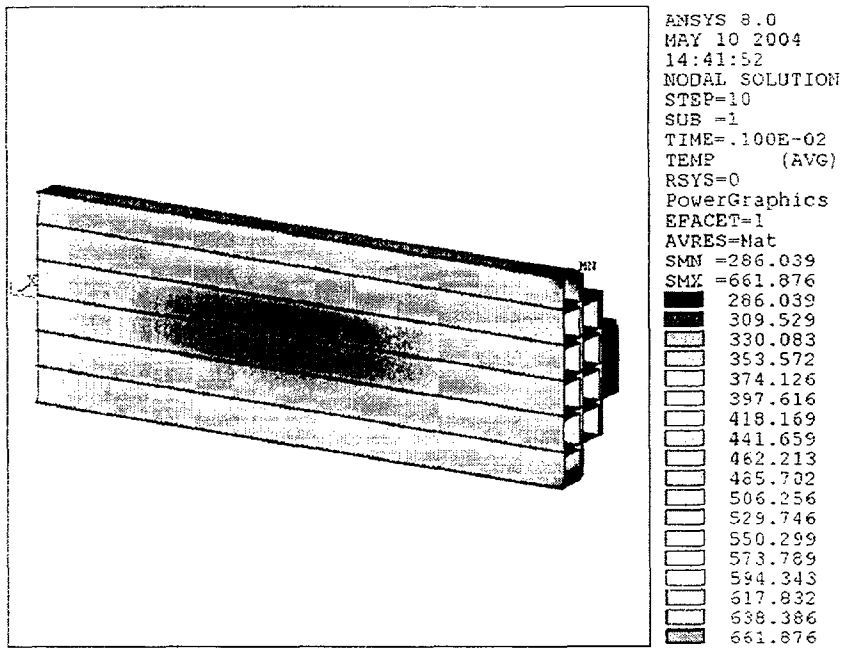

Figure E.7. Basket Axial Temperature Distribution - Normal Transport Conditions.

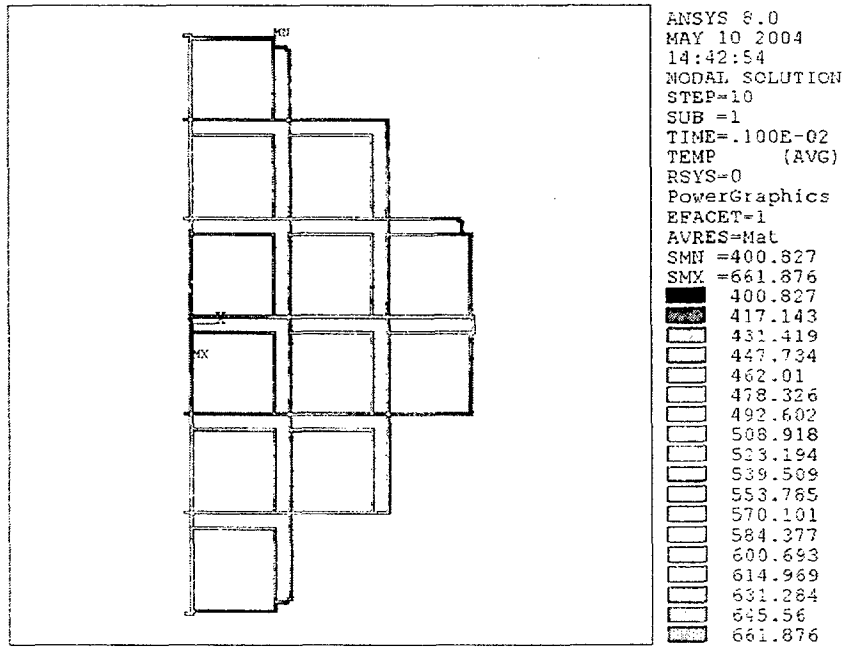

Figure E.8. Basket Radial Temperature Distribution - Normal Transport Conditions.

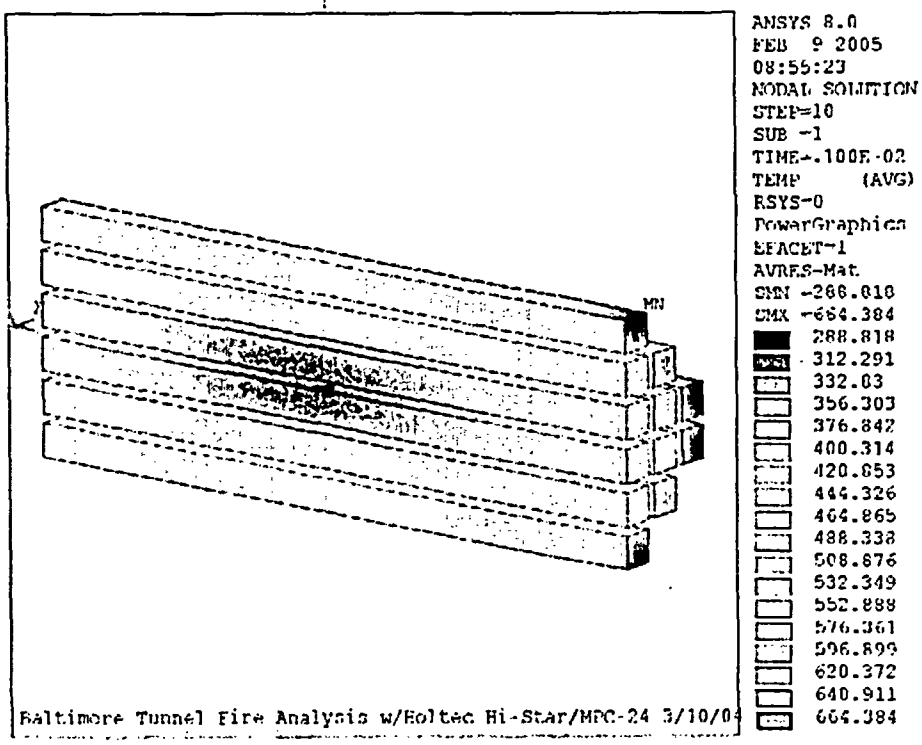

Figure E.9. Spent Fuel Axial Temperature Distribution - Normal Transport Conditions.

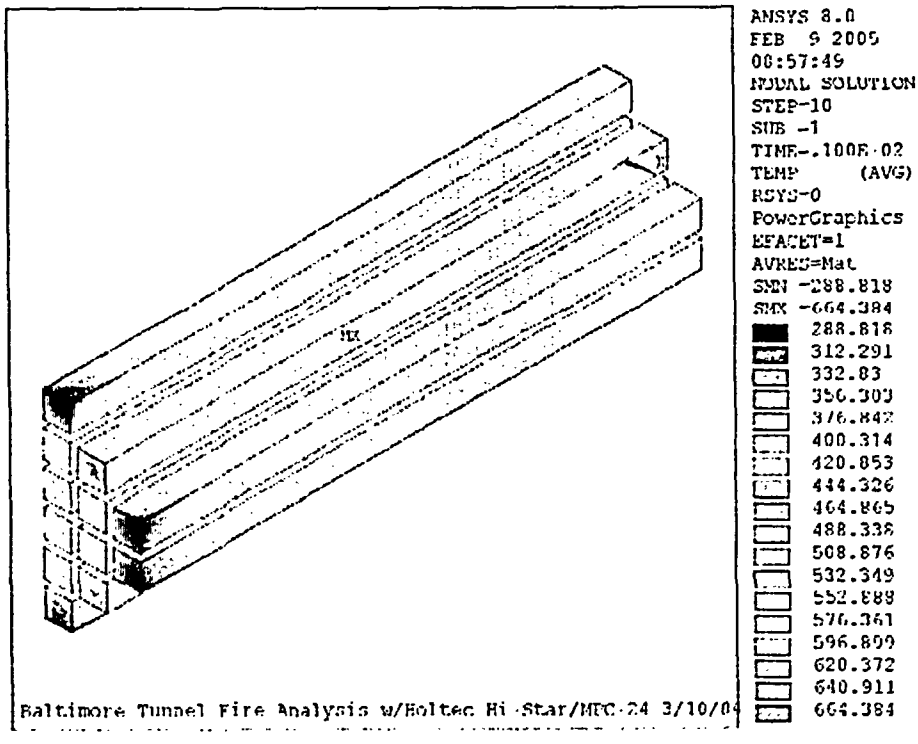

Figure E.10. Spent Fuel Axial Temperature Distribution - Normal Transport Conditions.

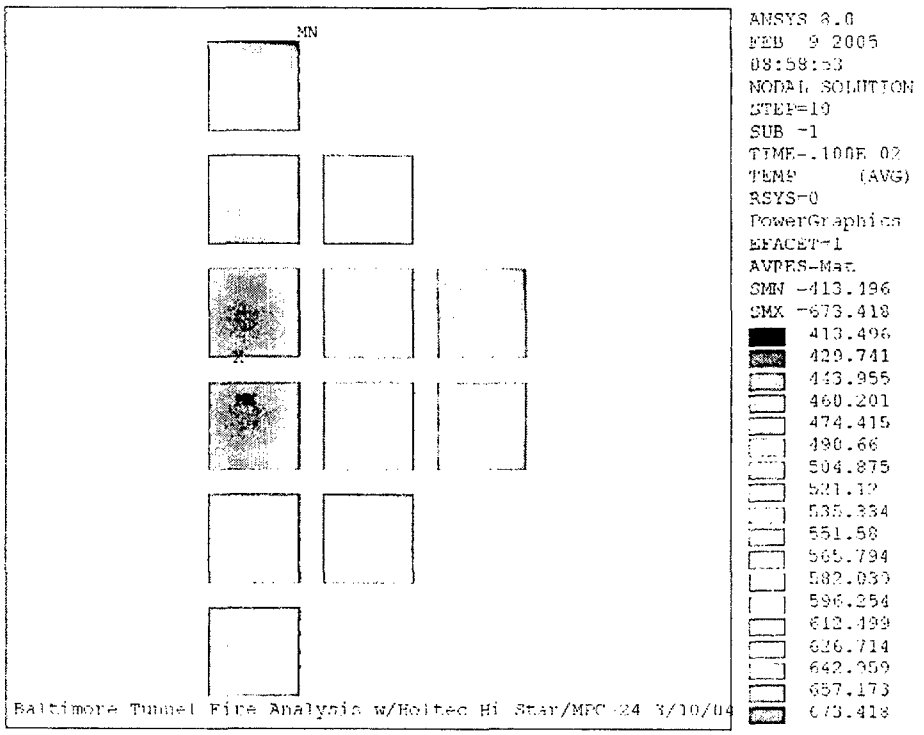

Figure E.11. Spent Fuel Radial Temperature Distribution - Normal Transport Conditions.

NRC FORM 335 (9-2004) NRCMD 3.7

U.S. NUCLEAR REGULATORY COMMISSION

BIBLIOGRAPHIC DATA SHEET

(See instructions on the reverse)

1. REPORT NUMBER (Assigned by NRC, Add Vol., Supp., Rev., and Addendum Numbers, if any.)

NUREG/CR-6886

2. TITLE AND SUBTITLE

Spent Fuel Transportation Package Response to the Baltimore Tunnel Fire Scenario

Draft report for comment

3. DATE REPORT PUBLISHED

MONTH	YEAR
November	2005

4. FIN OR GRANT NUMBER

J5167

5. AUTHOR(S)

H. E. Adkins, Jr.
J. M. Cuta
B. J. Koeppel

6. TYPE OF REPORT

Technical

7. PERIOD COVERED *(Inclusive Dates)*

8. PERFORMING ORGANIZATION - NAME AND ADDRESS *(If NRC, provide Division, Office or Region, U.S. Nuclear Regulatory Commission, and mailing address; if contractor, provide name and mailing address.)*

Pacific Northwest National Laboratory
Richland, WA 99352

9. SPONSORING ORGANIZATION - NAME AND ADDRESS *(If NRC, type "Same as above"; if contractor, provide NRC Division, Office or Region, U.S. Nuclear Regulatory Commission, and mailing address.)*

Spent Fuel Project Office
Office of Nuclear Material Safety and Safeguards
U.S. Nuclear Regulatory Commission
Washington, D.C. 20555-0001

10. SUPPLEMENTARY NOTES

11. ABSTRACT *(200 words or less)*

On July 18, 2001, a freight train carrying hazardous (non-nuclear) materials derailed and caught fire while passing through the Howard Street railroad tunnel in downtown Baltimore, Maryland. NRC staff undertook an investigation of the train derailment and fire to determine the possible regulatory implications of this particular event for the transportation of spent nuclear fuel by railroad.

The staff concluded that large transportation casks would withstand a fire with thermal conditions similar to those that existed in the Baltimore tunnel fire event with only minor degradation of peripheral components. The staff also concluded that some components of smaller transportation casks could degrade.

NRC staff evaluated the radiological consequences of the cask responses to the Baltimore tunnel fire. Though components in some casks heated up beyond their service temperatures, the staff determined that there would be no significant release as a result of the fire for any of these and similar casks.

12. KEY WORDS/DESCRIPTORS *(List words or phrases that will assist researchers in locating the report.)*

Spent fuel transportation
Cask thermal performance
Thermal analysis

13. AVAILABILITY STATEMENT

unlimited

14. SECURITY CLASSIFICATION

(This Page) unclassified

(This Report) unclassified

15. NUMBER OF PAGES

16. PRICE

PRINTED ON RECYCLED PAPER

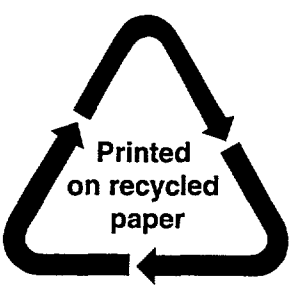

Federal Recycling Program